DOI:10.14753/SE.2020.2337

Mechanism of modulated electro-hyperthermia induced tumor destruction in C26 colorectal cancer models

PhD Thesis

Tamás Vancsik

Semmelweis University
Doctoral School of Pathological Sciences

Supervisor: Tibor Krenács, D.Sc.

Reviewers: Kinga Molnár, Ph.D.
István Kenessey, M.D., Ph.D.

Head of examining board: András Kiss, M.D., D.Sc.
Members of examining board: Tibor Glasz, M.D., Ph.D.
Lajos László, Ph.D.

Budapest
2019

DOI:10.14753/SE.2020.2337

Table of contents

Abbreviations

53BP1: p53 binding protein

5-FU: 5-fluorouracil

AIF: apoptosis inducing factor

APAF-1: apoptotic peptidase activating factor 1

APC: antigen-presenting cell

APO-1: apoptosis antigen 1

AST: astrocytoma

ATM: ataxia telangiectasia mutated protein

Bad: Bcl-2-associated death promoter

Bak: BCL2 antagonist/killer 1 protein

Bax: BCL2 associated X protein

Bcl-2: B-cell lymphoma 2 protein

BCL-W: Bcl-2-like protein 2

Bcl-XL: B-cell lymphoma-extra large protein

BH: BCL2 homology domain

Bid: BH3 interacting domain death agonist

Bim: Bcl-2-like protein 11

Bok: Bcl-2 related ovarian killer

CAD: caspase-activated DNase

CARD: caspase recruitment domain

casp: caspase

CCL21: chemokine (C-C motif) ligand 21

CD3/4/8: cluster of differentiation 3/4/8

CD40L: CD40 ligand

CDK2/4: cyclin-dependent kinase 2/4

c-FLIP$_L$: FLICE (FADD-like IL-1β-converting enzyme)-inhibitory protein long

CHF: congestive heart failure

CHIP: carboxyl terminus of the Hsc70-interacting protein

CHPP: continuous hyperthermic peritoneal perfusion

CpG: 5'—C—phosphate—G—3'

CR: complete response

CRT: calreticulin

CT: chemotherapy

CTL: cytotoxic T-cell

cyt-c: cytochrome-c

DAB: 3,3'-Diaminobenzidine

DAMP: damage associated molecular pattern

DAPI: 4', 6-diamidino-2-phenylindole

DC: dendritic cell

DD: dead domain

DED: death effector domain

DFFA/B: DNA fragmentation factor subunit alpha/beta

DiOC6: 3,3′-Dihexyloxacarbocyanine iodide

DISC: death-inducing signaling complex

Dox: doxorubicin

DR2: death receptor 1

DSB: DNA double strand break

EDTA: ethylenediaminetetraacetic acid

EGFR: epidermal growth factor receptor

EndoG: endonuclease G

ER: endoplasmic reticulum

ETA: effect-to-treatment analysis

FADD: Fas associated via death domain

FAS: First apoptosis signal

FasL: Fas ligand

FOV: field of view

FoxP3: forkhead box P3 protein

GBM: glioblastoma

GM1: monosialotetrahexosylganglio-side

H2AXγ: H2A histone family member X γ protein

H60: histocompatibility 60

HER-2: human epidermal growth factor receptor 2

Hif1/2: Hypoxia-inducible factor 1/2

HIPEC: hyperthermic intraperitoneal chemotherapy

HMGB1: high mobility group box protein 1

HRK: harakiri protein

HSE: heat shock element

HSF: heat shock transcription factor

Hsp70: 70 kDa heat shock protein

HT: hyperthermia

IAP: inhibitor of apoptosis protein

ICAD: inhibitor of caspase-activated DNase

ICD: immunogenic cell death

IDO: indoleamine 2,3-dioxygenase

IFN-γ: interferon-γ

IL-2/7/12: interleukin-2/7/12

IP: intraperitoneal

IR: infrared

LACC: locally advanced cervical tumors

LD: lethal dose

LVEF: left ventricular ejection fraction

MAPK: Mitogen-activated protein kinase

MBC: metastatic breast cancer

MCL1: myeloid leukemia cell protein 1

MDC1: Mediator of DNA damage checkpoint protein 1

Mdm2: Mouse double minute 2 homolog protein

mEHT: modulated electro-hyperthermia

MHC-I/II: major histocompatibility complex class I or II

MICA: major histocompatibility complex class I-related chain A

MOMP: mitochondrial outer membrane permeabilization

MTE: Marsdenia tenacissima extract

mTOR: mammalian target of rapamycin

NBS1: nibrin

NF-κβ: nuclear factor κ-light-chain-enhancer of activated B cells

NK: natural killer cell

NKG2D: natural killer group 2D

NKT: natural killer T-cell

NOXA: (Latin for damage) Phorbol-12-myristate-13-acetate-induced protein 1

NSCLC: non-small cellular lung cancer

OMM: outer mitochondrial membrane

OS: overall survival

p21: cyclin-dependent kinase inhibitor 1

p53: tumor protein p53

p62: nucleoporin 62kDa

PARP1: poly-ADP ribose polymerase 1

PBMC: peripheral blood mononuclear cells

PCD: programmed cell death

PCMA: peritoneal carcinomatosis with malignant ascites

PI3K: phosphoinositide 3-kinase

PMAIP1: phorbol-12-myristate-13-acetate-induced protein 1

PS: phosphatidylserine

PTEN: phosphatase and tensin homolog protein

PUMA: p53-upregulated modulator of apoptosis

Rae-1: retinoic acid early inducible 1

RIP1,-3: receptor-interacting serine/threonine-protein kinase 1, 3

rMA: relative masked area

ROS: reactive oxygen species

RpLp0: ribosomal **protein** lateral stalk subunit P0

RT: radiotherapy

RTK: receptor tyrosine kinase

SAR: specific absorption rate

SA-β-gal: senescence-associated beta-galactosidase

Smac: second mitochondria-derived activator of caspases

SMC1: structural maintenance of chromosomes protein 1

TAA: tumor-associated antigen

TBST: tris-buffered saline with Tween 20

Tc: cytotoxic T-cell

TCM: traditional Chinese medicine

TCR: T-cell receptor

TCRβ: T-cell receptor β

TDR: tumor destruction ratio

TE: tris-EDTA

TGF-β: tumor growth factor- β

Th1/2/17: type 1/2/17 T helper cell

TMA: tissue micro-array

TNF: tumor necrosis factor

TNFR1: TNF receptor 1

TNFRSF: TNF receptor superfamily member

TRAIL: TNF-related apoptosis-inducing ligand

TRAILR: TNF-related apoptosis-inducing ligand receptor 1

T_{reg}: regulatory T-cell

TUNEL: terminal deoxynucleotidyl transferase nick end labeling

ULK1: Unc-51 like autophagy activating kinase

VEGF: vascular endothelial growth factor

VEGFR: vascular endothelial growth factor receptor

VHL: von Hippel–Lindau tumor suppressor

WBH: whole body hyperthermia

WGA: wheat germ agglutinin

XIAP: X-linked inhibitor of apoptosis

DOI:10.14753/SE.2020.2337

1. Introduction

Modulated electro-hyperthermia treatment (mEHT, also called “oncothermia”) is a non-invasive complementary to chemo- and radio-therapy using electromagnetic field generated by amplitude modulated 13.56 MHz radiofrequency (1). The electromagnetic field, which can instantly penetrate into cancer lumps, induces heat shock response and cell stress at controlled 42^{o}C, besides interfering with gathered receptor molecules in cell membrane lipid rafts (2). Tumor selectivity of mEHT is linked to elevated glucose uptake (which has already been utilized in FDG-PET CT) glycolysis (also known as the Warburg effect) and the concomitant ion concentration and conductivity of tumors compared to adjacent normal tissues (3).

Loco-regional mEHT treatment has been exploited in combinations with chemo- and radio-therapy for successfully treating e.g. human gliomas, soft tissue sarcomas as well as cervical, colorectal and breast adenocarcinomas (3-8). Complementary mEHT treatment is financed by the national health insurance e.g. in Germany, Switzerland, Italy, Canada, South-Korea and Japan. In spite of these, the mechanism of action of tumor damage induced by mEHT and its molecular background have long been insufficiently understood. Therefore, we set up *in vitro* and *in vivo* tumor models to get a better insight into the underlying molecular background.

We selected C26 an aggressive mouse colorectal adenocarcinoma cell line in our mEHT treatment models. Colorectal cancer is one of the most common fatal malignancies worldwide, affecting more than 1.2 million new patients every year (9, 10). At least 50% of the cases relapse after surgical removal of the tumor without distant metastasis, but 20% of colorectal cancers have distant metastasis at the time of diagnosis (11). Though the 5-year survival of localized cancer is over 90%, it is sharply reduced to <12% in patients with distant tumor spread (12).

Besides their potential benefits, chemotherapeutics can produce serious and systemic side-effects including acute gastrointestinal, blood/bone marrow, neurological symptoms or such late adverse effects as cardiomyopathy, infertility, secondary malignancy etc. (13, 14). We choosed doxorubicin (Dox) in our mEHT studies presented in this dissertation, which is an anthracycline anti-tumor antibiotic, frequently used in first-line chemotherapy. It can destruct cancer cells both by preventing DNA repair in proliferating cells and by generating reactive oxygen species (ROS) which can disrupt cell membranes

and proteins (15). However, its use carries the risk of cardiotoxicity either through mitochondrial damage by ROS (16) and/or by interfering with iron metabolism through producing reactive Dox-Fe(II) complexes (17), mitochondrial proton pumps, calcium pumps in the sarcoplasmic reticulum, and Na^+/K^+ pumps in the cell membranes (18). Accordingly, any treatment combination which can support the anti-tumor effect of chemotherapy e.g. of doxorubicin without increasing the risk of side or adverse effects or allow drug use at lower concentrations with the same efficiency, would be of great benefit.

Furthermore, boosting of the host's immune response can be another promising addition to the efficiency of tumor therapy as it has been shown by clinical trials utilizing e.g. immune checkpoint inhibitors (10, 19). Our group earlier has shown that mEHT treatment can effectively damage colorectal cancer allografts in immunocompromised mice and provoke the release of damage associated molecular pattern (DAMP) signals relevant for inducing immunogenic tumor cell death (ICD) (16, 20). In line with these, mEHT pre-treatment has recently been described to augment tumor antigen primed dendritic cell immunotherapy through supporting T-cell, macrophage and eosinophil leukocyte invasion of CT26 (C26 from different vendor) murine colorectal cancer allografts (21).

We tested the molecular background of cell stress, apoptosis and DAMP related effects of mEHT treatment using C26 colorectal adenocarcinoma. Our *in vitro* model was also used to investigate the mechanism of action of Dox treatment on C26 cells and how its combination with mEHT can improve the treatment efficacy. We studied the mEHT induced tumor stress, cell death and immune response in C26 cancer allografts of immunocompetent mice both locally and at distant tumor sites either alone or after combining with a T-cell promoting agent.

For better understanding the effect of hyperthermia and in particular of mEHT on malignant tumors, below we overview the basic mechanisms of cell death, the relevant oncotherapy options including chemo-, radio- and immunotherapy. These methods have already been combined with conventional hyperthermia and/or mEHT, here we discuss the theory and practice of using moderate heat (~42oC) for experimental or human cancer treatment.

1.1. Stress response: heat shock proteins

Anti-tumor therapies are intended to destroy the inoperable malignancies, stop their growth, and/or reduce tumor volumes, thus increasing the feasibility for surgical resection. These therapies usually cause a high level of cellular stress which is not tolerable (22). Stress can be any kind of acute changing or chronic harmful effect on cells. It can come from both the extracellular (thermal-, or osmotic shock, hormonal effect, redox changing in the environment etc.) intracellular space (lack of ATP, surplus Ca^{2+}, toxins etc.). Nevertheless, the function of proteins which are crucial for maintaining the cell homeostasis can be disrupted by causing irreversible conformational changes. Stress-response can be identified by the synthesis of heat shock proteins (23). Aberrant proteins might distort their native conformation became denatures and thus unable to perform their normal functions. They impose severe stress for the host cells, by overloading the capacity of the proteolytic system, and their accumulation may cause cytotoxicity. If a protein undergoes an inappropriate folding during its expression or an extrinsic impact posttranslational harbors the native form, heat shock proteins can help to avoid the consequences (24). They also take part in the posttranslational folding of proteins to reach the native conformation, furthermore in the repair of those which lost this structure. Some of them functioning by binding and stabilizing the normal proteins (for example the Hsp90). Based on their expression pattern the chaperones have three subtypes; constitutive, constitutive and inductive and only inductive (23, 24). All expressed forms have their cell-organelle specific types; the most relevant examples can be seen in **table 1**.

Table 1. Some examples for the molecular chaperones regarding their expression and cellular location. Note that the carboxyl terminus of the Hsc70-interacting protein (CHIP) is a co-factor and works along with chaperones (24, 25).

Heat shock proteins				
	Extracellular space	Cytoplasm	Endoplasmic reticulum	Mitochondrium
Constitutive	Less known	Hsp33, Hsp40, Hsp60, Hsc70, Hsp90, moonlight chaperones (f.g. Prx)	Grp78 (BiP), ERdj1-5, Grp94, calnexin, calreticulin, (CHIP)	Less known
Inductive	Hsp22, Hsp27, Hsp70	Hsp22, Hsp27, Hsp33, Hsp40, Hsp70, Hsp70i	(CHIP)	Mortalin, TRAP-1

1.2. Cell death

Numerous ways of cell death have been described which are part of a redundantly regulated system. During the years of intensive studies, it has been concluded that these pathways are difficult to be separated from each other, since their induction mechanisms and molecular background show overlapping mechanisms. Here we highlight two clinically relevant pathways of cell death relevant to our work: apoptosis and necrosis.

1.2.1. Apoptosis

Recently it is well known that the regulated elimination of cells (programmed cell death; PCD) in different tissues are necessary for maintaining the homeostasis and the well balanced function of every organ in the body. The driver signaling can be induced from the extracellular space: extrinsic- or can be started intracellularly: intrinsic apoptotic pathway (26) (**Figure 1**).

In contrast to necrosis apoptosis is considered as the form of physiological cell death, which is tolerable for the immune system. The micromorphology of apoptosis includes the rounding-up and shrinkage of cells (pyknosis), chromatin condensation, nuclear fragmentation (karyorrhexis), few ultrastructural modifications of organelles and plasma membrane blebbing (27). The cells are fragmented into many membrane-bound apoptotic bodies, which are phagocytosed by macrophages or the neighboring cells. Important to note, that apoptosis is an energy-saver process, thus the membrane integrity and metabolic activity of cells can be maintained till the last stage, which allows enough time for the clearance of the dying cell portion (28). If there is no clearance, the end-stage apoptosis is followed by the degradation of the plasma membrane and appearance of the necrotic morphology (29).

DOI:10.14753/SE.2020.2337

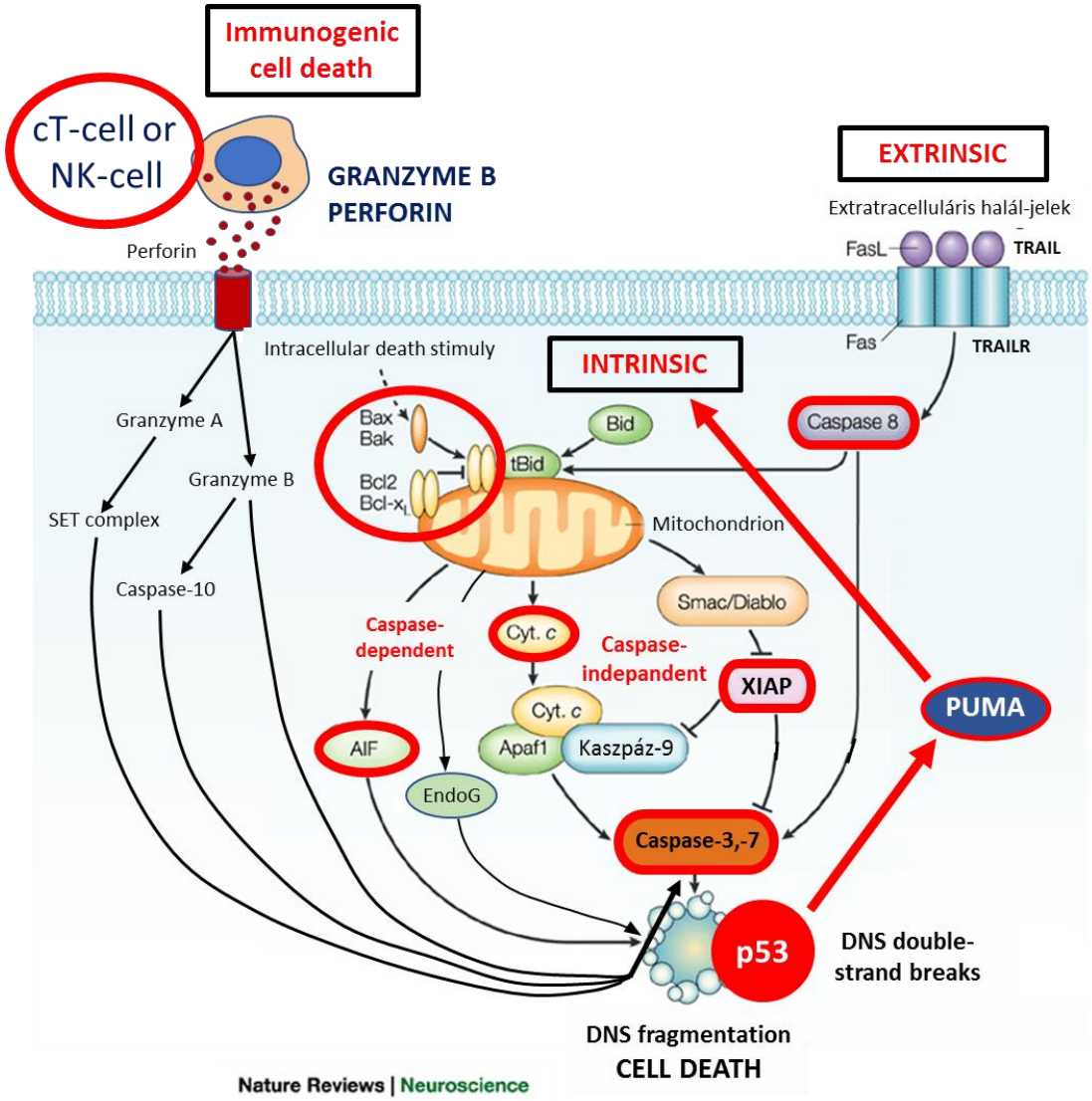

Figure 1. Red frames highlight the measured signal elements. Upon intracellular apoptotic stimuli Bax/Bak proteins are released under the inhibition of Bcl-2/-XL, thus they can be oligomerized and form the mitochondrial outer membrane pores (MOMPs). This moment also supported by the cleavage of Bid to truncated Bid (tBid). The pro-apoptotic proteins can be released through the MOMPs. Apoptosis-inducing factor (AIF) and endonuclease G can induce the DNA fragmentation on a caspase-independent manner, while cytochrome c and apoptotic peptidase activating factor 1 (APAF1) responsible for the activation of caspase cascade. The caspase-dependent way is also stimulated by the release of smac/diablo protein which can suppress the function of caspase inhibitor IAP proteins (e.g. XIAP) (30). On the other hand, DNA double-strand breaks can trigger the activation of the native p53, which can promote the transcription of pro-apoptotic P53-upregulated modulator of apoptosis (PUMA), thus can also induce the intrinsic apoptosis (31). On the extrinsic way the death receptors are activated and these promote the cleavage of caspase-8 which can directly activate the effector caspases and further enhance the intrinsic pathway by generation of tBid. In case of immunogenic cell death the secreted enzymes (perforin, granzyme B) of cytotoxic T- and NK-cells can induce the caspase-dependent way (32). Modified from the original figure of Vila and Przedborski (2003) (30).

The intrinsic apoptosis can be initiated by different adverse micro-environmental effects such as growth factor withdrawal, DNA damage, endoplasmic reticulum (ER) stress, high amount of reactive oxygen species, replication stress, microtubular alterations or mitotic defects (29). The intrinsic pathway is usually triggered by the mitochondrial outer membrane permeabilization (MOMP). This step is controlled by pro-apoptotic and anti-apoptotic members of the BCL2 protein family. BCL2 associated X (Bax), and/or BCL2 antagonist/killer 1 (Bak; encoded on BAK1 gene) proteins. In normal conditions, Bax is trafficking between the OMM and the cytosol, where it can be found in monomeric or inactive dimeric conformation. In contrast to this Bak constitutively abundant on the OMM. Upon apoptotic stimuli, Bax retro-translocation stops and it accumulates in the OMM. Both Bax and Bak can oligomerize and form ring-like lipidic pores on the outer mitochondrial membrane (OMM). These alters mitochondrial permeability and polarity, thus causes aberrations in the mitochondrial function and ultrastructure (27). The pro-apoptotic BH3-only proteins which can trigger the assembly of the OMM pores can be activated transcriptionally or post-translationally as a cell organelle or cellular compartment got perturbations. P53-upregulated modulator of apoptosis (PUMA), Bcl-2-interacting mediator of cell death (Bim), and phorbol-12-myristate-13-acetate-induced protein 1 (PMAIP1 or NOXA) are mostly gone through on transcriptional, while BH3 interacting domain death agonist (Bid) probably undergoes post-translational activation (33). MOMPs induce the cytosolic release of apoptogenic proteins from the intermembrane space of mitochondria including cytochrome-c (cyt-c) which is a member of the mitochondrial respiratory electron-transport chain, and the second mitochondrial activator of caspases (smac or diablo). The cytosolic pool of cyt-c, apoptotic peptidase activating factor 1 (APAF1) and pro-caspase-9 in a deoxy-ATP-dependent manner can form the apoptosome complex, which can cleave, thus activate the pro-casp-9. Activated casp-9 induces the proteolytic activation of the effector (or executioner) caspases: pro-casp-3 and pro-casp-7 (33). Smac released into the cytosol can enhance the apoptotic signaling by binding to the members of the inhibitor of apoptosis (IAP) protein family, including X-linked inhibitor of apoptosis (XIAP), which from the IAP protein family solely can block the apoptotic caspase-cascade by direct association (**Figure 2**). A major activator of XIAP is the Akt kinase (34). Akt signaling has important role in tumor-cell

survival through the inhibition of p53 and the induction of NF-κβ pathway (**Figure 2**) (35).

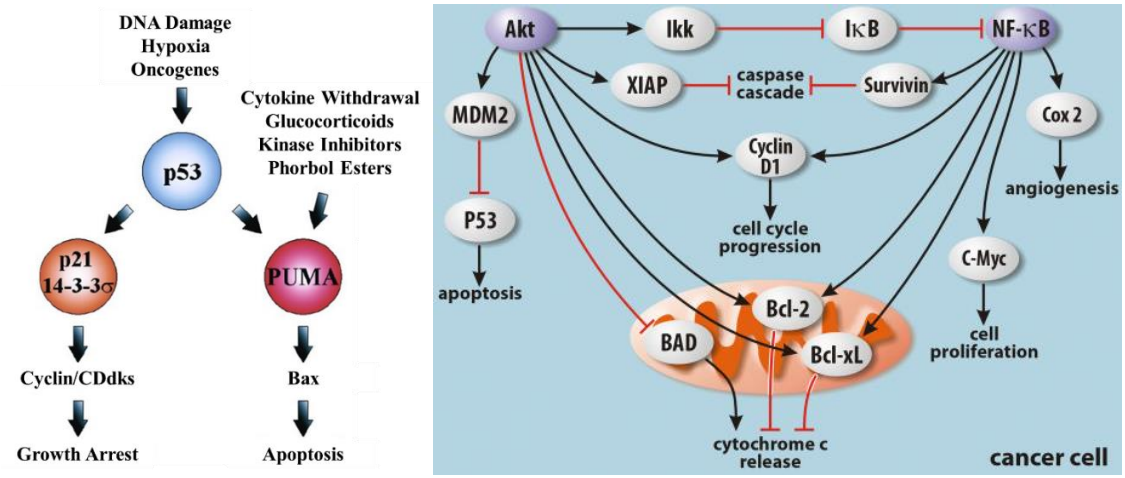

Figure 2. Upon different perturbations p53 can be activated and it triggers cell cycle arrest through p21 signaling or promotes intrinsic apoptosis by inducing the transcription of PUMA protein (Yu J and Zhang L 2003) (31). Akt kinase has numerous targets which are directly related to cell death, proliferation or even angiogenic machinery. The function of Akt promotes survival and tumor progression through the induction e.g. the NF-κβ pathway, which makes it an ideal target for therapies. Modified from the original figure of Niero EL et al. (2014) (35).

The catalytic activity of effector (or executioner) caspases triggered by cellular demise and responsible for morphological and biochemical aspects of apoptosis, such as DNA fragmentation, phosphatidylserine (PS) exposure (flip-flop) and the formation of apoptotic bodies. Casp-3 promotes DNA fragmentation by cleaving and inactivating the inhibitor of caspase-activated DNase (ICAD or DNA fragmentation factor subunit alpha: DFFA), to uncover the catalytic activity of caspase-activated DNase (CAD or DNA fragmentation factor subunit beta: DFFB) (36). Casp-3 promotes PS exposure by activating the elements of PS externalization (phospholipid scramblases) and inactivating proteins involved in PS internalization (phospholipid flippases) (37). PS has immunogenic properties; it can be recognized by macrophages. Macrophages and immature dendritic cells as well as epithelial and mesenchymal cells are capable for recognizing and engulfing apoptotic cells by phagocytosis (38, 39). On the other hand, DNA fragmentation can be induced in a caspase-independent manner. Upon the MOMP the apoptosis-inducing factor (AIF) and endonuclease G (endoG) are released and both are able for direct DNA-fragmentation (**Figure 2**) (40).

The anti-apoptotic members of the Bcl-2 family: Bcl-2, B-cell lymphoma-extra large (Bcl-XL or Bcl-2 like 1: BCL2L1), myeloid leukemia cell protein 1 (MCL1, Bcl-2 like 2: BCL2L2 or BCL-W), and Bcl-2 related protein A1 (BCL2A1 or BFL-1). These pro-survival proteins can antagonize the MOMP formation and generally are located in the OMM or in the ER membrane (29). Different BH3-only proteins have been defined as sensitizers of apoptosis, since they can bind anti-apoptotic proteins from Bcl-2 family. Bid, Bim, and PUMA potently bind all anti-apoptotic Bcl-2 members; Bad can interact with Bcl-2, Bcl-XL, and Bcl-W; NOXA inhibits MCL1; and harakiri protein (Hrk) binds Bcl-XL. The balance of inhibitors and sensitizers can be controlled by their transcription (41).

Extrinsic apoptosis is initiated by disturbance from the extracellular space mediated by ligand binding to death receptors which transduce and transmit these signals and activate downstream response elements. On the other hand, it can be induced by dependence receptors, which are growth factor receptors, when the levels of growth factors drop below a critical threshold, e.g. at growth factor withdrawal (29). Malignant cells commonly overexpress such receptor tyrosine kinases, which can be selectively blocked by targeted therapies. Since our studies did not focus directly on growth factor receptors, here we show details only of the death-receptor mediated pathways.

Death receptors are cell surface death receptors including Fas (known also as CD95 or APO-1, DR2), and tumor necrosis factor receptor 1 (TNFR1 or DR1), TNF-related apoptosis-inducing ligand receptor 1 (TRAILR1 or DR4), and TNF-related apoptosis-inducing ligand receptor 2 (TRAILR2 or DR5). Generally, upon the binding of their ligands, death receptors can assembly in stable homotrimers through the connection of intracellular domains and distinct adaptor proteins via their dead domain (DD). This stable multiprotein structure is called “death-inducing signaling complex” (DISC), “complex I”, and “complex II”, which are able to activate the pro-casp-8 (or pro-casp-10 in a limited way). The adaptor proteins contain the death effector domain (DED), which can bind both pro-casp-8 and the long form of FLICE/caspase 8-like inhibitory protein (c-FLIP$_L$). If the balance shifts towards to pro-casp-8, apoptosis can be triggered, but if the amount c-FLIP$_L$ and its cleaved product will be raised, that can induce survival through the activation of NF-κβ signal pathway (42).

Extrinsic apoptosis can activate two distinct downstream pathways. In case of "type I cells" (e.g., thymocytes and mature lymphocytes) the pro-casp-3 and pro-casp-7 proteolytic maturation by casp-8 can trigger the PCD. This cannot be inhibited by the transgene-driven overexpression of anti-apoptotic Bcl-2 proteins, the co-deletion of Bax and Bak1 genes, or the suppression of Bid (29, 43). In "type II cells" (e.g. hepatocytes, pancreatic β cells, and a majority of cancer cells) extrinsic apoptosis requires the mitochondria for execution of DNA fragmentation. Here the proteolytic cleavage of Bid by casp-8 and the activation of pro-casp-3 and pro-casp-7 is detained by XIAP (29, 42). Upon the cleavage of Bid by casp-8 a truncated form tBid is generated which translocates to the OMM. At the OMM, tBid works as an activator to engage Bax/Bak-dependent MOMP-driven release of cyt-c and APAF1 and consequent casp-9-driven PCD (43).

1.2.2. Necrosis

Necrosis is described as a type of unregulated or pathologic cell death, which is caused by traumatic and overwhelming external perturbations or damage on cell membranes including all types of cell organelles. It was morphologically characterized by the swelling of cell organelles, the changes in the nuclear ultrastructure such as dilatation and disruption of the nuclear (karyolysis) and organellar membranes. Furthermore, the overall increase of cell volume (oncosis), finally the split of the plasma membrane and the loss of intracellular contents are also well known characteristics of the necrotic phenotype. Necrotic cells are not fragmented into discrete and stable particles as it happens with in apoptotic cells (26). Since necrosis is characterized by severe and large-scale membrane damage and release of necrotic cell debris it is accompanied by a massive inflammatory response, resulting imposing heavy burden and adverse effects on the quality of life cancer patients (44).

Recently, it has been well known that the necrotic termination can be regulated by a subset of the apoptotic machinery. This type of cell death is known as necroptosis. Necroptosis can be induced by TNF-R1 (DR1), Fas (DR2) and TRAIL-R1/2 (DR4/5) receptors, but the serine-threonine kinase RIP is also needed. For the assembly of active necro(pto)some the phosphorylation of RIP1 and RIP3 is necessary (both are able for the autophosphorylation) (45). Necroptosome can directly induce the elevation of ROS,

organellar membrane disruption (mitochondria, lysosomes etc.) and the prompt decrease of ATP levels. Controversy to the apoptosis, that PARP1 is also activated during necroptosis and promote ATP depletion (46).

1.2.3. P53 induced apoptosis and senescence following DNA-damage

Sublethal dose of stress either in normal and tumor cells can induce transient or permanent cell cycle arrest called senescence. Cancer therapeutics supposed to induce the apoptosis of tumor cells, however in normal cells numerous tumor suppressor and oncogene regulate this process (47). Deregulated senescence signaling support the tumorigenesis. Senescence limits DNA replication, thus inhibits the proliferation of malignant cells. Besides the cellular stress, DNA damaging agents and factors are able to induce this cellular mechanism. Senescence can be characterized based on the phenotype of cells; a large, flat morphology and the presence of the senescence-associated beta-galactosidase (SA-β-gal) marker (47).

In normal cells telomere shortening- or uncapping-induced DNA damage can be sensed by ataxia-telangiectasia mutated kinase (ATM), which activates the p53 pathway and results proliferation arrest (48, 49). Similar signaling can be triggered upon double-strand DNA breaks (DSB). Depending on the severity of the genomic damage, p53 can block the cell cycle in G_1/S phase transiently or permanently (ends with apoptosis or senescence). P53 can induce p21 activation which inhibits cyclin dependent kinase 2 (CDK2)/Cyclin E and CDK4/6/Cyclin D (50). CDK inhibition results in hypo-phosphorylation of phosphorylated retinoblastoma protein, which allows the inhibition of transcription factors for the S-phase. Retinoblastoma is an important component of cell cycle arrest in senescence. In senescent cells the phosphorylated histone H2AXγ (pH2AXγ) positive foci are enriched in the nuclei; furthermore, p53 binding protein 53BP1, NBS1, the phosphoS966 form of SMC1, and MDC1 levels also increase (47).

Normally, P53 degradation is induced by the mouse double minute 2 homolog protein (Mdm2) ubiquitin ligase. Mdm2 activity is maintained by the active phospho-Akt (51), which has a great role in the cell survival in numerous ways, such like maintain the activation of anti-apoptotic proteins (XIAP, Bcl-XL, Bcl-2 etc.), inhibit some of the pro-apoptotic proteins (Bad), and induce the NF-κβ pathway (35). ATM can inhibit Mdm2,

thus p53 can release under control, which can promote the Akt destruction (51) (**Figure 2**).

1.3. Oncoimmunologic aspects

1.3.1. Tumor immunoediting

It is well known that in the development of malignancies the deficiency of immune system is also involved. If cells undergo malignant transformation and their intrinsic tumor-suppression (senescence, repair, apoptosis) fails, the malignant progression may be controlled by the immune response induced by the tumor-associated immunogenic signals (tumor-antigens, released "danger" signal/DAMP proteins, NK-cell receptor antigens etc.). Depending on the inherent conditions tumor-cells can be eliminated, kept in an equilibrium or they can escape from control ("3 E") (52).

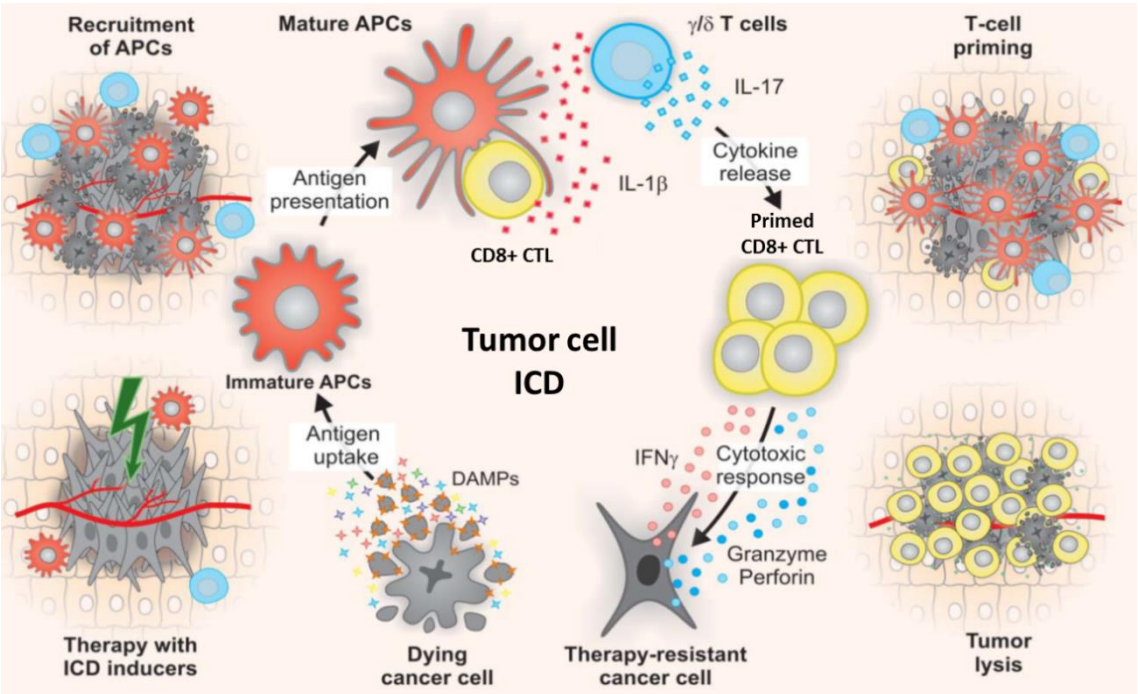

Figure 3. Particles released from the dying tumor cells can attract the immature dendritic cells, which are able to take up and show the tumor associated antigens for the effector CD8+ T-cells in the peripheral lymphoid organs and promote their expansion and maturation. The effectors can attack the tumor cells with their secreted enzymes and might induce the immunogenic cell death. Modified from the original figure of Kepp O et al. (2014) (53).

Cancer cells can be eliminated by immunogenic tumor cell death (ICD) (**Figure 3**) triggered by the classical danger signals such as type I IFNs which are induced early under

tumor development, promoting the activation of primer antigen-presenting (S100+) dendritic cells (DC) and the adaptive immune response (53). One of the best described part of ICD is the damage associated molecular pattern signaling. This includes the extracellular release of high mobility group box protein 1 (HMGB1) and ATP which act similarly to cytokines (54) and cell membrane localization and access by antigen presenting and immune cells of the chaperons Hsp70 and calreticulin (20). Complex DAMP signals can activate antigen-presenting cells (APC) by promoting the uptake and presentation of tumor antigens through Toll-like-, purinergic- and pattern recognition receptors for enhancing tumor-specific T-cell response (53).

Tumor-associated antigens (TAAs) are peptide fragments derived from proteins, that are important for cell-differentiation and from mutated proteins or proteins with elevated expression during tumorigenesis compared to normal conditions (55, 56). The T-cell receptors (TCRs) in the tumor microenvironment can interact with TAA-derived peptides in context of either MHC class I or MHC class II presentation by all nucleated cells, or restricted cell types capable of antigen presentation, which activate CD8+ cytotoxic T-cells, or CD4+ helper T-cells (57). It is therefore not surprising that tumor-infiltrating CD8+ and CD4+ T-cell populations are considered to be good prognostic factors in cancers (52). The resting T-cells are mostly activated by the antigen presenting dendritic cells (DCs or APCs) carrying cognate MHC/TAA in the secondary lymphoid organs (spleen and lymph nodes) (58). Endogenous proteins, processed in the cytosol of APCs, are mainly presented by the MHCI pathway, while exogenous proteins are taken up by APCs via phagocytosis or receptor-mediated endocytosis are presented through the MHCII pathway (59). CD8+ T-cells, also known as “cytotoxic” T-cells (CTL or Tc) are the most well-known effectors in tumor immune-surveillance (60). The TCR–MHCI/TAA interaction is required for clonal expansion of resting CD8+ T-cells and expression of their effector enzymes; perforin and granzymes (58). Perforin can open pores on the membranes of the target-cell, thus the granzymes can enter the cytoplasm and their serine protease function induces the activation of caspase cascade and apoptosis (61). CD4+ T helper (Th) cells catalyze the activation of CD8+ function by producing high levels of mitogenic cytokines (IL-2, IL-12) (62). DCs which are expressing cognate MHCII/peps can interact with TAA-specific CD4+ T-cells (63). TAAs can also be presented via the MHCII pathway by uptake and cross-presentation similar to those

presented by the MHCI pathway (64). Specific receptor-ligand interactions can (for example CD40 on DCs with CD40L on CD4+ T-cells) trigger DCs to activate resting CD8+ T-cells (65, 66). Basically, we can divide CD4+ T-cells for 4 subsets regarding their cytokine-expression profile: Th1, Th2, Th17 and regulatory T-cells (67). During anti-tumor immune response Th1 cells can produce pro-inflammatory cytokines, for example IL-2, IL-12 (62). Th1 cells can also express perforin and granzymes, thus these have direct effect in preventing tumor-progression (68). Regulatory T-cells (T_{reg}) cells identified by their FoxP3 and +/CD25 expression are immune-regulators with the primary role of controlling Th1 type anti-tumor immune response (60). Therefore, T_{reg} infiltration into the tumor microenvironment is considered as a poor prognostic factor (69). T_{reg}s suppress effector T-cells either by direct contact and immunoregulatory cytokine expression (60). TGF-β secreted by T_{reg}s suppresses the gene transcription required for cell survival and effector functions (52). Furthermore, high level of the α-chain of IL-2 receptor (CD25) is constitutively expressed, which can bind and consume up large amounts of IL-2 and thus act as an IL-2 sinker (70). Furthermore, T_{reg}s can affect DCs to turn them into tolerogenic towards antigens. Priming of T-cells with antigens presented by tolerogenic DCs results in peripheral T-cells tolerance in the form of anergic (unresponsiveness) or clonal deletion (71, 72).

Malignancies can be developed not only due to the insufficient immune response, but also because of the selection of tumor-cell populations which can modify the anti-cancer immunity (52). Immunosuppression can help tumor cells to escape from elimination. Malignant cells usually express immunomodulator molecules which help to hide their antigens from the microenvironment, suppress the activation or induce programmed cell death of the immune-effector cells (73). There are numerous ways how the tumor cells can impair the systemic defense mechanisms, such as by secreting/producing cytokines (TGFβ-1) and death ligands (FasL, Apo2L/TRAIL), microparticles, ganglioside shading and IDO (indoleamine 2,3-dioxygenase). These factors usually facilitate the development or polarization of native immune cells towards suppressive subtypes, which can promote the tumor cell survival and metastatic abilities (74).

1.3.2. Connection between hyperthermia and the anti-tumor immune response

Hyperthermia especially whole-body hyperthermia can induce the expression of homeostatic chemokines including chemokine (C-C motif) ligand 21 (CCL21) and adhesion factors such as L-selectin, integrin and ICAM in high endothelial venules (75). These are important for the homing of DCs and T-cells to these sites, furthermore, hyperthermia can increase the migration capacity of DCs *ex vivo* (76).

It was demonstrated that incubation of peripheral blood mononuclear cells (PBMCs) at 39°C for 2 h in a water bath, then co-culturing with anti-CD3/CD28 monoclonal antibodies for 24 h at 37°C, induced significantly higher IFN-γ and IL-2 secretion in T-cells compared to that at 37°C (77).

Other studies suggest that heat-induced increased membrane fluidity can be a key factor for cytokine-production, resulting in the promotion of an enhanced T-cell and APC crosstalk. Mild hyperthermia at 39.5°C can induce the cluster formation of the GM1+ (monosialotetrahexosylganglioside) CD-microdomain in CD8+ T-cells. Also this heat can promote the clustering of TCRβ and the CD8 co-receptor and enhance the antigen-specific conjugate formation between T-cells and APCs in mice (78).

Increased expression of heat shock proteins was shown to increase in fever-range whole-body hyperthermia for protecting proteins from the heat induced conformation-changes with their chaperone function. DCs can deliver chaperoned antigenic peptides to MHC-I, thus induce antigen-specific T-cell activation (79). It was shown that under insufficient conditions for T-cell activation the presence of recombinant Hsp60 promotes antigen-specific IFN-γ secretion, thus effector T-cell maturation (80).

NK-cells as a part of the innate immune response can attack their targets without exposure to specific antigens. All normal nucleated cells express MHC class I molecules, which can be downregulated in aberrant cells such as cancer cells, as a part of an immune escape mechanism from anti-tumor immunity by T-cells (81). NK-cells target cells which lack MHC-I molecules, because MHC-I inhibits NK-cell functions which can be released in this situation. Activated NK-cells can attack tumor cells by secreting cytotoxic molecules; perforin and granzyme and death receptors such as FasL, TRAIL, and TNF-α (82). Heat stress can enhance the clustering of NK-cell-activating receptors such as NKG2D, and the expression of NK-cell-activating ligands, including MHC class I-related chain A (MICA) (83). Furthermore, activated NK-cells produce such cytokines like IFN-

γ and IL-2 (84), which can induce immunoglobulin production from B-cells and activation of T-cells (85). This observation was suggestive that hyperthermia-mediated NK activation could improve not only the native but the tumor-specific adaptive immune response (84).

Regulatory T-cells down-regulating or suppressing the induction and proliferation of immune cells including T-cells, DCs and NK-cells (70). T_{reg}s usually extend for about 4% of CD4+ T-cell population, but it can raise to 20-30% in the tumor microenvironment and imply poor prognosis. In animal models, the suppression of T_{reg}s can increase the efficacy of immunotherapy, so depletion of T_{reg}s can be a desirable target for cancer immunology. Hyperthermia is considered to reduce the induction and enhance the apoptotic signaling of T_{reg}s. Furthermore, the irradiation of fever-range hyperthermia on the upper abdominal region of healthy volunteers caused a significant decrease in the number of T_{reg}s in peripheral blood samples, while the percentage of NK-cells and their activity was increased (86).

1.4. Standard therapy options in the oncology

For patients diagnosed with malignant disease, the recommended first line therapies will be offered, based on standard guidelines regularly published under WHO supervision. The first treatments are usually integrated in a standard set of protocols ("gold standard"). There are many therapeutic options offered including surgery, radio-, chemo-, targeted-, hormone or immunotherapies, some of which discussed below, have been successfully combined with different forms of hyperthermia.

1.4.1. Chemotherapy

The chemotherapeutic drugs inhibit or interrupt cell proliferation, so their targeting mechanism is based on the higher proliferation capacity of tumor cells compared to normal cells. We can differentiate alkylating agents, antibiotics, antimetabolites, anti-tubulin agents and topoisomerase-inhibitors as the basic types of cytostatics (87-89).

The family of alkylating agents contains for example the nitrogen mustards, aziridines and epoxides, alkyl sulfonates, nitrosoureas, cisplatins (and derivatives such as carboplatin etc.) which can covalently bind to the DNA. Antibiotics like anthracyclines (for example doxorubicin), actinomycin-D or mitoxantrone intercalates with the DNA

strand thus interrupt the DNA replication and mRNA synthesis. The antimetabolites can disrupt the nucleotide synthesis or replace them under DNA replication. The basic antimetabolites are the purine-analogues, pyrimidine-analogues and folate-antagonists. The anti-tubulin agents (vinca-alcaloids and taxanes) disrupt the microtubule spindles. The topoisomerase-inhibitors such as the anthracyclines and campothecin-derived agents can block the function of the topoisomerase-I and-II, thus these can induce both single- and double strand DNA breaks (87, 89).

1.4.2. Radiotherapy

Radiation therapy applies ionizing radiation for eliminating tumor cells through DNA damaging. DBS can directly induce programmed cell death, while single-strand DNA damage can be passed through on cell division, but it can accumulate and causing cell death or makes slower the proliferation (90).

DNA damage can be caused by either direct or indirect ionization of those atoms which makes up the DNA chain. Indirect ionization creates free oxygen radicals derived from the water content of cells which cause the majority of the effects on DNA breaking (90). Oxygen is a radiosensitizer, since it increases the efficacy of the radiation therapy; because it gives the source for DNA-damaging radicals (91). Solid tumors often become deficient in oxygen, this hypoxic condition can raise 2-3 times higher the resistance of tumor cells for radiation than in normal oxygen environment (92, 93). Overcoming hypoxia including the use of high-pressure oxygen tanks, blood substitutes that carry increased oxygen, hypoxic cell radiosensitizer drugs (misonidazole, metronidazole and hypoxic cytotoxins like tirapazamine) (91). Furthermore, hyperthermic therapies are also used for dilating the vessels and increase the blood-flow to the tumor site (94).

1.4.3. Immunotherapy in oncology

Immunotherapies in oncology are intended to activate the immune system against tumor cells. These therapies are thought to have fewer side-effects than drugs applied for chemotherapy. It can be used alone on some malignancies, but for others it seems to work better in combination to other treatments (10, 19, 95, 96). Immunotherapies can be applied as a complementary with administration of soluble factors (97-99), TAA-primed native (100-103) or chimeric antigen receptor containing effector cells (100, 102). On the other

hand, such immune checkpoint inhibitors like pembrolizumab, nivolumab (104) which target PD-1, PD-L1, CTLA-4 molecules (105) are become the part of the first-line regimen in metastatic melanoma, non-small cell lung cancer, head and neck squamous cell carcinoma, renal cell carcinoma, and Hodgkin's lymphoma (106).

1.5. Hyperthermia as a complementary therapy

Complementary treatments are not considered as first-line therapies in the oncology. They are offered by some clinics and a few of these have been proven physiological effects enabling them to be covered by the health insurance systems (107, 108). These methods are allowed to be used along with standard treatments such as chemo-radiotherapy, and more recently targeted or immunotherapy. The complementary treatments may help some people to cope with the side-effects of cancer and cancer treatments (109, 110). Hyperthermic methods on cancer patients have being used since the early 20th century for attenuate the effect of conventional treatments (111).

1.5.1. Hyperthermia

Hyperthermia (HT, usually high fever-range heating) in oncology is intended to increase the local or whole-body temperature in patients. Based on the location and extension of the heating, we can define three types of hyperthermia; whole body, regional and local HT. HT modalities are intended to be complementaries besides surgery, radiation- and chemotherapy or immunotherapy. HT is mostly defined between 40°C to 48°C on the treated part what can be maintained for one or more hours. At higher temperatures such as 50°C references are given for coagulation, from 60°C to 90°C for thermal ablation, which can be applied directly in small tumors (112).

The effect of HT can be manifested on multiple sites of malignancies. Although it has direct cell-stress and killing effect on the tumor cells, the application of HT as a complementary is more important. HT can be a radiotherapy-sensitizer (113) besides it can enhance the liposomal (114, 115) and non-encapsulated (116, 117) cytostatic drug uptake.

1.5.1.1. Whole body hyperthermia

Whole-body hyperthermia (WBH) is usually used as a complementary therapy of patients with advanced metastatic malignancies, for example: melanoma, soft tissue sarcoma or ovarian cancer. It was reported to be a chemosensitizer of refractory malignant childhood tumors. It can be applied in thermal chambers, hot water blankets or infrared radiators under the maintenance of electrolyte balance. Homogenous distribution of heating can be used for 3-4 hours of 39.5-41°C WBH or in extreme WBH the patients are treated in anesthesia for 1 hour up to 42°C as a maximal temperature (112).

1.5.1.2. Regional hyperthermia

The regional hyperthermia is intended to heat up large parts of the body which involves malignancies. Most commonly it is used for tumors situated in the major and minor pelvis, abdomen (cervical, prostate, bladder, colorectal and ovarian carcinomas) or thighs (soft tissue sarcomas). Three main types can be defined: deep-positioned tumors heated with external applicators; limbs or organs heated by thermal perfusion and continuous hyperthermic peritoneal perfusion (CHPP) (112).

External applicators can commonly be dipole antenna pairs surrounding the patient which emit radiofrequency or microwave focused on the tumor containing part of the body. Other devices integrate the targeted body part in an electric circuit and heat up with capacitive or inductive manner. Both methods operate with radiofrequency which can be controlled to generate specific absorption rate (SAR) distribution. SAR is a descriptive physical parameter for the interaction between the electric field and the material (see in chapter 1.7.1. Mechanism of modulated electro-hyperthermia) (112).

If malignancies affect distinct limbs or organs (liver, lung), they can be treated with regional perfusion. For this procedure a large artery of the limb or organ and a draining vein is bypassed in order to heat up the blood extracorporeally. This method induces less systemic side-effects than the WBH (112, 118, 119).

Continuous hyperthermic peritoneal perfusion (CHPP) is used perioperatively delivering warm washing fluid (41.0-42.5°C). It can be completed with the addition of chemotherapeutic agents to a hyperthermic intraperitoneal chemotherapy (HIPEC). These treatments are supposed to deal with disseminated tumors within the abdominal cavity, such as multifocal ovarian or colorectal metastases, carcinomatosis of unknown origin,

stomach cancer and mesothelioma. The therapeutic strategy involves the resection of the primary tumor and cytoreduction of its peritoneal metastases (112).

1.5.1.3. Local hyperthermia

Local hyperthermia is dedicated to small (up to 5–6 cm diameter) tumors located superficially or within an approachable body cavity like in the rectum or esophagus. Superficial, interstitial, intraluminal or intracavital applicators can be applied and most commonly microwaves, radio waves or ultrasound are used to deliver heat to the tumors. Local HT has less side-effects than WBH or some regional techniques, since heating of small cancerous areas can spare the normal environment. Furthermore, cooling of the surface (tempered around 37°C) on the treatment site usually applied during the electromagnetic-delivered therapies to avoid skin irritation or burnings (112).

Tumors located on the skin or right bellow can be targeted by surface-placed antennas or superficial applicators. The body cavities can be used for inserting the hyperthermia applicators to treat the prostate (urethra, rectum), rectal, vagina, cervix or esophagus cancer. In case of tumors which can be treated with brachytherapy (head and neck tumors, prostate cancer, breast cancer or brain malignancies), thin microwave antennas, radiofrequency electrodes, ultrasound transducers, heat sources or laser fibers are inserted into the tumor tissue via brachytherapy applicators. This can be applied before (up to 2 hours) or right after the brachytherapy. This HT method can be used on lesions not larger than 5 cm. It is an invasive method and the thermal conditions are needed to be controlled, thus arrays of the applicator are inserted inside the HT device or separately (112, 120).

Thermoablation with radio waves (radiofrequency ablation) is needed to be mentioned between the interstitial HT methods. The applicator is inserted within the tumor tissue and heats it up above 50°C and maintains it for 4-6 min or for more than 512 CEM43°C*. It directly causes vascular stasis, cellular coagulation and necrosis. Electric ablation is used for small tumors located in the liver, kidney, lung or bones (121).

Iron-oxide or gold nanoparticles can be injected in the tumor site and be heated up by electro-magnetic field or ultrasound, which can give an opportunity to heat tumors situated in deep body regions such as the skull (recurrent glioblastoma) or pelvis (prostate and cervical carcinoma) (122).

*CEM43°C: This metric, first proposed by Sapareto and Dewey, quantifies thermal exposure in terms of the number of min of heating at 43°C needed to obtain equivalent effects in biological tissues (123).

1.5.2. Adverse effects of hyperthermia

Adverse effects are rarely caused and usually quite slight by regional hyperthermia. These include skin burns and (skin) pain, which can be healed spontaneously. In case of therapies combined with hyperthermia, it was concluded that the toxicity of radiation is not increased, but regarding chemotherapy it might be enhanced due to increase in drug efficacy. In rare cases of combination with chemotherapy, severe subcutaneous fat or muscle necrosis was formed, which required surgery for curing. Regional hyperthermia can have variable side-effects with different heating devices and targeted organs, nevertheless whole-body hyperthermia often more invasive. Whole body hyperthermia can be accompanied by the feeling of heat, tiredness, and loss of sweat due to an elevation of the body core-temperature. Furthermore, dehydration, heat illness, cardiac disease or thrombosis and toxicity to the peripheral nervous system might be observed depending on the background of disease or physical condition. Thus, this method is contraindicated for patients with neurodegenerative diseases, like multiple sclerosis (86).

Regarding the biological effects, there are no reports which showed that hyperthermia treatments have a positive effect on tumor progression (86).

1.6. Standard therapies in combination to hyperthermia

1.6.1. Chemotherapy with hyperthermic treatments

Evidences suggest that chemotherapy combined with hyperthermic treatments would not cause additional toxic effects; furthermore, it can promote the therapeutic index of the cytotoxic agents. Hyperthermia was described as a suitable complementary besides alkylating drugs such as carboplatin and cisplatin *in vitro*, *in vivo* and on clinical trials (124-126).

Furthermore, neoadjuvant chemotherapy with anthracyclines on patients with high-risk soft tissue sarcoma had better effects if it was combined with regional hyperthermia (127, 128).

Hyperthermia induced chemosensitivity to cisplatin, cetuximab, mitomycin-C in gastrointestinal, head and neck cancer patients, in case of triple combination therapy with HT, RT and chemotherapy (129).

Interestingly, a study showed that the combination of WBH and chemotherapy can induce immunogenicity. Intracellular concentrations of interferon-gamma and/or TNF-alpha in CD8+ T-cells were elevated 24 h after the combined treatment, while it could not be observed in patients receiving chemotherapy alone. NK-cell, cytotoxic T lymphocyte (CD56), CD69+ (T-cell activation marker) expressing CD4+ T-cell numbers and the concentration of the soluble IL-2 receptor increased significantly 48 h after the combined treatment only (130).

Patients with locally advanced breast cancer who subsequently underwent a modified radical mastectomy or lumpectomy with axillary node dissection followed by radiation therapy and then eight cycles cyclophosphamide, methotrexate, 5-fluorouracil chemotherapy were involved in a phase I/II study. Paclitaxel, liposomal doxorubicin and hyperthermia (HT) were combined in the study. The thermal dose CEM 43 T90 was significantly correlated with achieving a pathological response (131, 132). Four-year overall survival (OS) was 75% (131), while a randomized trial showed 56% three-year OS rate after similar chemotherapy (133).

The first randomized phase 3 trial described the effect of etoposide, ifosfamide, and doxorubicin (EIA) chemotherapy alone or complemented with regional hyperthermia on 341 patients with localized high-risk soft-tissue sarcoma (STS). A significant difference in local progression-free survival (LPFS) at 2 years of 15% (76% after EIA+HT and 61% after EIA) was observed. The treatment response rate was significantly higher in the EIA+HT group (28.8%) than in the EIA alone group (12.7%). The OS was also higher in the combination group, but interestingly, leucopenia was also more frequent (128 of 165 vs. 106 of 167). Adverse effects of hyperthermia were pain, bolus pressure and skin burn which was mild/moderate in 40.5%, 26.4% and 17.8%, while severe 4.3%, 4.9% and 0.6% of the cases respectively. Two deaths were occurred in the combined treatment group and one in EIA-alone group (128).

1.6.2. Radiotherapy in context to hyperthermic treatments

The heat shock can be a radiosensitizer, especially if the timing of its application is close enough for the irradiation. Heat shock induces the release of heat shock transcription factor (HSF1) which is normally bound by an Hsp70-Hsp90-Hsp40 complex, and can activate the heat shock responsive elements (HSE) in the nucleus. The transcription and translation of HSE will provide the inductive chaperones which can protect the tumor-cells from the irreversible damages (134). Although if hyperthermia is applied simultaneously or close enough (less than 30 min) in time to the irradiation, (before the protein-chaperones appear) a high radiosensitization effect can be observed, which is significantly reduced over time after radiation therapy in superficial, breast, cervical and lung cancer metastasis. It can be explained by the heat-induced damage of the DNA-repair molecules. Other studies reported that 1-4 hours after RT could raise the complete response (CR) rate and 3-year OS for cervical cancer patients. Furthermore, there are examples showing that not only the concurrent combination (HT twice, RT five times per week) had beneficial effects on the CR without affecting the OS. The irregular use of HT did not have additional effect on the RT. Concluding these clinical observations the validation of molecular mechanism of hyperthermic methods would be pivotal to define the best setup for its combination with the standard therapies (129, 135).

It can be observed in some cases when local radiotherapy can cause tumor growth suppression in distant tumor sites as well. This phenomenon is not fully understood, but it thought to be caused by the awakening of specific anti-tumor immunity. Current studies reported that hyperthermia-induced immunogenic-reaction can support the therapeutic efficacy of radiotherapy through the abscopal effect. Magnet-mediated hyperthermia improved the CD4+/CD8+ T-cell ratio in sarcoma-bearing rats, what could promote an abscopal effect (other examples will be given later in chapter 1.7.2.2.1. Experimental studies) (129).

114 patients with locally advanced cervical cancer attended in a randomized study from 1990-1996. Standard radiotherapy (RT) and hyperthermia (HT) (42°C interstitially in tumors) protocols were applied individually and in combination. The median follow-up time was 43 months. CR rates were 57% after using RT alone and 83% following RT+HT (p=0.003). During the follow-up period the difference in pelvic control (PC) was maintained, the 3-years local control (LC) rates were 41% after RT and 61% following

RT + HT. The OS rates following RT and RT+HT was 27% and 51%, respectively (p=0.009). It was not observed that HT enhance the toxicity of radiation therapy (136).

This study was completed with a 12-years following-up period, where the local control remained better in the RT+HT group (37% vs. 56%; p=0.01). The overall survival rates stayed significantly better: 20% after RT and 37% following the RT+HT (p=0.03). HT had beneficial prognostic values regarding the International Federation of Gynecology and Obstetrics (FIGO) stage, and tumor diameter. Cancer Grade 3 or higher radiation-induced late toxicities were similar in both groups based on the European Organization for Research and Treatment of Cancer (137).

In this study from 1996 to 2005 involving 378 patients with locally advanced cervical cancer (International Federation of Gynecology and Obstetrics Stage IB2-IVA) standard dose of external RT was used in combination to brachytherapy or supplemented with HT once in a week. CR was observed in 77% of patients. 5 years later the LC, disease-specific survival, and incidence of late toxicity Common Terminology Criteria for Adverse Events Grade 3 or higher were 53%, 47%, and 12%, respectively. In multivariate analysis, the number of HT treatments identified as a beneficial prognostic factor for the outcome (138). This study concluded that hyperthermia in addition to standard radiotherapy of locally advanced cervical tumors should be considered for patients who can not receive chemotherapy.

1.6.3. Combination therapy with immunotherapy and hyperthermia

168 advanced or recurrent breast cancer patients were treated with hyperthermia and immunotherapy, who were either non-responders or refused standard therapy. In case of 26 patients, clinical benefit (CR, partial response and long stable disease) was observed. The rate of effective immunotherapy increased from 9.1% to 23.9% after combining with hyperthermia. It was concluded when hyperthermia and immunotherapy were used together, it improved the treatment efficacy in 20 cases who had distant metastases to solid organs (139).

Later the same group treated 74 patients with advanced or recurrent head and neck cancer, who have not given response to the standard therapy or it was refused by them. In 15 cases they observed clinical benefit (CR, partial response and more than 6 months

long-term stable disease). Hyperthermia applied alone was effective in one patient only. Dendritic cell therapy combined with hyperthermia was beneficial on 14 patients (140).

1.7. Modulated electro-hyperthermia

Modulated electro-hyperthermia is a non-invasive loco-regional hyperthermic method for selective treatment of malignant tissue (141). The clinical mEHT applicators use 13.56 MHz frequency amplitude modulated electric field, which is generated between two plan-parallel asymmetric condenser plates of the electric circuit. The lower plate is built in the bed (where the patient lies during the treatment) and the laying surface gives the contact area. The other plate (bolus) is connected to a moveable arm from upside and has a shape adapting and water-circulation cooling system. This bolus can be changed for different size in order to adapt for the tumor -affected area (142). The tumor bearing body part is embraced by the electrodes, thus it becomes part of the electric circuit by capacitive impedance coupling, allowing selective loco-regional heating (143). Some of the currently used modalities of the mEHT are shown on **Figure 4**.

Figure 4. A clinically used local mEHT modality is shown on **A**. The electromagnetic heating is generated between the surface of the bed and a mobile water-cooled shape-adapting bolus. On **B**, a pillow-like textile-covered electrode pair is used to carry out the therapy with lower electric power. The devices can be used with catheter-like applicators (**C**) for reaching cervical or prostate malignancies.

1.7.1. Mechanism of modulated electro-hyperthermia

The background of the selective heating is based on the different electric properties of tumors compared to normal tissue. The dielectric permittivity and the complex conductivity (σ and ε) are highly frequency dependent and varies between different tissues. Permittivity is a characteristic of the material and defines the amount of charge is needed to generate one unit of electric flux in a certain medium. In a biological medium with low permittivity the charge will yield more electric flux than in a medium with high permittivity. Permittivity is the ability to store electric field by the polarization of the medium. If the conductivity (frequency-dependent) in case of alternating currents is larger, the signal is absorbed more quickly by the material. The conductivity in context of the frequency in normal tissues for example the liver 0.15 S/m at 10 kHz, 0.16 S/m at 100kHz, 0.47 S/m at 10 MHz and 0.9 S/m at 100 MHz; the lung 0.11 S/m at 10 kHz, and 0.8 S/m at 100 MHz; the spleen 0.62 S/m at 100 kHz, 0.84 S/m at 10 MHz and 1.05 S/m at 100 MHz; the kidney 0.24 S/m at 100 kHz, 0.64 S/m at 10 MHz and 0.94 S/m at 100 MHz (144, 145). Malignant tumors can show a 4-fold increase in permittivity and 5 to 40-fold increase in conductivity compared to normal tissue. For example, in the range of 3 MHz-3 GHz frequency the permittivity of the normal tissue increases from 1.5 to 3 mS/cm in breast tissue, while it increases from 7.5-12 mS/cm in malignant breast tumors and the conductivity of normal tissue is 10 and it raises to 50-400 in malignant (146-149).

The elevated conductivity seems to be caused mostly by the Warburg effect of tumor cells, the metabolism is changed to aerobic glycolysis from oxidative phosphorylation, which increases the concentration of lactic acid in the extracellular matrix (ECM) (3, 150-152). Furthermore, increased cellular water could be detected in malignant tissue, metal-ion and salt content (also in the ECM) (146-149, 153).

Using the 13.56 MHz frequency can be explained with the proper penetration in the body (<25 MHz) and its safety regarding the neural excitation (10 kHz<); furthermore, its practical benefits, since this free frequency range is not required to be shielded for avoiding the interference with other electronic devices (3).

The thermal effect of the electromagnetic field is the result of dielectric heating mechanism; which heating is caused by molecular dipole rotation within the dielectric material (154). The thermal effect of this dielectric heating can be defined by the absorbed energy in the tissue with the specific absorption rate (SAR) (155).

$SAR = \sigma E^2/\rho = J^2/\sigma\rho$ (W/kg)

where: J = current density (A/m^2), σ = conductivity (S/m), ρ = density (kg/m^3) E = electric field strength (V/m). SAR is connected to temperature rise; a direct calculation of the expected temperature increase (ΔT Kelvin) in tissue exposed to RF for a time (t seconds) can be made from the equation:

$\Delta T = (SAR)\ t/C$

where C is the specific heat ($J\ kg^{-1}\ K^{-1}$) of the biological material (156).

From these equations it can be seen that the SAR and consequently the temperature can be increased by the applied power of the electric field and by conductivity. Since the conductivity of the tissue cannot be substantially changed during a treatment the SAR difference between the normal and tumor tissue can explain the selective heating (157).

1.7.2. Effects of modulated electro-hyperthermia

1.7.2.1. Non-thermal effect of modulated electro-hyperthermia

A non-thermal interaction between the electric field and the biological material was also described (155). The tumor-killing efficacy of 30 min of mEHT and conventional radiation hyperthermia with infrared light was compared using HT29 human colorectal carcinoma xenografts inoculated in BALB/C nude mice. 24 hours after the interventions tumors showed 6.1% tumor destruction ratio (TDR; calculated by the ratio of damaged to the whole area of the section) at 38°C in the control group and conventional infrared heating at 42°C induced 17.9%, while mEHT at 38°C caused 45.9% and 57.1% at 42°C (**Figure 5**) (157).

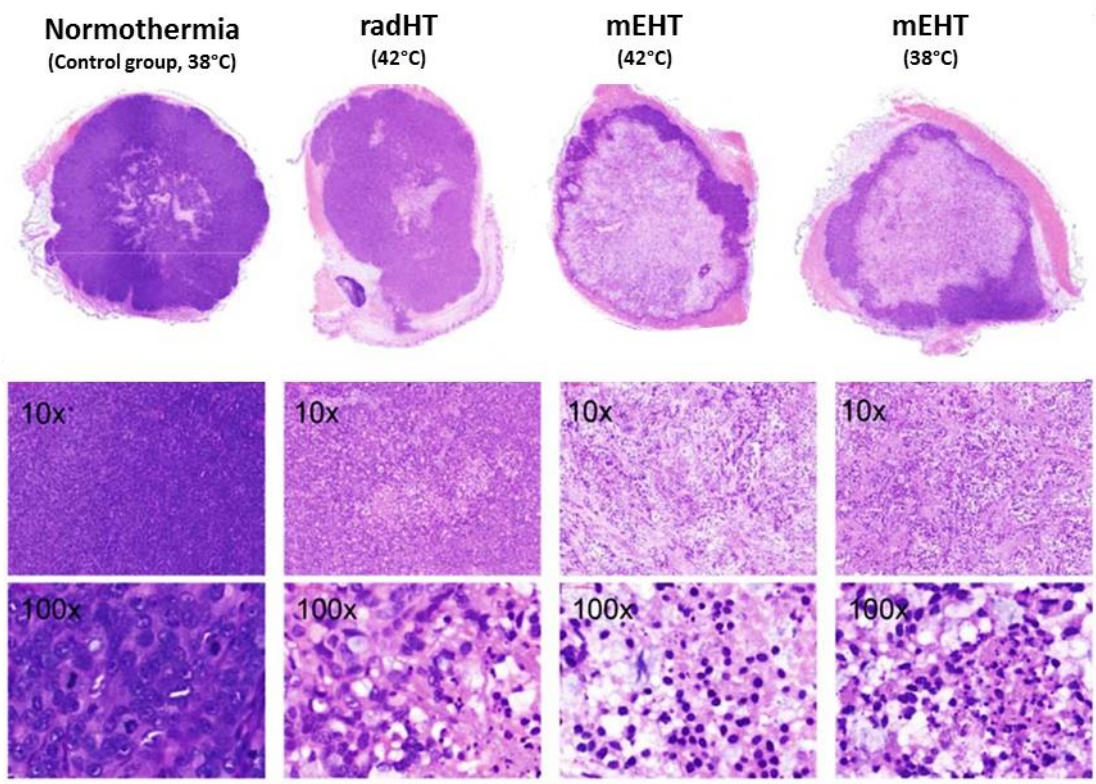

Figure 5. Differences in tumor destruction in human HT29 colorectal cancer xenografted into mice after using 38°C normothermia, 42°C infra-red radiation hyperthermia, 41°C mEHT and 38°C mEHT. Modified from the original figure of Andocs G et al. (2009) (157). Hematoxylin and eosin.

In line with these findings *in vitro* studies showed similar results. On CT26 mouse colorectal carcinoma cell cultures ten times higher annexin V+ apoptotic population (35.1%) was occurred 24 hours after 30 min of mEHT at 42°C, compared to the 42°C water bath (2.98%) which did not show significant difference compared to the 37°C control (2.76%). Furthermore, they showed that mEHT induced significantly higher not only intracellular but extracellular release of Hsp70 (which has immunogenic properties *in vivo*) compared to the same temperature water bath heating (21). In another study Yang et al. made comparison between the conventional water bath, the capacitive impedance-matched mEHT (13.56 MHz) and capacitive (8 MHz) hyperthermic methods in HepG2 human hepatocellular carcinoma cell line. mEHT induced significantly larger annexin V+ population, and apoptotosis was confirmed by subG_1 and cleaved-caspase-3, -8, -9 measurement. A higher release of such stress-proteins like Hsp70 (intra- and extracellular) and calreticulin was observed, which can promote ICD of tumor cells in *in*

vivo condition. Interestingly the expression of β-catenin and E-cadherin adhesion molecules were increased only after mEHT (1).

The electromagnetic field-related effects can be explained by the electric properties of the cell membrane. *In silico* data showed that the lipid fraction of the membranes has high impedance (resistance in AC), which is feasible to insulate the cytosol against the current. On the other hand, higher electric energy absorption was observed in lipid rafts, which leads to increased heating production compared to the lipid parts of the cell membrane (2).

1.7.2.2. Experimental and clinical results of modulated electro-hyperthermia treatment on different tumor-types

1.7.2.2.1. Experimental studies

It was found that 15 min of 43°C mEHT treatment induced the phosphorylation of the stress-dependent p38 kinase (on Thr180/Tyr182) in OVCAR-3, SK-OV-3, HeLa and SNU-17 ovarian and cervical cancer cells. Upon mEHT significant increase in the population of subG_1 with higher cleaved caspase-3 and poly-ADP ribose polymerase (PARP) levels were observed in OVCAR-3 and SNU-17 cells. mEHT reduced both the weight and the volume of human ovarian and cervical cancer cell lines and patient-derived primary cancer cell line xenografts in mice. Autophagy is frequently associated with tumor recovery after mEHT treatment, consequently mEHT and 3-methyladenine (autophagy inhibitor) were applied in combination, which inhibited the tumor growth more effectively than the individual treatments (158).

U87-MG and A172 human glioma cell lines were used and exposed to 60 min of 42°C mEHT three times with 2-days intervals. mEHT inhibited the growth of glioma cultures through the increase of p53 and the decrease of PARP1 (essential for recovery from DNA damage; often overexpressed in cancer). Furthermore, the pro-apoptotic E2F1 and CPSF2 gene expressions were elevated, while the suppression of the positive growth regulators PSAT1, ADAR was observed. mEHT significantly suppressed the growth of human U87-MG glioma xenografts in nude mice. mEHT reduced the amount of CD133+ glioma stem cell population and suppressed cancer cell migration and sphere formation (159).

In our earlier study, HT29 colorectal cancer was inoculated into both femoral sites of BALB/c (nu/nu) immunocompromised mice and the right-side tumors were treated once

using 30 min of mEHT. mEHT induced significant increase in the tumor destruction ration (TDR, damaged area per whole tumor area), where the highest difference was 7 fold compared to the untreated controls. Significant mitochondrial accumulation of Bax and cytosolic release of cyt-c (at 8 and 14 h) was observed, while there were no relevant changes in the level of cleaved caspase-3. Detection of significantly higher DNA fragmentation 24 and 72 h post-treatment were suggestive for intrinsic apoptotosis. We assumed that the nuclear relocalization of AIF (14-24th h) was the effector of programmed cell death induced by mEHT (16). In this model we also observed that the apoptosis was accompanied by the early upregulation (4 h after treatment) of heat shock protein (Hsp70 and Hsp90) mRNA levels. The *in situ* occurrence of DAMP including calreticulin (at 4 h), Hsp70 (14-24 h) and Hsp90 (24-216-h) were significantly higher. Furthermore, the clearance from cell nuclei of HMGB1 from 24-h post-treatment and its disappearance from tumor cells by 48 h was also detected. In spite of the immunodeprived model, the mEHT-related DAMP release was suggestive for the promotion of immunological cell death response in colorectal cancer xenografts (20).

Qin et al. used either intratumoral DC injection, mEHT or combined therapy to treat C3H/He mice inoculated with squamous cell carcinoma SCCVII cells subcutaneously in the left leg, and in the chest to assess the systemic anti-tumor effect. mEHT was only applied locally on the left leg for 30 min, with the protocol for 10 min preheating and 20 min keeping the temperature at 42°C in the tumor core. Higher mean of tumor volume was observed in the control group, than in case of DC injection alone. mEHT and the DC+mEHT therapy caused the greatest suppression in tumor growth; furthermore, this tendency was also significant in the distant untreated tumor of the chest. Significantly higher number of CD3+ and CD8+ cells were detected in the draining lymph node of DC+mEHT treatment group. CD8 and S100 markers were expressed stronger in the DC+mEHT treatment group in the untreated tumor-site, while the Foxp3 expression was higher in the controls. GP96 is an ER analogue of the Hsp90, which has DAMP function as well. The gene expression level of GP96 in the untreated tumors of the chest in the mEHT group was significantly higher than the control. It was concluded that a distant anti-tumor (abscopal) effect may be induced by mEHT, and the effect of immunotherapy with DCs was enhanced by the overexpression of GP96. These results indicated that the

combination therapy of an intratumoral DC injection and mEHT evoked systemic anti-tumor activity in a distant non-treated tumor site (**Figure 6**) (160).

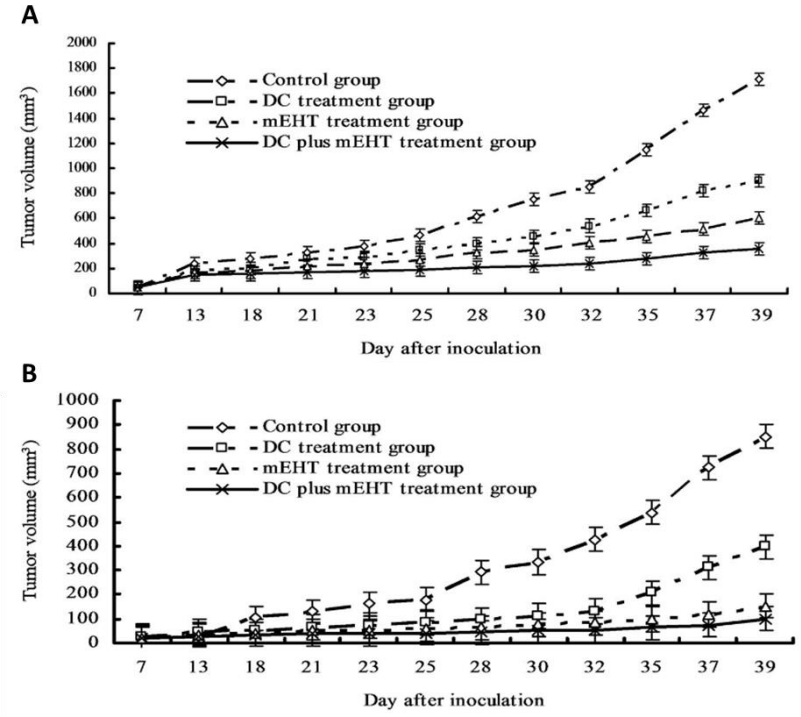

Figure 6. The growth of the locally treated tumor was suppressed by each therapy, however the mEHT+DC injection was the most effective (**A**). Interestingly the same tendency was observed in the tumors which was implanted in the chest and was not treated locally (**B**) (Qin W et al. 2014) (160).

In another study it was found that mEHT can induce significantly higher intra- and extracellular release of Hsp70 than a conventional water bath heating at the same temperature in CT26 mouse colorectal carcinoma cell line *in vitro*. So, they used Hsp70 beside to CT26-derived epitope (AH1) what was presented by H-2Dd -a major mouse histocompatibility antigen- for stimulating DC maturation. CT26 murine colorectal cancer allografts were treated either with mEHT for 30 min at 42°C, or gave matured synergetic DCs intratumorally 24 h following mEHT or used a combined treatment of these. mEHT+DC treatment significantly inhibited CT26 tumor growth compared to DCs or mEHT alone. They saw a secondary tumor protection effect in case of mEHT+DC treatment upon rechallenging by injecting tumor cells again. Immunohistochemical staining of CD45 and F4/80 revealed that mEHT-DC treatment increased the number of lymphocytes and macrophages. Most interestingly, mEHT also induced infiltrations of eosinophil granulocytes, which can be a positive signal for specific T-cell response. A

tumor-specific cytotoxic T-cell activity was revealed by T-cell- and ELISpot assay. This study showed that mEHT induces tumor cell apoptosis and increase the release of Hsp70, but conventional hyperthermia does not. mEHT can create a desirable tumor microenvironment for an immunological response, which improves the efficacy of intratumoral DC therapy (**Figure 7**) (21).

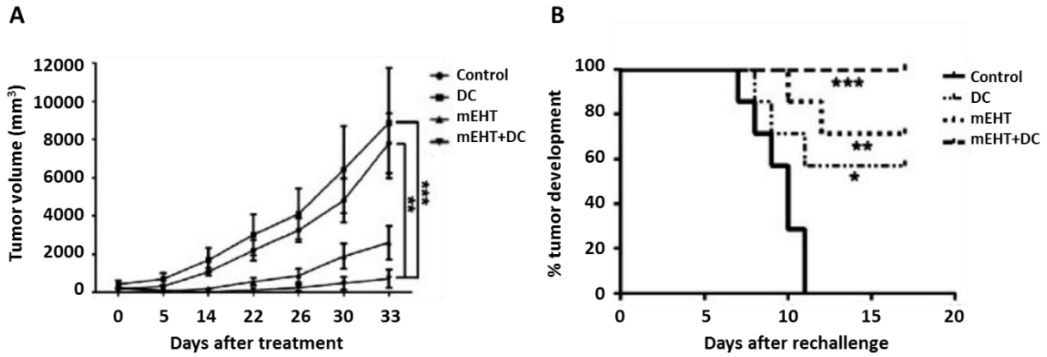

Figure 7. MEHT only and mEHT+DC caused significant decrease in the CT26 tumor growth (**a**). 30 days after the first intervention a secondary rechallange was done by injected CT26 on the contralateral leg of the mice. The Kaplan-Meier plot indicates the percentage of tumor development (**b**) (Tsang YW et al. 2015) (21).

1.7.2.2.2. Clinical studies

In a clinical study the pelvic area of 20 patients with cervical carcinoma was heated for 60 min with mEHT. The peri-tumoral temperature was measured with an internal temperature probe placed into the cervix over the tumor area. The tumor blood flow was measured by 3D color Doppler ultrasound. The mean peri-tumoral temperature raised from 36.7 ± 0.2 °C to 38.5 ± 0.8 °C during the treatment. The decline in the peak systolic velocity/end-diastolic velocity ratio (S/D ratio) and the resistance index (RI) values within blood vessels were suggestive for increased tumor blood perfusion. These results support the theory of the clinical observations that hyperthermia improves the response of cervical cancer to radiotherapy or chemotherapy (5).

A cohort of 54 patients with recurrent glioblastoma (GBM) treated with dose-dense temozolomide and mEHT (ddTMZ+mEHT) between 2000 and 2005 was systematically retrospectively compared with five pooled ddTMZ 21/28 days cohorts (114 patients) from 2008 to 2013. Effect-to-treatment analysis (ETA) suggests that mEHT significantly enhances the efficacy of the ddTMZ 21/28 days regimen (p=0.011), with significantly

less toxicity (no grade III-IV toxicity vs. 45%-92%, $p<0.0001$). Based on this study, mEHT could be a cost-effective enhancer of ddTMZ regimens in recurrent GBM (6).

A randomized, controlled, single-center, open-label clinical trial (phase II) with two parallel groups (allocation ratio, 1:1) was carried out for investigating the efficacy and safety of mEHT combined with the traditional Chinese medicine (TCM) “Shi Pi” herbal decoction (study group; SG), compared with standard intraperitoneal chemo-infusion (IPCI, control group; CG) on patients with peritoneal carcinomatosis with malignant ascites (PCMA). A total of 260 patients with PCMA were randomly allocated into the two groups (130/130); 60 min of mEHT was applied per session every second day for 4 weeks, in a total of 14 sessions. TCM decoction was administered orally on every day. In CG, occlusive IPCI with cisplatin and 5-fluorouracil was applied twice, biweekly. The objective response rate in SG was 77.69% vs. 63.85% in CG ($p<0.05$). The quality of life in SG was 49.23% vs. 32.3% in CG ($p<0.05$). The adverse event rate in SG was 2.3% vs. 12.3% in CG ($P<0.05$). It was concluded that mEHT with TCM was non-toxic, well-tolerable and had better control on PCMA than the conventional IPCI, thus the combination offered a better benefit-harm balance (161).

DOI:10.14753/SE.2020.2337

2. Aims of the thesis

The studies summarized in the thesis aimed at investigating the molecular background and the dynamics of mEHT induced cancer damage in C26 colorectal adenocarcinoma cell line models by focusing on:

- The heat and cell stress responses induced by single, or repeated mEHT treatment *in vitro*.
- The cell death pathways activated by mEHT treatment *in vitro.*
- The tumor damage mechanisms induced by doxorubicin monotherapy and combined with mEHT treatment *in vitro*.
- The heat, cell stress and programmed cell death pathways induced by mEHT treatment in C26 tumors allografted into immunocompetent BALB/c mice. The compatibility of the *in vitro* and *in vivo* model systems.
- The spatio-temporal expression and release of DAMP signaling molecules in the loco-regionally mEHT treated tumors.
- The spatio-temporal occurrence of immune cells in and around the treated tumors in relation to tumor damage.
- The potential systemic anti-tumor effect of mEHT treatment.

3. Materials and methods

3.1. *In vitro* experiments

3.1.1. Cell culturing

C26 murine colorectal adenocarcinoma cell line (CLS Cell Lines Service GmbH, Eppelheim, Germany, #400156) was grown in RPMI 1640 with 300 mg/l L-glutamine content (#LM-R1640, Biosera, Boussens, France) including 10% heat inactivated fetal calf serum (#FB-1090/500, Biosera) and 80 mg gentamicin (Sandoz GmbH, Basel, Switzerland). Cells were released from sub-confluent monolayers using 0.25% trypsin and 0.22 mg/ml ethylenediaminetetraacetic acid (EDTA) for 5 min, suspended in fresh medium and $4x10^5$ cells were grown using 4 ml medium in 60 mm Petri dishes, containing a 24x40 mm coverslip each.

3.1.2. *In vitro* doxorubicin and modulated electro-hyperthermia treatments

After 48 h growth, coverslip cultures were mEHT treated 2x30 min (with 5 min preheating) at 42°C between two plan-parallel electric condenser plates by using the Lab-EHY 100 device (Oncotherm Kft, Budaors, Hungary) with a 120 min break in between treatments (**Figure 8**). After the second treatment coverslip-cultures were transferred into fresh culture medium. At this point for the combined treatment the medium contained 1 μM Dox. For identifying the optimal Dox concentration $2x10^4$ cells/well were treated using 0, 0.01, 0.1, 1, or 10 μM Dox in 96 well plates. 24 hours post-treatment resazurin viability assay was performed expecting, based on preliminary experiments, that 1 μM drug concentration can lead to sufficient tumor death, which was used either for Dox monotherapy or in combination with mEHT treatment. Each group included 3-5 independent experiments.

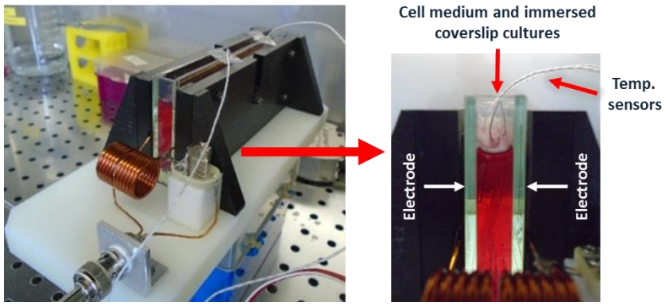

Figure 8. The *in vitro* applicator includes two plan-parallel copper condenser plates as the electrodes. Between the electrodes a medium containing chamber stands where the coverslip cultures and the thermo-sensors are placed.

3.1.3. Gene expression analysis using qRT-PCR

The expression of mEHT-induced apoptosis and cell cycle control related genes were tested. mRNA was extracted 1, 3, 9 and 24 h after mEHT treatment using RNeasy Mini Kit (#74104, Qiagen, Venlo, Netherlands). cDNA synthesis from RNA template was done with RevertAid First Standard cDNA Synthesis Kit (#K1622, Thermo Scientific, Waltham MA, USA). Quantitative PCR testing of RpLp0 (housekeeping gene), PUMA, BAX, BAK1, XIAP, BCL-2, BCL-XL, and P21 target gene expression (**table 2**; all primer pairs were purchased from Sigma-Aldrich, St Luis, USA was performed with CFX Connect TM Real-Time PCR Detection System (Bio Rad, California, USA) using the SsoAdvanced™ Universal SYBR Green Supermix (#1725271, Thermo Scientific) according to the vendors instructions. The fold change of the genes of interest relative to RpLp0 was defined as $2^{-\Delta\Delta CT}$ method.

Table 2. Primer sequences used for measuring pro- and anti-apoptotic mRNA levels.

Gene	Forward primer (5'-3')	Reverse primer (5'-3')
BAK-1	CAGCTTGCTCTCATCGGAGAT	GGTGAAGAGTTCGTAGGCATTC
BAX	AAGCTGAGCGAGTGTCTCCGGCG	GCCACAAAGATGGTCACTGTCTGCC
BCL-2	CTCGTCGCTACCGTCGTGACTTCG	CAGATGCCGGTTCAGGTACTCAGTC
BCL-XL	AACATCCCAGCTTCACATAACCCC	GCGACCCCAGTTTACTCCATCC
P21	GCAGAATAAAAGGTGCCACAGG	AAAGTTCCACCGTTCTCGGG
PUMA	TCTATGGGTGGAGCCTCAGT	GAGGGCTGAGGACCCATTAAA
RPLP0	CTCTCGCTTTCTGGAGGGTG	ACGCGCTTGTACCCATTGAT
XIAP	ATGCTTTAGGTGAAGGCGAT	CATGCTGTTCCCAAGGGTCT

3.1.4. Cell counting, viability and doxorubicin uptake measurements

For measuring Dox uptake cultured samples were collected in Fluoroskan Ascent™ Microplate Fluorometer (Thermo Scientific) using 530/590 or 570/590 nm (excitation/emission) filter pairs. Cell viability assay was done using a homemade stock solution of 0.3 mg/ml resazurin (#R7017-5G, Sigma-Aldrich) dissolved in sterile-filtered PBS, which was used in 0.03 mg/ml both in treated and control cell culture medium and in plain medium for calculating background intensity. Fluorescent intensity was measured

after 1 h resazurin incubation using the 570/590 nm (excitation/emission) filter pair, since this provided better separation for Dox fluorescence intensity measurements.

3.1.5. Measurement of apoptosis-necrosis ratio

Apoptotic cell fractions were identified using flow cytometry (BD FACSCalibur®, BD Bioscience, San Jose, USA). The supernatant was collected and cells were trypsinized 24 h after treatment, all further steps were done at 0-4°C to avoid Dox diffusion out of cells. Samples were washed in 2 ml PBS for 3 times by centrifuging for 5 min each time at 500 G. A mixture of 1 µl FITC-Annexin V stock solution (#640906, Biolegend, San Diego, CA, USA) and 1 µl of 1mg/ml propidium-iodide (PI, # P4170, Sigma-Aldrich) was added to 10^5 cells in 100 µl PBS. Samples were incubated for 15 min in dark , then supplemented with 400 µl Annexin V Binding Buffer (#422201, Biolegend). Argon Ion laser at 488 nm excitation wavelength was used for both fluorochromes. FITC-Annexin V was measured on FL1 (filter: 530/30 nm), while PI on FL2 channel (filter: 585/42 nm) by counting $2x10^4$ events per sample using flow cytometry (BD FACSCalibur™, BD Bioscience, San Jose, USA). Data analysis was done with FlowJo v10 software (FlowJo LLC, Ashland, Oregon, USA).

3.1.6. Cell cycle analysis and counting of subG$_1$ fraction

For confirming the termination of apoptosis subG$_1$-phase cell fractions were tested using flow cytometry. 10^5 tumor cells were fixed in 1 ml 70% ethanol at room temperature for 20 min then they were kept for at least 30 min at -20°C, washed and resuspended in 250 µl PBS and incubated for 15 min with 20 µg/ml RNase (#R6513, Sigma-Aldrich). Finally, PI stain was applied for 15 min and the fluorescence intensity of $2x10^4$ events was measured in the FL2 channel. BD CellQuest™ Pro software (BD Bioscience) was used for data analysis.

3.1.7. Polarized membrane staining

Mitochondrial membrane integrity was tested using 3,3′-Dihexyloxacarbocyanine iodide (DiOC6, # 318426, Sigma-Aldrich) flow cytometry (22). 10^5 tumor cells were rinsed in PBS and treated with 10 nM/ml DiOC6 solution made from 1 mM stock solution for 15 min, which was prepared with absolute ethanol, and $2x10^4$ events were measured

in the FL1 channel. BD CellQuest™ Pro software (BD Bioscience) was used for data analysis.

3.1.8. Immunohistochemistry, hematoxylin-eosin staining and image analysis

Cell cultures were fixed in 4% paraformaldehyde/PBS solution for 10 min at 4°C then washed three times in TBS. For permeabilization 0.05 M tris-buffered saline (TBS) pH 7.4 containing 0.3% Tween-20 (#P9416, Sigma-Aldrich; 0.3% TBST) was used for 20 min and after washing in 0.1% TBST the samples were used either for hematoxylin-eosin (H&E) staining or for immunocytochemistry. Later, non-specific binding sites were blocked for 20 min using TBST containing 3% BSA (#82-100-6, Merck, Darmstadt, Germany). Antibodies produced in rabbit host for calreticulin (1:200, clone: D3E6, #12238), cleaved caspase-3 (1:100, clone: 5A1E, #9664), Hsp70 (1:50, #4872, polyclonal) and phosphor-H2AXγ^{Ser139} (1:150, clone: 20E3, #9718) (all from Cell Signaling, Danvers, MA, USA); and goat polyclonal antibody for p53 (1:350, #AF1355, Bio-Techne Minneapolis, MN, USA) diluted in 1% BSA/TBST were used for overnight incubations at room temperature. For immunofluorescence Alexa Fluor 546 (orange-red) coupled anti-rabbit Ig (1:200) was used for 90 min, and cell nuclei were stained with 4', 6-diamidino-2-phenylindole (DAPI, blue) (both from Invitrogen/Molecular Probes, Carlsbad, CA, USA). EnVision polymer-peroxidase conjugated anti-rabbit Ig (Dako, Glostrup, Denmark) was used for immunoperoxidase reactions for 40 min followed by DAB chromogen/hydrogen peroxide kit (Leica-NovoCastra, Newcastle Up-on-Tyne, UK). Cell nuclei were counterstained with hematoxylin and the stained coverslip cultures were mounted onto glass slides were digitalized and evaluated using the QuantCenter image analysis software package (3DHISTECH, Budapest, Hungary). The ratio of marker positive cells at different intensity ranges were calculated using the CellQuant module.

3.1.9. Immunostaining for flow cytometry

24 h after mEHT treatment supernatants were collected, coverslip cultures were trypsinized and washed in 2 ml PBS by centrifugation at 500 g 3x5 min. Cells were counted in Bürker-chamber. Next, fixation in 4% paraformaldehyde/PBS for 30 min at 4°C and washing 3 times in PBS was followed by permeabilization in 0.2% Tween-20/PBS for 20 min. After repeated centrifugations, the supernatants were discarded and

10^5 cells were immunolabelled for 30 min at 4ºC by using Alexa Fluor® 488 conjugated rabbit monoclonal phosphor-Akt^{Ser473} (1:100, clone: D9E, #4060) and cleaved caspase-8^{Asp387} (1:800, clone: D5B2, #8592) (both from Cell Signaling) and mouse monoclonal phosphop53^{Ser15} (1:50, clone:16G8, #9235) antibodies diluted in 1% BSA/PBS. For detecting unlabeled rabbit antibodies an Alexa Fluor 488 conjugated anti-rabbit Ig (1:200) (Invitrogen/Molecular Probes) was used for 30 min. All samples and negative controls were washed in PBS by 3-times centrifugation and measured in the FL1 channel. Data analysis was done with FlowJo v10 software (FlowJo LLC).

3.1.10. Clonogenic assay

24 h after treatment, cells were trypsinized and 500 cells/well were cultured in 6-well plates using 3 experimental parallels. 10 days after plating the cell medium was discarded and the wells were washed 3 times in PBS then fixed in 4% buffered formaldehyde for 30 min. After washing again in distilled water samples were dried out, stained with 0.1% crystal violet for 20 min, washed again and cell colonies were counted manually.

3.2. *In vivo* experiments

3.2.1. Tumor model

C26 murine colorectal adenocarcinoma cell line was maintained regarding the description in chapter 3.1.1. Cell culturing. After the cultures were trypsinized from sub-confluent monolayers, they were suspended in a serum free medium and reached the required 10^7 cell/ml concentration. All reagents were purchased from GIBCO (Invitrogen, Carlsbad, CA).

BALB/c mice (females) were maintained in sterile environment, kept on sterilized food and water *ad libitum* under 12 h dark/12 h light cycles. The C26 cell line was subcutaneously injected with 1 million cells/100 µl into both femoral regions of 6-week-old BALB/c mice, which were kept for 14 days until the diameter of symmetrical tumor implants reached ~1.5 cm diameter.

Laboratory animals were kept and treated in compliance with the Hungarian Laws No. XXVIII/1998 and LXVII/2002 on the protection and welfare of animals, and the animal welfare regulations of the European Union. The study was approved by the Governmental

Ethical Committee under No. SzIE ÁOTK MÁB 233/2012 and No. SzIE ÁOTK MÁB 26/2013.

3.2.2. *In vivo* modulated electro-hyperthermia and Marsdenia tenacissima extract (MTE) treatment

Right leg tumors were treated with mEHT ($mEHT_{right}$) of the symmetrical C26 implants using plan-parallel electric condenser plates embracing the tumors (**Figure 9A**). The left-leg tumors served both for untreated internal controls ($mEHT_{left}$) and for monitoring the potential systemic effect of the treatment options tested. A rectangular grounded (lower) aluminum electrode of 72.0 cm^2 (kept at 37 °C) was below the animals and a 2.5 cm^2 round copper-silver-tin coated flexible textile electrode was overlaid on the tumors, which were cooled under control using a wet pad. Electromagnetic heating was generated by capacitive coupled, amplitude modulated 13.56 MHz radiofrequency (LabEHY, Oncotherm kft., Budaors, Hungary). Animals were treated with a single shot of mEHT for 30 min using 1-3W average power during 100 mg/kg ketamine and 10 mg/kg xylazine anesthesia. Intratumoral temperature was measured with optical sensors (Luxtron FOT Lab Kit, LumaSense Technologies, Inc. CA) and kept at ~42°C (+/- 0.5°C) (**Figure 9B**). The subcutaneous temperature under the electrode was kept at ~40 °C and the rectal temperature at ~37°C.

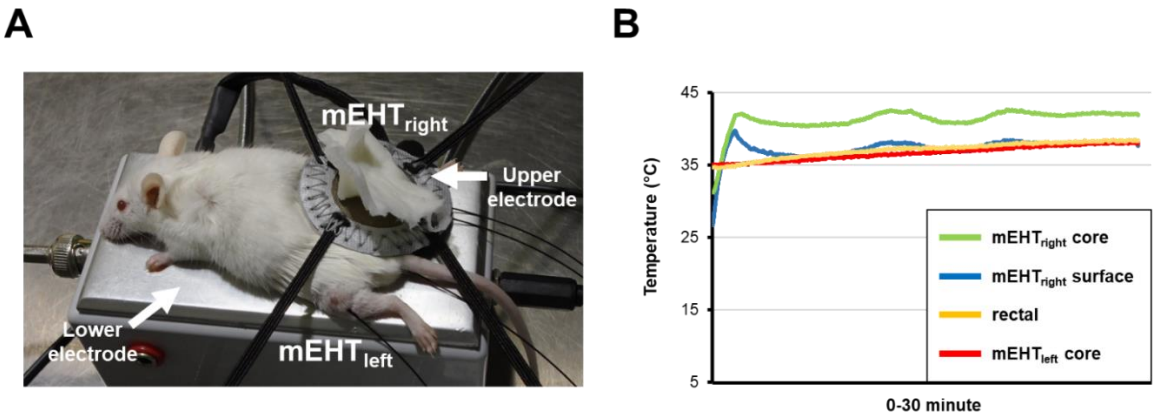

Figure 9. Experimental model of mEHT treatment (**A**). Temperature curves during treatment (**B**).

The chlorogenic acid rich Marsdenia tenacissima plant extracts (MTEs) (162), have been shown to increase chemosensitivity (163-166) of tumors and promote T-cell activation (167). The extract was obtained as a warm water decoctum, then precipitated

in 96% ethanol (MTE, Xiao-Ai-Ping, Sanhome Pharmaceutical Co., Nanjing, China). Mice were injected with 7.5 ml/kg extract intraperitoneally (i.p.). In the combined treatment group, MTE administration was followed 30 min later by mEHT treatment of the right-leg tumors (mEHT+MTE_{right}), as described above. In sham treated animals the experimental conditions were the same as in mEHT groups except that the electric circuit was turned off. Tumor samples were collected from at least 3 animals from each group at each time point (12, 24, 48 and 72 h) after treatment following the termination of mice by cervical dislocation. Excised tumors were fixed in 10% formalin, dehydrated and embedded into paraffin wax.

3.2.3. Measuring modulated electro-hyperthermia related tumor destruction

4 µm thick serial cross sections from whole tumor blocks were used both for H&E and immunostaining. H&E stained slides were digitalized using Pannoramic Scan and analyzed with the HistoQuant module of Pannoramic Viewer software (all from 3DHISTECH, Budapest, Hungary) based on image color and intensity segmentation. The whole tumor area (W) was correlated with the damaged (paler) tumor tissue (D) for calculating the tumor destruction ratio (TDR=W/D) (**Figure 10A**).

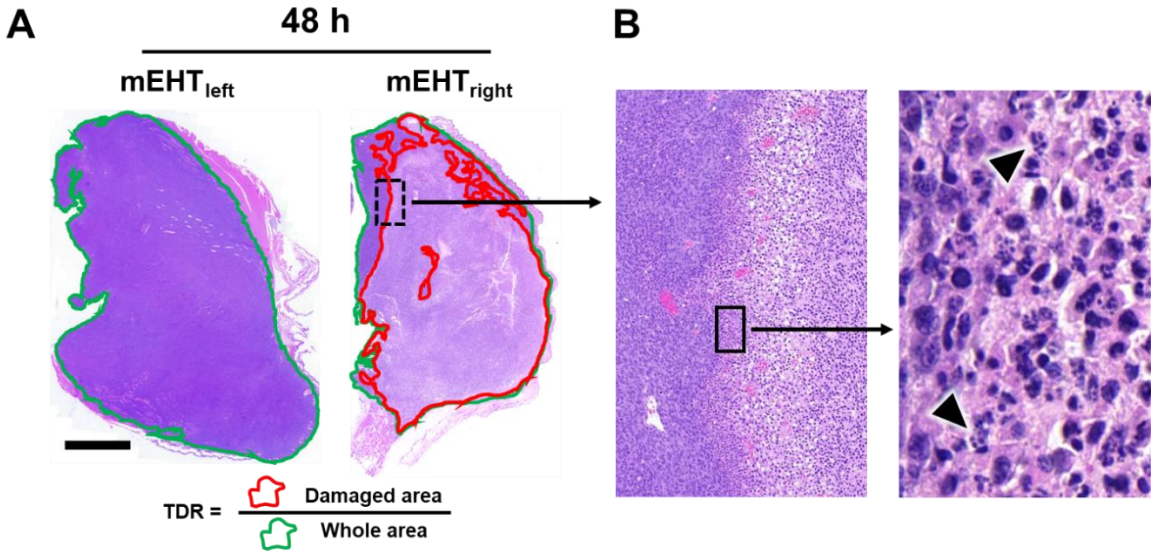

Figure 10. TDR was calculated from the ratio of the damaged to whole tumor area in H&E stained sections. Significantly increased TDR was observed after mEHT treatment of C26 colorectal cancer allografts (**A**). Chromatin condensation and apoptotic bodies (arrowheads) are regular signs of apoptosis (**B**). Scale bar shows 2 mm on A, 100 µm (left) and equal to 10 µm (right) on B.

3.2.4. Immunohistochemistry and TUNEL assay

Both whole cross sections and tissue microarrays (TMA) were used for immunohistochemistry. Three representative cores of 2 mm diameter were taken from standard areas of each tumor samples and were collected into TMA blocks. Two cores from the border between degraded and intact tumor regions and one from the degraded tumor center based on H&E stained slides using the computer-driven TMA Master (3DHISTECH). For antigen retrieval dewaxed, rehydrated and endogenous peroxidase-blocked (20 min in 1:60; H_2O_2:methanol) slides were heated at ~100^{o}C for 40 min using microwave oven (Whirlpool, Benton Harbor, MI) either in citrate buffer pH 6.0 (0.01 M sodium citrate-citric acid) or in Tris-EDTA (TE) buffer pH 9.0 (0.1 M Tris base and 0.01 M EDTA) followed by blocking in 0.1 M Tris-buffered saline (TBS, pH 7.4) containing 5% bovine serum albumin (BSA) and 0.1 % sodium-azide (all from Sigma-Aldrich, St Luis, MO) for 20 min. Then, sections were incubated in a humidity chamber at room temperature overnight (16 h) using the antibodies and conditions listed in **table 3**. For immunofluorescence Alexa Fluor 546 (orange-red) coupled anti-rabbit Ig (1:200) was used for 90 min. Cell membranes were highlighted with a wheat germ agglutinin (WGA) Alexa Fluor 488 conjugate (1:200) and cell nuclei were stained with DAPI. All fluorescence probes were from Invitrogen/Molecular Probes (Carlsbad, CA, USA). For immunoperoxidase staining, the labelled polymer-peroxidase anti-rabbit Ig detection system (Dako, Glostrup, Denmark) was applied for 30 min and the reactions were developed using DAB/hydrogen peroxide kit (Leica-NovoCastra, Newcastle Up-on-Tyne, UK). Between incubation steps the slides were washed 3x3 min in TBS (pH 7.4) buffer. Stained slides were digitalized, and the immunofluorescence reactions were evaluated using image (color, intensity and size) segmentation based software tools HistoQuant and CellQuant (3DHISTECH). Relative mask areas (rMA) representing positive immunoreactions were calculated from the ratio of stained and whole annotation area for cleaved-caspase-3, HMGB1, CD3 and S100 staining. For calreticulin and Hsp70 staining the number of biomarker positive cells was counted in 5 representative microscopic fields (FOV) at 40X objective magnification on each sample at each time point and experimental group. The number of cytoplasmic cytochrome-c positive and nuclear FoxP3 positive cells was counted in 3 FOV and 5 FOV/sample at 50X objective magnification, respectively.

Table 3. Antibodies and conditions used for immunohistochemistry and immunofluorescence. Vendor specification: Cell Signaling (Danvers, MA, USA); Thermo (Waltham, MA, USA); Dako (Glostrup, Denmark); eBioscience (San Diego, CA, USA); Sigma-Aldrich (St. Louis, MO, USA); T-E: Tris-EDTA, pH 9.0.

Antigen	Type	Reference no.	Dilution	Antigen retrieval	Vendor
AIF	Rabbit, pAb	#4642	1:25	T-E	Cell Signaling
Bax	Rabbit, pAb	#HPA027878	1:50	T-E	Sigma
Calreticulin	Rabbit, pAb	#12238	1:200	T-E	Cell Signaling
CD3	Rabbit, pAb	#IS503	1:2	T-E	Dako
Cleaved caspase-3	Rabbit, pAb	#9664	1:100	Citrate	Cell Signaling
Cleaved caspase-8	Rabbit, pAb	#8592	1:100	T-E	Cell Signaling
Cytochrome-c	Rabbit, pAb	#4280	1:50	T-E	Cell Signaling
FoxP3	Rat, pAb	#14-5773	1:600	T-E	eBioscience
HMGB1	Rabbit, pAb	#6893	1:200	Citrate	Cell Signaling
Hsp70	Rabbit, pAb	#4872	1:200	T-E	Cell Signaling
S100	Rabbit, pAb	#RB-9018	1:500	T-E	Thermo

Terminal deoxynucleotidyl transferase nick end labeling (TUNEL, Alexa Fluor 488 Assay, Invitrogen) assay was used according to manufacturer's instructions. This assay is based on the detection and linking of DNA nick ends by terminal deoxynucleotidyl transferase (TdT) with fluorochrome labeled deoxyuridine triphosphate (dUTP) nucleotides. Labeling of cell nuclei is proportional with the amount of fragmented DNA as a result of programmed cell death. Briefly, dewaxed and rehydrated slides were heated in a citrate-based (pH 6.0) antigen unmasking solution (H-3300, Vector Lab, Burlingame, CA) for 45 min using microwave oven (Whirlpool). Then slides were incubated at 37°C for 60 min with a cocktail of alkyne substituted dUTP and TdT followed by the fluorochrome for 30 min at room temperature which coupled to dUTP under copper (I) catalysis. Slides were digitalized using Pannoramic Scan after nuclear DNA was stained with DAPI. The TUNEL positive cells were counted at 100X objective magnification in 5 FOV in each sample.

3.3. Statistics

Statistical analysis for parametric variables was done with the independent two-sample t-test using Microsoft Excel Analysis ToolPak Add-In software. For non-parametric variables the Kuskal-Wallis test with the Mann-Whitney U-test for pairwise comparisons, were applied (SPSS15.0, Chicago, IL). Statistical significance was declared at p-values

of *p<0.05, **p<0.01 and ***p<0.001. Each *in vitro* result was calculated at least from 3 experimental and 3 biological parallels.

For the *in vivo* experiments the SPSS v.20 package was used for statistics (IBM, New York, NY). The non-parametric Kruskal-Wallis test was used, followed by Dunn's post hoc test with Bonferroni correction to see pairwise statistical significance between groups. Significance was declared at p<0.05 or less after correction.

4. Results

4.1. *In vitro* experiments

4.1.1. Modulated electro-hyperthermia monotherapy induced cell stress and alterations in programmed cell death

Similarly to our earlier *in vivo* studies (16, 20), cell- and heat-stress as well as apoptosis related markers showed major increase at protein level accompanied by programmed cell death response in subconfluent C26 colorectal adenocarcinoma cultures 24 h after 2x30 min mEHT monotherapy (at 42°C). Significant upregulation and relocalization of calreticulin from the endoplasmic reticulum to the cytoplasm and cell membranes was observed in treated cultures (40.02±2.05) compared to the untreated controls (21.70±0.69) (**Figure 11A**). Calreticulin positive cell membrane blebbing regions suggested the release of this antigen embraced within small extracellular vesicles.

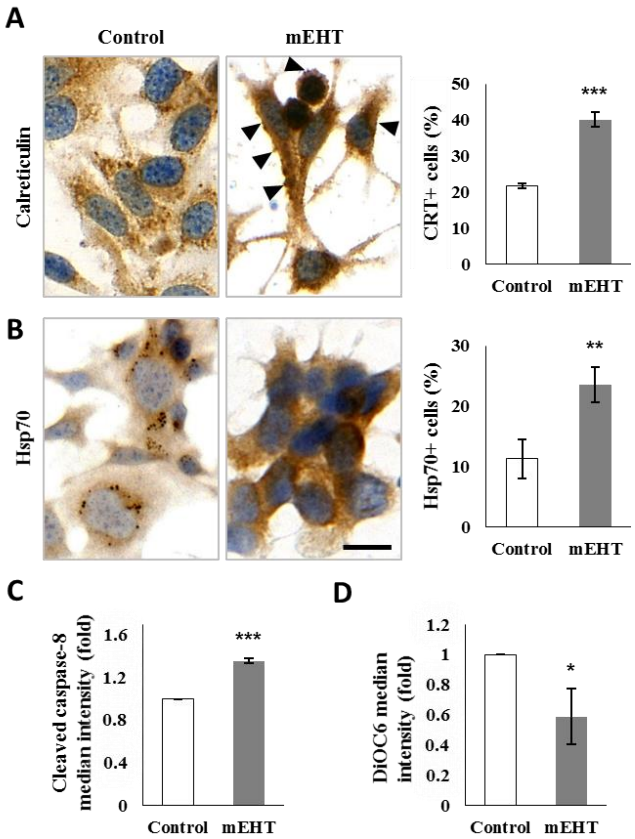

Figure 11. Signs of significant cell stress in C26 tumor cells 24 hours after mEHT treatment. Cytosolic release and cell membrane translocation of calreticulin with positive membrane blebs (arrowheads) (**A**). Elevated cytoplasmic Hsp70 reaction released from paranuclear vesicles (**B**). Scale bar: 20 μm. Significant increase of cleaved caspase-8 levels (C) and reduction of DiOC6 uptake by mitochondrial membranes (D) measured by flow cytometry indicate the induction of both the intrinsic and the extrinsic programmed cell death pathways, respectively. *p<0.05; **p<0.01; ***p<0.001.

Likewise, the proportion of tumor cells showing elevated Hsp70 levels with diffuse pattern (instead of concentrating in the endoplasmic reticulum-Golgi region) increased from 11.26±3.18 to 23.52±2.92 as a result of mEHT treatment (**Figure 11B**). Furthermore, the median intensity of the cleaved caspase-8 labelled cell fraction suggesting the activation of the extrinsic apoptotic pathway was also increased to 1.36±0.02 fold (**Figure 11C**), while the polarized membrane-staining of DiOC6 indicating intact mitochondrial membranes, was significantly reduced after mEHT (58.87±18.36%) compared to control cultures (**Figure 11D**).

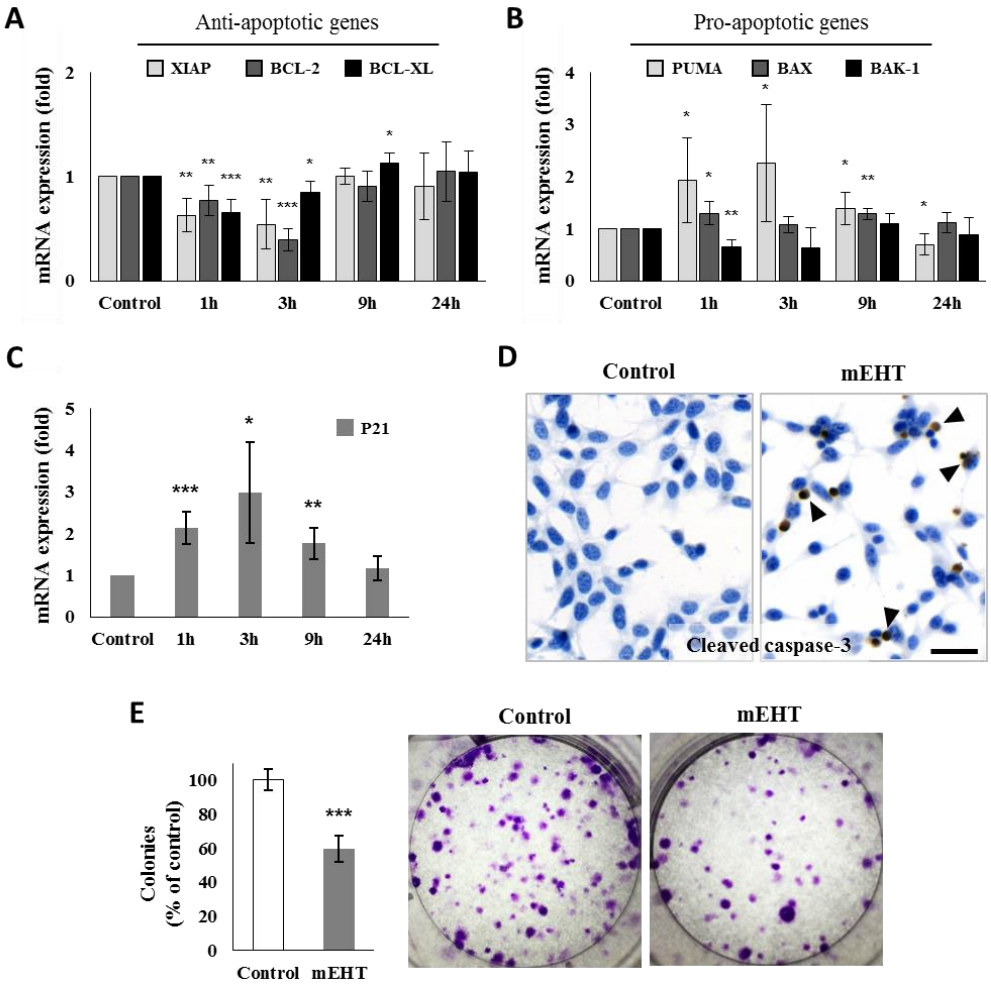

Figure 12. Expression of apoptosis regulation related genes in C26 tumor cells after mEHT treatment. Significant reduction of the anti-apoptotic XIAP, BCL-2, BCL-XL mRNA levels 1- and 3-hours post-treatment (**A**). Elevated pro-apoptotic PUMA mRNA levels at 1, 3 and 9 hours, and BAX levels at 1 and 9 hours after mEHT (**B**). Similarly increased temporal pattern of P21 mRNA levels to that of PUMA (**C**). In line with the apoptosis-promoting mRNA profile, cleaved caspase-3 protein expression (arrowheads) was significantly elevated 24 h after treatment as tested with immunocytochemistry (**D**). Scale bar: 100 µm. Significant reduction of colony-forming tumor progenitor-cell populations 10 days after mEHT treatment (E). *p<0.05; **p<0.01; ***p<0.001.

Apoptosis and cell-cycle regulation related gene expression was studied at mRNA level to see how the early response elements react to therapy. mEHT monotherapy induced a major mRNA fold-decrease of the anti-apoptotic BCL-2, BCL-XL and XIAP transcripts both after 1 h (0.77±0.14, 0.65±0.13, and 0.63±0.16 respectively) and 3 h (0.39±0.11, 0.85±0.1 and 0.54±0.24, respectively) post-treatment, then usually returned to the control levels between 9-24 h (**Figure 12A**). mRNA levels of the pro-apoptotic BAX showed moderate but prolonged increase which was significant at 1 h (1.3±0.23 fold) and 9 h (1.28±0.11fold) post-treatment (**Figure 12B**). The pro-apoptotic PUMA (**Figure 12B**) and the cyclin dependent kinase inhibitor P21 transcript levels also showed significant increase at 1 h (1.92±0.81, 2.13±0.38 fold), 3 h (2.25±1.12, 2.97±1.21 fold) and 9 h (1.38±0.31, 1.76±0.38 fold) post-treatment (**Figure 12C**). These changes were accompanied by the significant elevation of the cleaved/activated caspase-3 protein positive tumor cell fraction in the treated cultures compared to the controls (**Figure 12D**).

In clonogenic assay colony formation from tumor progenitor/stem cell clones was significantly reduced after mEHT monotherapy (59.55±7.73%; $p<0.001$) (**Figure 12E**).

4.1.2. Combination of mEHT and doxorubicin treatments

Serial dilutions of Dox were tested to optimize its therapeutic concentration in C26 cultures. Accordingly, treatment using 1 μM Dox concentration led to an ~LD40 value as measured with resazurin cell viability assay after 24 h incubation (**Figure 13A**), which was then applied in the relevant treatment protocols. In comparative testing, mEHT reduced tumor cell viability to 87.35±6.36%, Dox treatment to 56.92±2.62 while their combination resulted in only 25.00±3.31% surviving tumor cells at 24 h (**Figure 13B**). After 48 h mEHT treatment cell viability was further reduced to 78.82±5.84%, 29.06±1.89% and 13.17±2.48%, respectively (**Figure 13B**). After 24 h the number of surviving tumor cells also showed strong correlation with the resazurin assay particularly after combined treatment. This was also significant after mEHT monotherapy 49.61±7.12% while Dox monotherapy revealed less correlation with the resazurin test (45.14±6.31%) (**Figure 13C**). Dox concentration in the medium was also tested based on its fluorescence intensity using 570/590 nm excitation/emission filter pair. When the drug treatment was combined with mEHT, Dox levels in culture supernatants were reduced to 0.70±0.07 fold of those of Dox monotherapy suggesting the promotion of drug uptake

(**Figure 13D**). Dox at 1 μM concentration, both alone and in combination with mEHT, completely killed tumor progenitor cell clones (not shown).

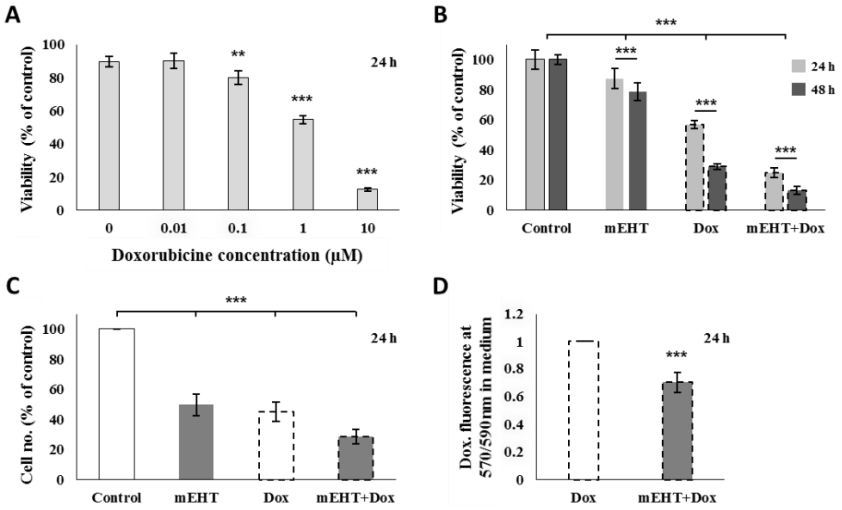

Figure 13. Comparison and combination of doxorubicin (Dox) and mEHT treatments in C26 tumor cell cultures. 1 μM Dox, reducing cell viability (resazurin assay) by ~40%, was chosen for further investigations (**A**). Progressively and significantly reduced tumor cell viability (**B**) and numbers (**C**) 24 and 48 h after mEHT, Dox and combined (mEHT+Dox) treatments. Enhanced effect of the combined treatment might be due to the reduced Dox concentration (elevated Dox uptake) in the culture supernatants (**D**). **p<0.01; ***p<0.001.

4.1.3. Treatment related changes in Akt and p53 activation

The potential influence of mEHT treatment on the survival related Akt kinase activation was measured through the phospho-Akt^{Ser473} positive cell fractions, which showed a strong tendency of reduction after both mEHT (85.01±10.06%, p=0.061) and mEHT+Dox treatments (76.33±15.64%, p=0.059) compared to control (95.97±1.89%) (**Figure 14A**). At the same time, the activated tumor-suppressor phospho-p53^{Ser15} protein positive cell populations were significantly increased from 4.27±0.99% base level up to 34.7±2.4% after mEHT, to 63.3±5.96% after Dox and to 65.13±6.95% after combined treatments (all p<0.001) (**Figure 14B**). Elevated number of tumor cells showing nuclear translocation of the p53 protein was detected by immunocytochemistry in the treated cultures, indicating the stabilization and activation p53 protein (**Figure 14C**).

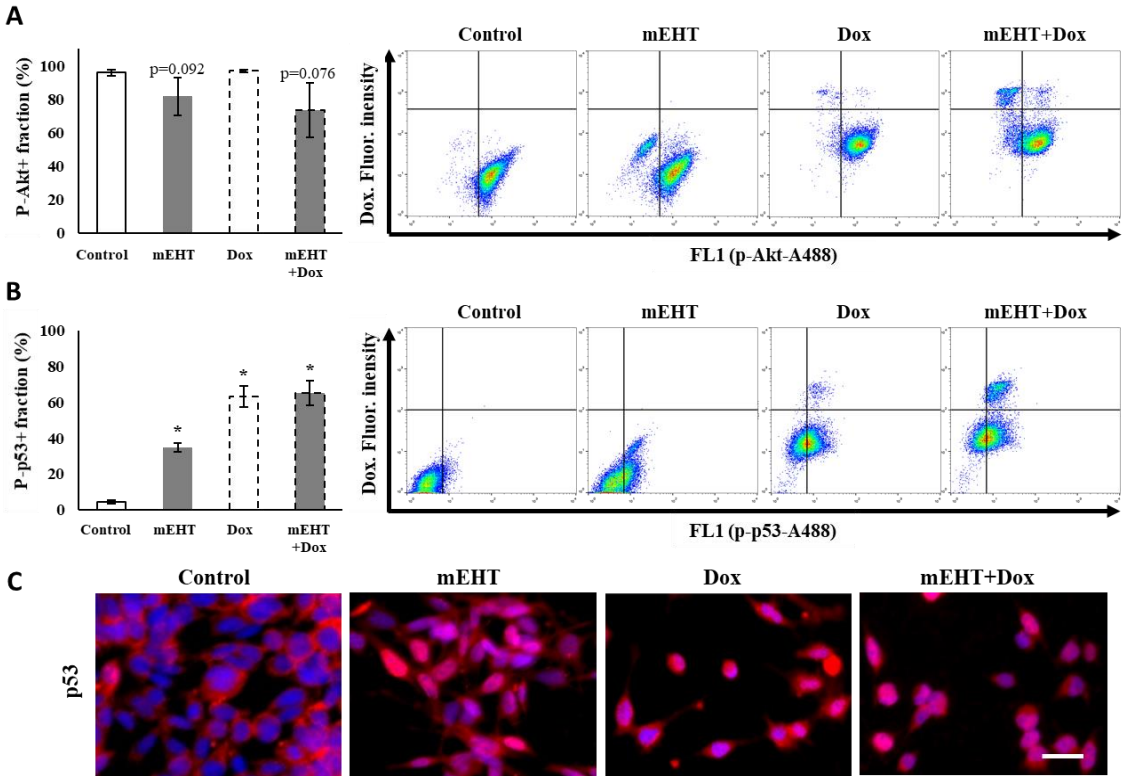

Figure 14. Comparison of phospho-Akt and -p53 levels 24h after treating cultured C26 tumor cells. Reduced phospho-Akt^{Ser473} kinase positive cell populations after mEHT and mEHT+Dox treatments (**A**). Significantly elevated post-treatment phospho-p53^{Ser15} levels showing the same highest values after Dox and the combined treatments (**B**). Increased cytoplasmic to nuclear relocalization of phospho-p53^{Ser15} indicated p53 activation (**C**). Scale bar: 100 µM. ***p<0.001.

4.1.4. Mechanism of tumor cell death induced by doxorubicin and mEHT

In line with the results from our earlier *in vivo* studies (168), mEHT monotherapy induced a significant increase of the apoptotic tumor cell fractions *in vitro* (14.53±2.99%) compared to the untreated cultures (1.94±0.36%). At the same time, apoptosis was not significant (2.31±0.73%) after Dox treatment (**Figure 15A**). This finding was further supported by the combined mEHT+Dox treatment resulting in only similar proportions of apoptotic cell populations (16.67±3.69%) to mEHT monotherapy (**Figure 15A**). Necrotic cell populations were detected also in the control cultures (6.24±2.64%), which are increased more after Dox monotherapy (11.18±1.50%) than after mEHT (9.84±1.25%) and these were added together after combined treatment (20.63±11.36%) (**Figure 15A**).

DOI:10.14753/SE.2020.2337

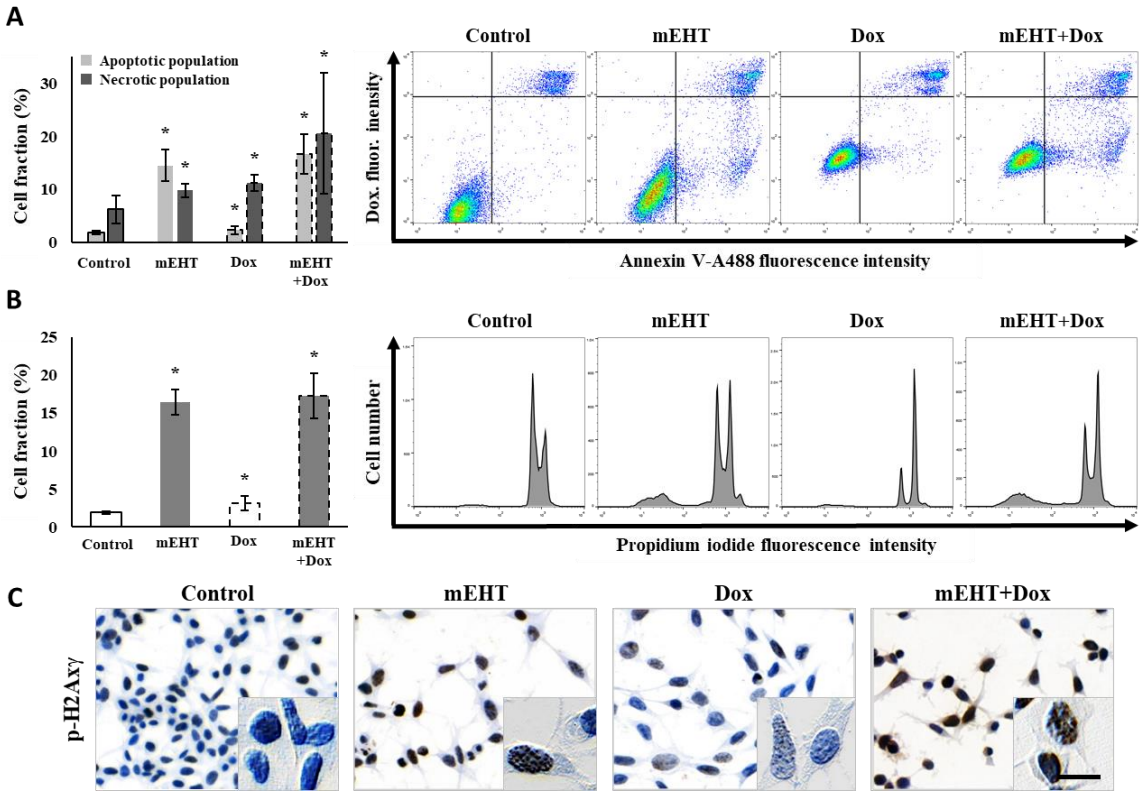

Figure 15. Comparison of the ratio of cell and DNA damage 24h after treating cultured C26 tumor cells. Significantly elevated apoptotic cell fractions after mEHT and necrotic cell fractions after Dox treatments and their additive, merged effect after combination (mEHT+Dox) therapy (**A**). Significant increase in subG$_1$ phase cell fractions both after mEHT and combined treatments refer to the apoptosis-related DNA damage (**B**), where DNA double strand breaks were indicated by upregulated H2AXγ granular positivity (brown) in cell nuclei using immunocytochemistry (**C**). Scale bar is 100 μM on the larger FOVs. *p<0.05; **p<0.01; ***p<0.001.

4.1.5. Treatment related DNA fragmentation and damage response

The proportion of cells with apoptosis-related fragmented DNA was grown significantly from 1.92±0.16% to 16.47±1.64% after mEHT, to 3.13±0.94 after Dox and to 17.27±2.99% after combined mEHT+Dox treatments (**Figure 15B**). DNA double strand-breaks indicated by the increased intensity and granularity of the H2AXγ immunoreaction in tumor cell nuclei, was also detected at high levels both after mEHT monotherapy and after combined mEHT+Dox therapy compared to controls (**Figure 15C**).

4.1.6. Treatment related inhibition of cell cycle and tumor colony-formation

G_1-phase cell populations in the cell cycle were significantly reduced to 38.89±0.97% after mEHT, to 21.41± 1.84% after Dox and to 32.81±4.67% after mEHT+Dox treatments compared to the control cultures 48.81±2.91% (**Figure 16A-B**). S-phase cell populations showed decrease only after Dox monotherapy, while G_2-phase cell fractions were increased after both monotherapies, to 38.24±1.81% after mEHT, and to 65.69±1.82% after Dox, but only to 42.97±1.05% upon mEHT+Dox treatments compared to the control (29.37±2.4%) levels **(Figure 16A-B**).

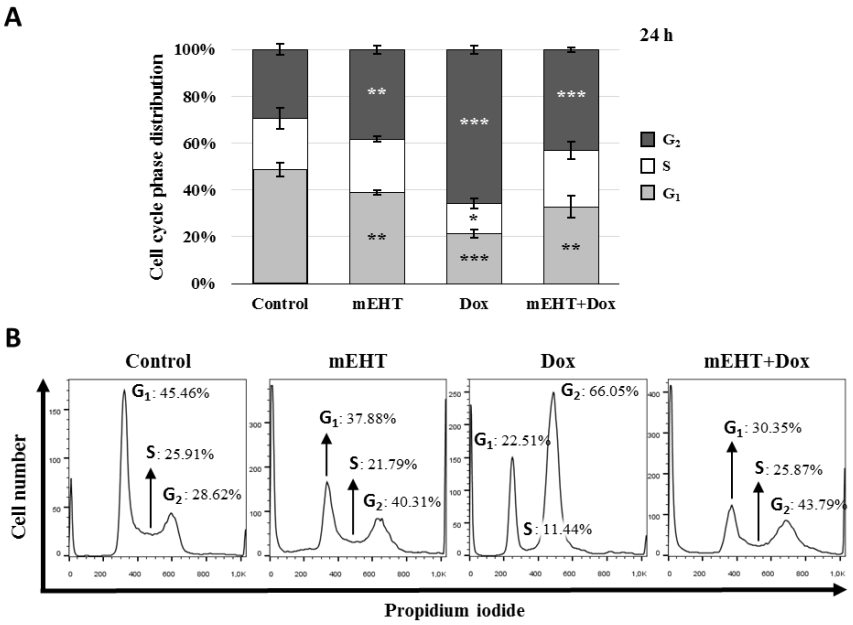

Figure 16. Summary graph (**A**) of flow cytometry analysis (**B**) of the treatment related cell cycle fractions. Significant but less G_2-phase cell cycle arrest was shown 24 h after mEHT than after Dox treatment, where the sizes of G_1 and G_2 populations in the combined (mEHT+Dox) group show about the averages of the single treatments. *p<0.05, **p<0.01 and ***p<0.001.

4.2. *In vivo* experiments

4.2.1. mEHT induced programmed tumor cell death

TDR was calculated by dividing the damaged areas with the whole tumor areas (**Figure 10A-B**), measured in H&E stained digital slides, was significantly higher in mEHT treated ($mEHT_{right}$) than untreated sides ($mEHT_{left}$) or sham control tumors between 24-72 h post-treatment (**Figure 17A-B**). Combination therapy (mEHT+MTE) led to tumor damage not only in the treated right tumors ($mEHT+MTE_{right}$) but also in the untreated left tumors ($mEHT+MTE_{left}$) within the same time-frame (**Figure 17C**). Kruskal-Wallis test showed highly significant differences ($p<0.001$) among groups 24 h ($\chi^2(5)=26.081$), 48 h ($\chi^2(5)=20.911$) and 72 h ($\chi^2(5)=28.297$) post-mEHT treatment. The effect of MTE administration alone was not significant.

Nuclear chromatin condensation and widespread apoptotic bodies indicated mEHT induced programmed cell death response (**Figure 10B**), which was confirmed by elevated DNA fragmentation from 24 h post-treatment ($\chi^2(5)=72.415$, $p<0.001$) (**Figure 17D**). Post hoc test revealed significantly elevated TUNEL positivity in: $mEHT_{right}$ vs. $sham_{right}$ and $sham_{left}$; in the $mEHT+MTE_{right}$ or $mEHT+MTE_{left}$ vs. sham controls and $mEHT_{left}$ (**Figure 17E).**

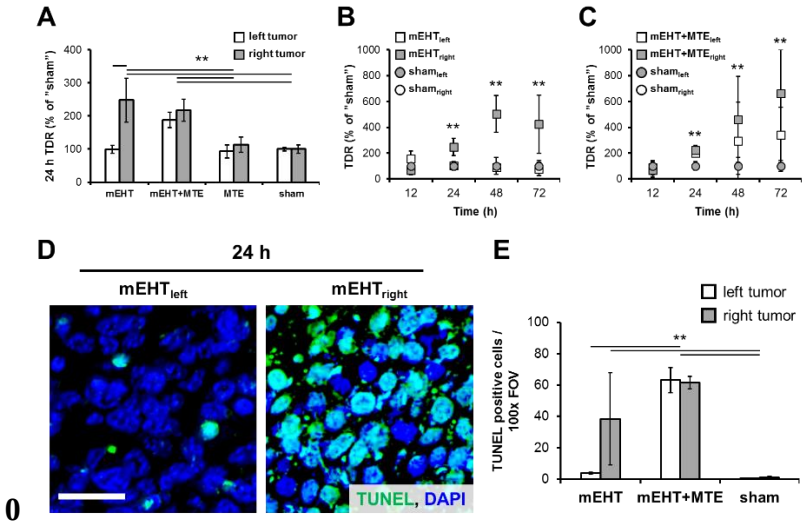

Figure 17. Elevated TDR both in the mEHT treated right-leg tumors compared to the untreated left sides or sham controls in monotherapy. Also increased TDR in both tumor sides after combing mEHT and MTE (mEHT+MTE) compared to the sham controls, 24 h after treatment (**A**). Progressive tumor damage both after single (**B**) and combined mEHT+MTE treatments (**C**). Significantly elevated numbers of TUNEL positive cell nuclei (green) in the mEHT-treated (right) tumor (**D**), and in both sides of the mEHT+MTE combination group compared to sham controls 24 h post-treatment (**E**). p**<0.001. Scale bar shows 20 μm (D-E).

4.2.2. Mechanism of mEHT induced programmed tumor cell death

mEHT treatment induced the significant mitochondrial translocation of Bax protein and the cytoplasmic release of cytochrome-c between 12-24 h ($\chi^2(5)=11.989$, $\chi^2(5)=14.497$, $p<0.05$) in the treated ($mEHT_{right}$) tumors either after single or combined mEHT treatment (**Figure 18A-B**). Cytochrome-c became significantly delocalized ($\chi^2(5)=11.943$, $p<0.05$) also in the mEHT untreated (left-leg) tumors of the combined mEHT+MTE group between 48-72 h (*not shown*). Major elevation of cleaved/activated caspase-3 positive cell numbers was detected from 12 h post-treatment compared to sham controls ($\chi^2(5)=9.842$, $p<0.05$) (**Figure 18C-D**). Overlapping cleaved caspase-8, -caspase-3 and TUNEL positive cell fractions were significantly elevated in the apoptotic tumor regions including the intact-damaged marginal zone, particularly at advanced stages, 48-72 h post-mEHT treatment (**Figure 18E-F**). These findings are consistent with the activation of caspase-dependent extrinsic and intrinsic apoptotic pathways. After treatment, the nuclear Ki67 protein expression disappeared completely from tumor cells which showed minor morphological signs of apoptosis (**Figure 19**).

There was no significant difference in nuclear AIF levels between the treated and untreated tumors (*not shown*).

DOI:10.14753/SE.2020.2337

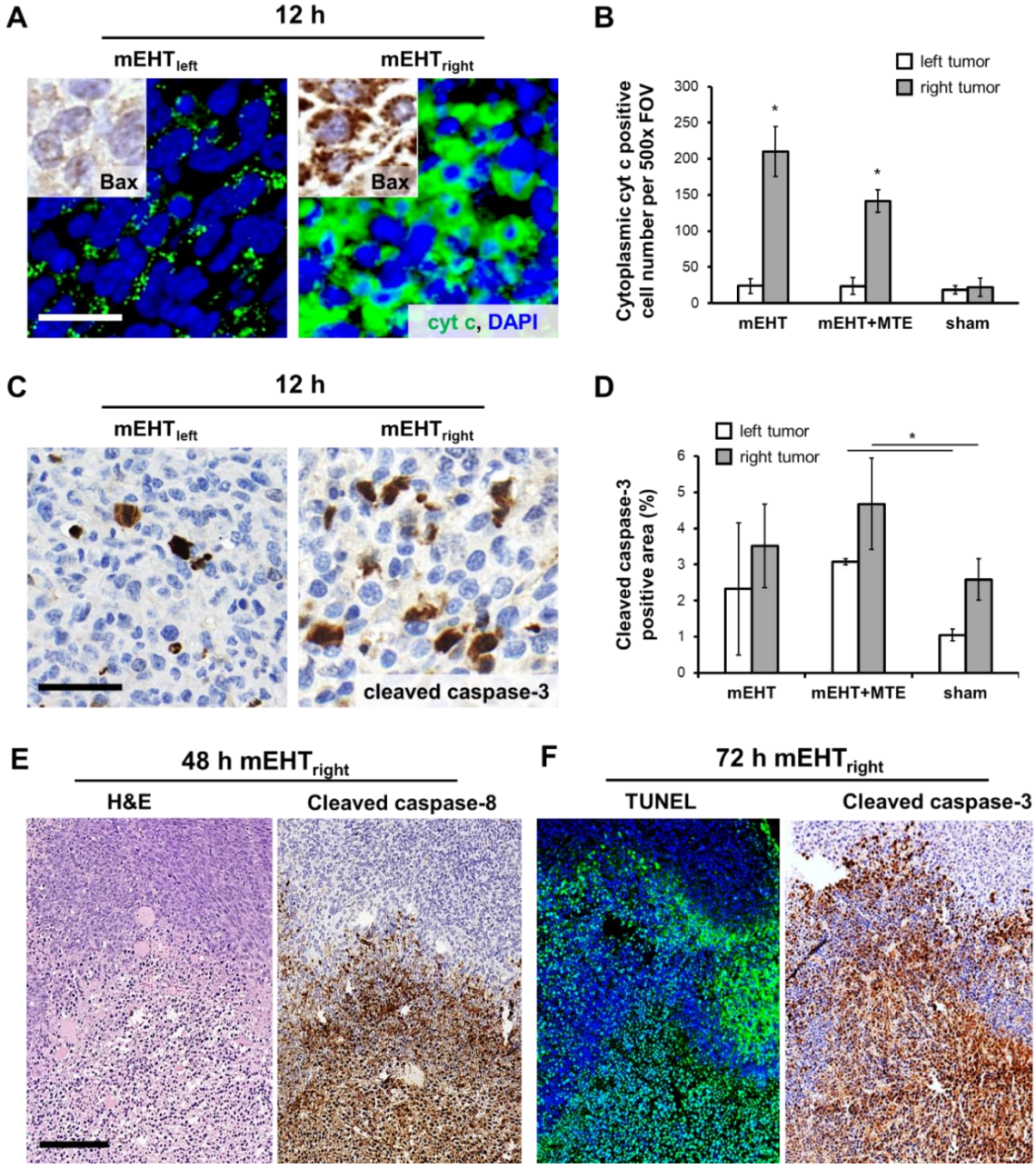

Figure 18. The mEHT induced pro-apoptotic factors. Mitochondrial cytochrome-c in untreated tumors show significant cytoplasmic (green, immunofluorescence) after mEHT treatment (**A**) in parallel with the mitochondrial translocation of Bax protein (insets in A, brown; immunoperoxidase) in 12 h samples ($p^*<0.05$) (**B**). At the same time, cleaved caspase-3 positive cells (brown) are also significantly more abundant at both tumor sides after combined (mEHT+MTE) treatment (**D**). Overlapping areas of cleaved caspase-8 (brown) (**E**), TUNEL (green fluorescence) and cleaved caspase-3 (brown) positive cell fractions (**F**) concentrated in damaged tumor regions proved both extrinsic and intrinsic caspase dependent apoptosis 48 h and 72 h after treatment, respectively. Scale bars, A and C: 20 μm; E and F: 100 μm.

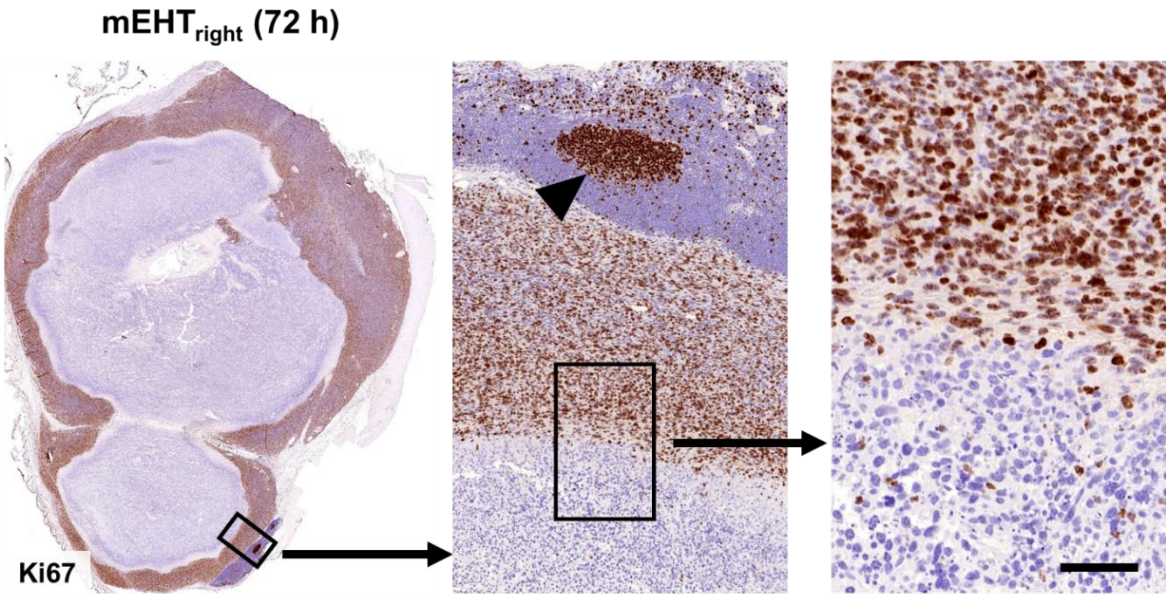

Figure 19. mEHT induced cell cycle blocking. Nuclear Ki67 positivity indicating tumor cell proliferation is ceased in the mEHT damaged central tumor regions (left), even in cells showing only early signs of apoptosis on higher magnifications (middle and right). The lymphoid germinal center (middle, arrowhead) serves for Ki67 positive control. Scale bar shows 2 mm on the left, 200 μm on the middle and 60 μm on the right image.

4.2.3. mEHT induced DAMP signals

Massive cytoplasmic to cell-membrane relocalization of calreticulin was observed after 12 h post-treatment ($\chi^2(5)=44.720$, $p<0.001$). Pairwise statistical analysis confirmed significant cell membrane concentration in $mEHT_{right}$ (mEHT treated) vs. $mEHT_{left}$ and sham control tumors; and in $mEHT+MTE_{right}$ or $mEHT+MTE_{left}$ vs. $mEHT_{left}$ and sham control tumors (**Figure 20A-B**).

The release of calreticulin was followed by a significant accumulation of cell-membrane localized Hsp70 protein in the mEHT-treated groups peaking at 48 h post-treatment ($\chi^2(5)=54.912$, $p<0.001$). Pairwise significance was seen in $mEHT_{right}$ vs. $mEHT_{left}$ and sham control tumors; and in $mEHT+MTE_{right}$ or $mEHT+MTE_{left}$ vs. $mEHT_{left}$ and sham control tumors (**Figure 20C-D**).

Significant nuclear to cytoplasmic release or complete loss in the damaged areas of HMGB1 protein was also seen at 48 h post-mEHT treatment ($\chi^2(5)=12.969$, $p=0.024$). Post hoc test confirmed significant disappearance of HMGB1 in $mEHT_{right}$ vs. sham controls; and in $mEHT+MTE_{left}$ vs. $mEHT_{left}$ tumors (**Figure 20E-F**).

DOI:10.14753/SE.2020.2337

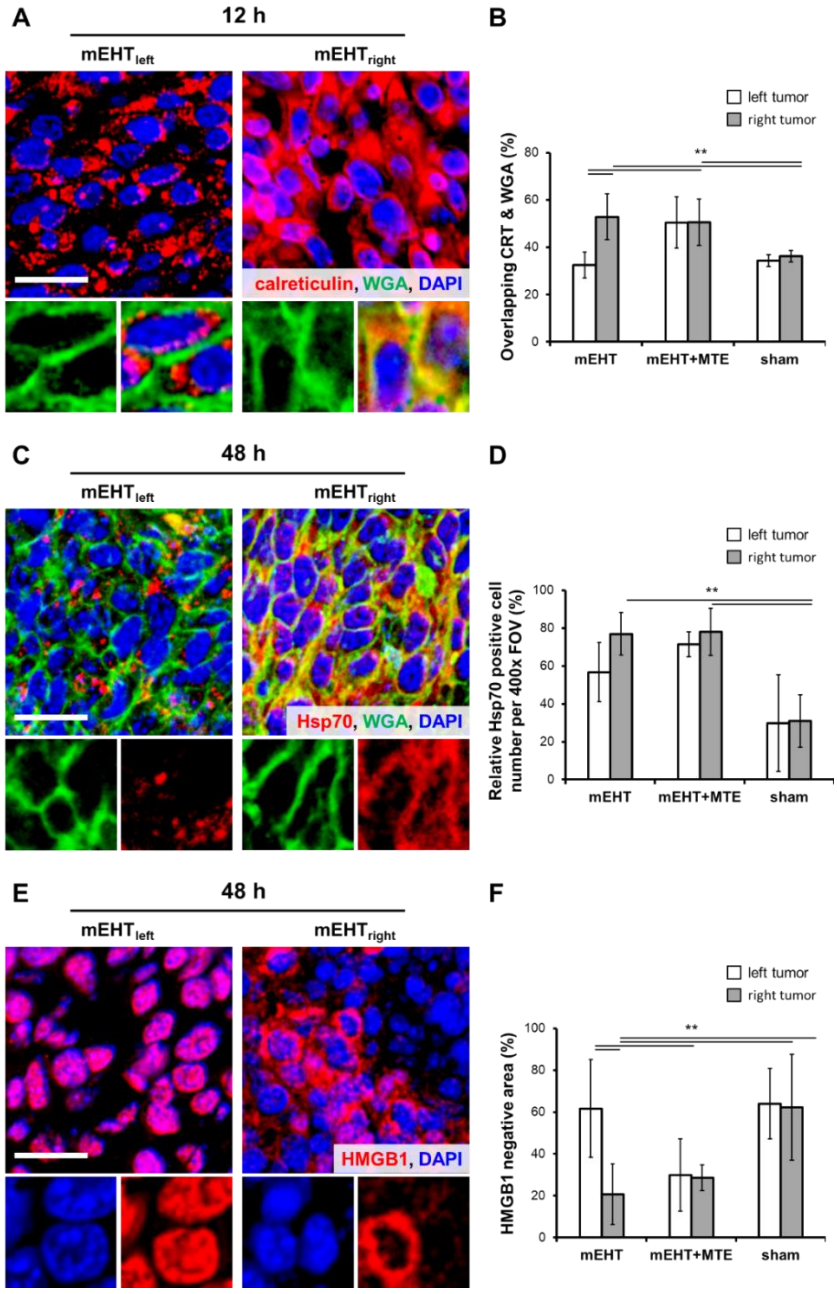

Figure 20. mEHT induced damage signaling. Release of calreticulin (red) protein from the endoplasmic reticulum and colocalization with the cell membrane marker WGA (green) confirms its membrane accumulation (yellow) after mEHT treatment (**A**). Significantly increased proportion of tumor cells with overlapping WGA and calreticulin reactions in both treatment groups (p**<0.001) compared to sham controls (**B**). Elevated intracytoplasmic Hsp70 protein (red) overlapping with the cell membrane WGA (green) 48 h after treatment. The number of Hsp70 positive cells was significantly increased (p**<0.001) in the $mEHT_{right}$ and in both tumors of mEHT+MTE groups compared to sham controls (**D**). Early nuclear to cytoplasmic release of HMGB1 (red) group 48 h after treatment (**E**). The proportion of HMGB1 negative areas (indicating extracellular release) was significantly lower (p*<0.05) in the $mEHT_{right}$ and in both tumor sides of mEHT+MTE groups compared to sham controls (**F**). Scale bar shows 20 μm, and 10 μm in the insets.

4.2.4. mEHT induced tumor infiltration by antigen presenting cells and T-cells

DAMP signal sequence was accompanied by the massive tumor infiltration by S100 positive APC from 48 h post-treatment ($\chi^2(5)=12.483$, $p=0.029$). Significant numbers of APC in $mEHT_{right}$ vs. $mEHT_{left}$ and $sham_{right}$ and $sham_{left}$ tumors; and in $mEHT+MTE_{right}$ vs. sham tumors were revealed (**Figure 21A-B**). Also, significant numbers of CD3 positive T-cells infiltrated the treated tumors with a peak at 72 h post-mEHT treatment ($\chi^2(5)=14.156$, $p=0.015$) (**Figure 21C**). Pairwise testing confirmed significantly more T-cells in $mEHT_{right}$ vs. $mEHT_{left}$ tumors; in $mEHT+MTE_{right}$ vs. $sham_{left}$ and $sham_{right}$ tumors (**Figure 21C-D**). APC and T-cell invasion also showed a nearly significant trend between $mEHT+MTE_{left}$ and sham control tumors. A dense ring of T-cell invasion was seen in the margin between the damaged and the "intact" tumor regions, furthermore, the latter was also infiltrated heavily (**Figure 21E**). A scant number of FoxP3 positive T-cells were observed and no difference can be seen between the treated and untreated tumors.

DOI:10.14753/SE.2020.2337

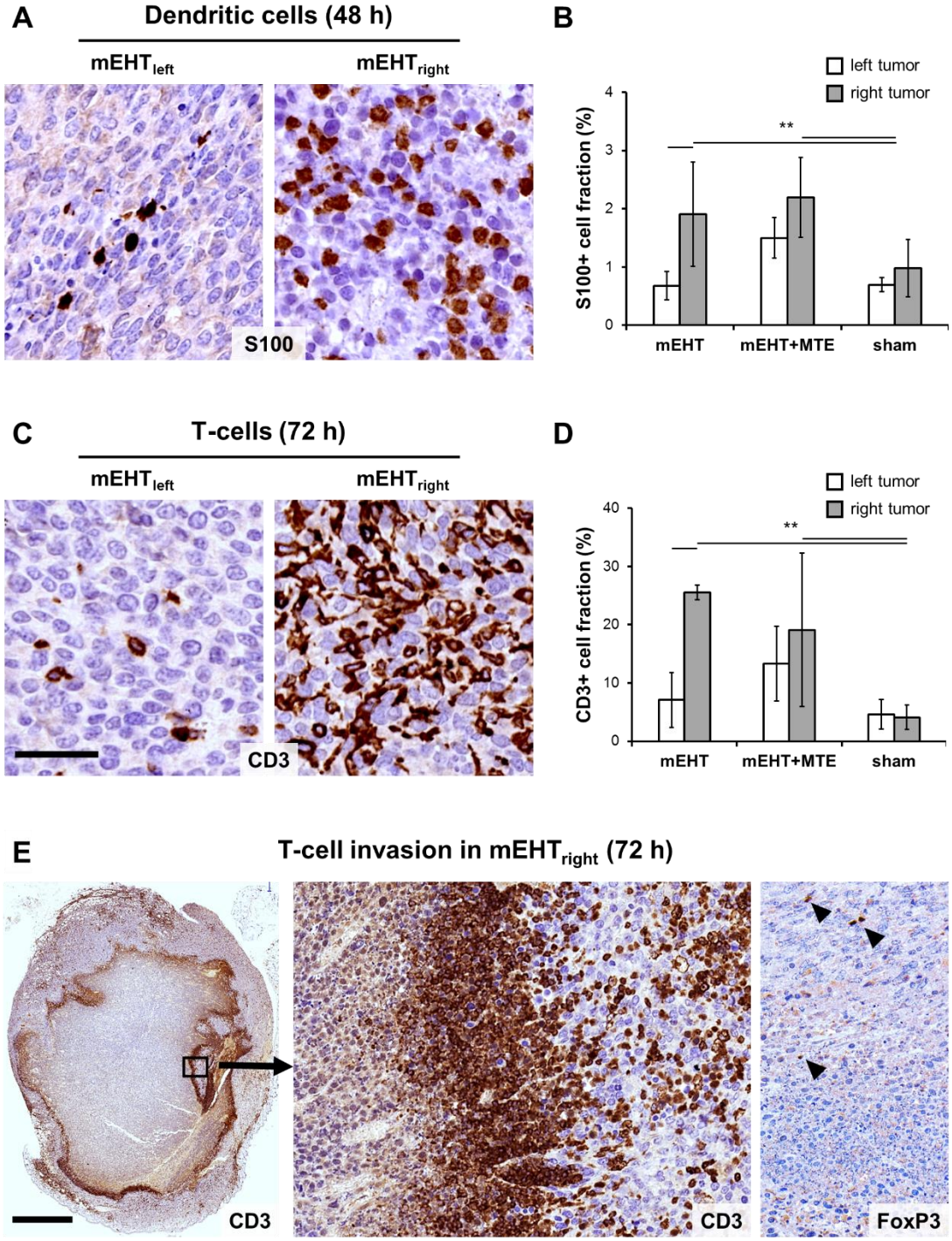

Figure 21. mEHT induced tumor infiltration by immune cells. Significant elevated S100 positive (brown) APC was counted in the $mEHT_{right}$ tumors, and in both tumor sides of the mEHT+MTE combined group 48 h after treatment (**A**), as summarized in a graph (**B**). Increase in T-cell numbers also proved to be significant ($p^*<0.05$) in the $mEHT_{right}$ tumors, and in both tumor sides of the mEHT+MTE combined group 72 h after treatment (**C**), shown also in a graph (**D**). Massive T-cell infiltration rim separates damaged central tumor regions from the intact periphery (**E**), while the latter was also heavily infiltrated as seen at higher magnification (middle), with only scant FoxP3+ T-cells (right). Scale bars in A-B and D-E: 40 μm. Scale bar in C-left: 2 mm, middle and right: 100 μm.

5. Discussion

5.1. *In vitro* study of mEHT treated C26 colorectal adenocarcinoma

Earlier studies confirmed that mEHT treatment used as a complementary to chemo- and radiotherapy of human cancer can induce tumor destructions by itself both by provoking apoptosis through irreversible heat and cell-stress, and by affecting cell membrane-fluidity and targeting dielectric membrane receptor molecules concentrated in lipid rafts (2, 169). These effects and the increased loco-regional blood perfusion by mEHT added to those of the combination partner are likely to contribute to the improved treatment efficacy of these combinations (5, 8). However, the molecular mechanisms of interactions between mEHT and chemotherapy, which could help in designing better treatment protocols, still need to be clarified. Here we set up an *in vitro* test system for rapid analysis of mEHT effects using C26 a mouse colorectal cancer cell line, which earlier made it possible to follow the treatment related immunological events *in vivo* in allografts (168). A similar tumor destruction mechanism revealed in the two models, so it validated our *in vitro* model that it is appropriate for feasible testing of mEHT in combinations with other treatment modalities, which worth for further *in vivo* analysis. Combination of mEHT with Dox chemotherapy resulted in an additive tumor cell destruction and control by merging efficient apoptosis and necrosis induction of mEHT and Dox, respectively (170). The cell cycle arrest contributed by both components.

In line with our *in vivo* allograft results, mEHT applied in monotherapy provoked cell- and heat-stress in cultured C26 tumor cells, indicated by the upregulation and cytoplasmic translocation of Hsp70 and calreticulin proteins (168). In culture, the latter was obviously enriched in tiny cell membrane blebs of damaged tumor cells suggesting its release within extracellular vesicles possibly including exosomes that may form protective shells around their content (171, 172). Hsp70 and calreticulin are part of the DAMP signaling, which can augment the receptor mediated uptake, processing and presentation of tumor antigen to promote anti-tumor immune response (53, 173-175). Indeed, we confirmed this by showing that after a single mEHT treatment CD3+ (very rarely FoxP3 positive) T-cells and S100 positive antigen presenting cells showed progressive accumulation accompanied by an ongoing tumor damage (168). After mEHT treatment, the upregulation of pro-apoptotic (PUMA and BAX), the downregulation of anti-apoptotic gene (XIAP, BCL-2 and BCL-XL) transcripts (between 1-3 h) followed by the significant

elevation of cleaved/activated caspase-3 protein positive cultured tumor cells (after 24h) were consistent with caspase dependent apoptosis (31, 176, 177). The increased cleaved/activated caspase-8 protein levels and damaged mitochondrial membrane permeability (reduced DiOC6 absorption) suggested the activation of both the extrinsic and the intrinsic programmed cell death pathways (178, 179). However, less subG_1 phase fraction indicating DNA fragmented apoptotic cell population was measured than it was expected from the increase of annexin-V positive cell fractions (early sign of apoptotic membrane damage), implying that cell cycle progression was also hindered by mEHT treatment (180). This was supported by the P21 transcript upregulation, what was found between 1-9 h after mEHT treatment, since P21 encoding the cyclin dependent kinase inhibitor $p21^{waf1}$ protein, which can mediate cell cycle arrest (and senescence) (50).

Both caspase dependent apoptosis through the upregulation of pro-apoptotic and downregulation of anti-apoptotic mediators and cell cycle arrest through inducing $p21^{waf1}$ expression are likely to be orchestrated by the upregulated nuclear phospho-$p53^{Ser15}$ protein (181, 182). Activation of p53 could be induced both by heat and cell-stress and the DNA double strand breaks as the latter was indicated by the accumulation of nuclear H2AXγ protein after mEHT treatment (183). Here we detected the phosphorylation of p53 protein at Ser15, what is known to prevent p53 ubiquitination by Mdm2 and thus can promote p53 functions (51). Akt can also interfere with p53 activation and inhibit its function on the mitochondria including apoptosis (51, 184, 185). Thus reduced survival-related phospho-Akt^{Ser473} levels were measured (though only at a level of strong tendency) after mEHT treatment, it can further support p53, since activated Akt could promote Mdm2 control of p53 and the anti-apoptotic XIAP for interfering with caspase-3 activity (186-188).

Dox monotherapy of cultured C26 colorectal cancer cells was feasible at 1 μM concentration relevant for reducing tumor cell viability up to 40% (189, 190). Under comparable conditions this decrease significantly exceeded that of mEHT, but instead of inducing apoptosis, necrosis was the dominant cell damage mechanism by Dox with significantly less DNA double strand breaks measured than after mEHT. However, Dox contributed more significantly to p53 activation and killing of tumor stem cell clones than mEHT. Comparative analysis of cell cycle fractions also revealed a major G_2-phase arrest

after Dox treatment and less but still significant G_2 arrest after mEHT compared to untreated cultures.

Combination of Dox with mEHT treatments resulted in an additive reduction of tumor cell viability (almost reaching synergy level) and number as well as cumulated the effects on the apoptotic, necrotic and the whole lost/damaged cell fractions. Our results also suggest that mEHT can promote the uptake of Dox by tumor cells, which may further raise the sensitivity and/or reduce the therapeutic concentration and side-effects of Dox, is in agreement with the observation that alternating current (also delivers mEHT) can enhance Dox uptake (191).

In conclusion, here we introduce an *in vitro* mEHT treatment model of C26 mouse colorectal cancer useful for feasibility studies of the molecular background of combining mEHT with other treatment modalities, starting with Dox chemotherapy. Besides validating similar cell stress and programmed cell death pathways in this model to our allograft system using the same cell line, we also extended our focus to refine cell damage pathways involved in the mEHT effect. Our results show that mEHT monotherapy can induce irreversible cell stress both through caspase-dependent apoptosis and $p21^{waf1}$ mediated cell cycle arrest, which are likely to be driven by p53 activation. Elevated phospho-$p53^{Ser15}$ and reduced phospho-Akt^{Ser473} are known to promote p53 escape from Mdm2 control. In combination, mEHT seems to promote the uptake and significantly potentiate tumor destruction and cell-cycle control by Dox through merging efficient apoptosis, necrosis and cell cycle arrest induction by mEHT and Dox. This model can serve for pilot testing of mEHT combinations prior to comprehensive investigations of allografted C26 cells using immune competent animals.

5.2. *In vivo* study of mEHT treated C26 colorectal adenocarcinoma

Previously we showed that the mEHT can trigger a programmed cell death response in HT29 human colorectal cancer xenografts of immunocompromised mice, which was dominantly mediated by caspase independent AIF activation (16). This was accompanied by the translocation and release of DAMP signal elements relevant to inducing ICD and the tumor infiltration by immature immune cells (20). In the current study, C26 colorectal cancer allografts grown in immunocompetent mice were used to test mEHT induced cell stress, programmed cell death and anti-tumor immune responses. Here we also detected

apoptosis mediated tumor damage, followed by a caspase-dependent subroutine. It seems that the preferred programmed cell death pathway after mEHT treatment is rather dependent on the inherent genetic and epigenetic set-up of the given tumor cell line, than the treatment itself. This view is supported by detecting the same death pathways after mEHT treatment in small damaged areas, probably induced by hypoxia, in the untreated sham tumors both in the HT29 and C26 models. In this study, the mEHT induced DAMP signal sequence was followed by significant APC and T-cell invasion of the treated tumors, which was also seen in the untreated contralateral neoplasms when mEHT was delivered together with MTE, a T-cell promoting agent (summarized in **Figure 22**). These data suggest that besides its loco-regional effect mEHT can also contribute to tumor damage distant from the directly targeted regions.

It has already been revealed that mEHT treatment more effectively destroys tumor cells than conventional hyperthermia at the same (42°C) intratumoral temperature (157). This and all of our earlier works suggest that modulated electric field can instantly penetrate deep into tumors and provoke tumor damage spreading inside-out from tumor centers (16, 20, 157). It can efficiently mediate an irreversible cell stress by inducing heat shock and affecting charged molecules particularly in tumor cell membranes (2). In human cancer therapy, mEHT (oncothermia; and traditional hyperthermia too) is used in sequentially repeated treatment modules, usually alternating either with radio- or chemotherapy. So far experimentally, we only characterized the effects of single mEHT treatment. Therefore, in our present model, we standardized the single treatment with precisely measuring and keeping the intratumoral temperature at 42^{o}C. We demonstrated that mEHT treatment caused significant destruction of C26 colorectal cancer cells by inducing apoptosis confirmed by chromatin condensation and nuclear DNA fragmentation. C26 cell line form aggressive tumors showed almost 100% proliferation index by detecting Ki67 protein *in vivo*, a general cell cycle marker expressed from G_1- to the end of M-phase (192). Furthermore, we showed that early apoptotic commitment induced by mEHT can result in the complete blockade of the cell cycle regulation machinery indicated by the loss nuclear Ki67 expression.

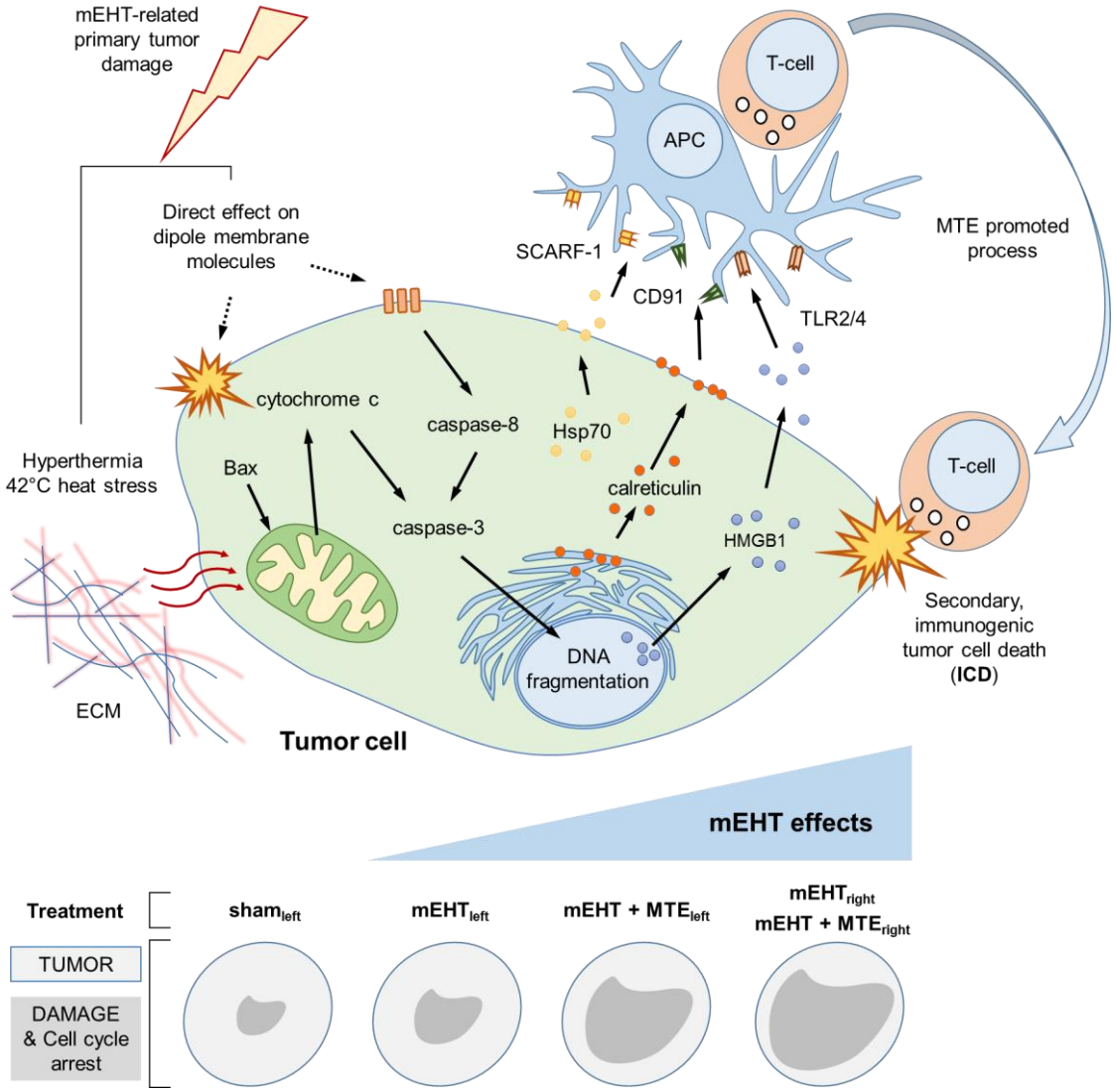

Figure 22. On mEHT induced anti-tumor damage mechanisms. Upper panel. Heat stress at 42°C and direct effect of electric field on dipole molecules both in the ECM and the tumor cell membrane induce caspase-dependent apoptosis resulting in DNA fragmentation. The concomitant release of DAMP signals (Hsp70, calreticulin and HMGB1) support the maturation of antigen presenting cells (APC), which activate cytotoxic T-cells for mediating a secondary, ICD response. Systemic mEHT effect is possibly facilitated by MTE promoted T-cell migration/activation. Lower panel sums up semi-quantitatively how mEHT induced pathways, tumor destruction effect and cell cycle arrest are manifested after using different treatment modules.

The progressive accumulation of DNA fragmentation and apoptotic bodies between 12-72 h post mEHT treatment was consistent with a programmed cell death response. The significant tumor damage caused by mEHT treatment proved to be caspase-dependent indicated by the massive expansion of the cleaved/activated caspase-3 positive apoptotic cell fractions. The upregulation of cleaved/activated caspase-8 protein in parallel with the

mitochondrial translocation of Bax and the mitochondrial release of cytochrome-c confirmed the activation of both the extrinsic and the intrinsic caspase dependent pathways (176). Elevated apoptotic signaling detected initially, between 12-24 h, only in the mEHT treated tumors became bilateral by 48 h post-treatment in mEHT+MTE treated animals. This finding suggests that apoptosis can be provoked by mEHT both directly and later on through mediators which recruit the immune system (*see* **Figure 22**). The latter may involve factors discharged by damaged tumor cells and those of MTE extract leading to a systemic effect on distant tumor sites.

In line with our *in vitro* findings, we proved mEHT induced DNA DSBs also in this *in vivo* C26 model. Since DNA DSBs are also provoked during tumor cell proliferation as a result of genetic instability and during the concomitant $p21^{waf1}$ mediated cell cycle arrest, we looked for and found H2AXγ positive cells beyond these processes confirming the extrinsic (mEHT) origin DNA damage (**Figure 23)**.

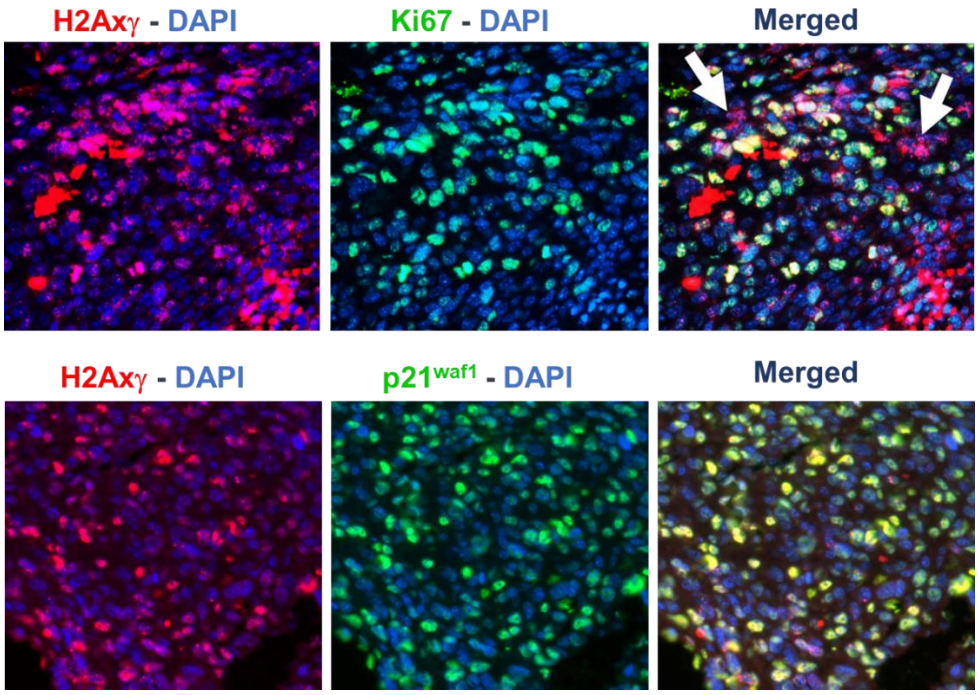

Figure 23. H2AXγ positive tumor cells (red) indicating DNA double-strand breaks. At the border of intact-damaged tumor region H2AXγ reaction is seen beyond Ki67 positive (green) proliferating cells (upper panel, arrows) suggesting an externally induced damage; while in the intact tumor regions its reaction mostly overlaps with that of the senescence associated $p21^{waf1}$ (lower panel).

Tumor treatment can contribute to the elimination of cancer cells through interactions between immune-independent (initial apoptosis) and immune-dependent (activation of

immune response) pathways (53). Immunogenic tumor cell death response can extend and maintain the treatment induced primary apoptotic tumor damage. ICD can be triggered by DAMPs including extracellular release of HMGB1 and ATP which act similar to cytokines (54). It is also supported by the cell membrane localization and access by antigen presenting and immune cells of the chaperons Hsp70 and calreticulin (20). Conventional hyperthermia can induce only partial DAMPs in tumors mainly through Hsp70 release which is less efficient by itself in supporting APC maturation as well as NK and cytotoxic T-cell functions (193-195). Complex DAMP signals can activate APC by promoting the uptake and presentation of tumor antigens through Toll-like-, purinergic- and pattern recognition receptors for enhancing tumor-specific T-cell response (53). In this study mEHT also induced complex DAMP signals including calreticulin, Hsp70 and HMGB1 release in line with our results on immunocompromised tumor model (20). The potential immune stimulatory effect of these signals was supported by the progressive tumor infiltration by S100 positive APC and CD3 positive T-cells in immunocompetent mice with only negligible number of FoxP3+ immune inhibitory T-cells **(Figure 21)**. Though elevated tumor damage, DAMP signaling, and immune cell infiltration was frequently seen in the contralateral (left) tumors after single mEHT treatment, this changed into significant only after combined mEHT+MTE treatment in the mEHT untreated left tumors.

Similar to our results, local mEHT treatment, in combination with antigen-primed syngeneic APC injection, significantly inhibited the growth of CT26 tumors (similar to C26 but from different vendor) and protected animals from developing new tumors after CT26 rechallenge (21). This intervention primed IFN-γ secretion and supported the recruitment of both the innate immunity and the adaptive cytotoxic T-cell mediated immunity. A similar mEHT primed APC treatment of squamous cell carcinoma allografts also induced elevated numbers of S100 positive APC and CD8 positive cytotoxic T-cells in line with the inhibition of tumor growth both in the treated and distant tumor sites (160). In agreement with our results, mEHT (when combined with APC therapy) did not influence the number of the immune-inhibitory FoxP3 positive regulatory T-cells (69). Thus, massive CD3 positive T-cell infiltration with insignificant number of FoxP3 positive regulatory T-cells, can mediate an effective anti-tumor immune response (69,

193-195). This was supported by the progressive nature of tumor damage and the positive correlation with the immune cell infiltration in our present study.

MTE treatment has been demonstrated to support the cellular immune response. MTE administration synergized with the growth inhibitory and apoptosis inducing effects of cisplatin in Lewis lung cancer xenografts and increased the number of tumor infiltrating CD8 positive T-cells and the expression of interferon-γ, perforin-1 and granzyme-B (165). It also contributed to the suppression of growth of EGFR inhibitor resistant, K-ras and EGFR-mutant non-small cell lung cancer cells through hampering downstream receptor tyrosine kinase (RTK) signaling pathways (Akt and MAPK) (196). This effect was primarily attributed to chlorogenic acid identified in MTE by enhancing IFN-γ, IL-2, IL-12, MCP-1 levels and promoting the recruitment of Th1 lymphocytes, as well as stimulating T-lymphocyte, NK-cell and macrophage functions (167, 197). The systemic effect of loco-regional cancer therapy, also known as abscopal effect, which was confirmed e.g. after chemotherapy or γ-irradiation, is most probably mediated by the immune system (198). Therefore, both published reports and our data suggest that MTE can contribute to APC and T-cell recruitment and tumor infiltration in synergy with DAMP signals and tumor antigen release induced by mEHT. However, the exact mechanism of action and the messengers involved need to be further clarified in molecular and functional studies.

6. Conclusion

Our data show that mEHT treatment can induce irreversible heat and cell stress leading to DNA double-strand breaks and the blockade of tumor cell cycle resulting in caspase-dependent programmed cells death in C26 colorectal cancer models both *in vitro* and *in vivo*. Both apoptosis and $p21^{waf1}$ mediated cell cycle arrest (senescence) are likely to be driven by p53 activation. Elevated phospho-$p53^{Ser15}$ and reduced phospho-Akt^{Ser473} are known to promote p53 escape from Mdm2 control (a simplified summary is shown in **Figure 24**).

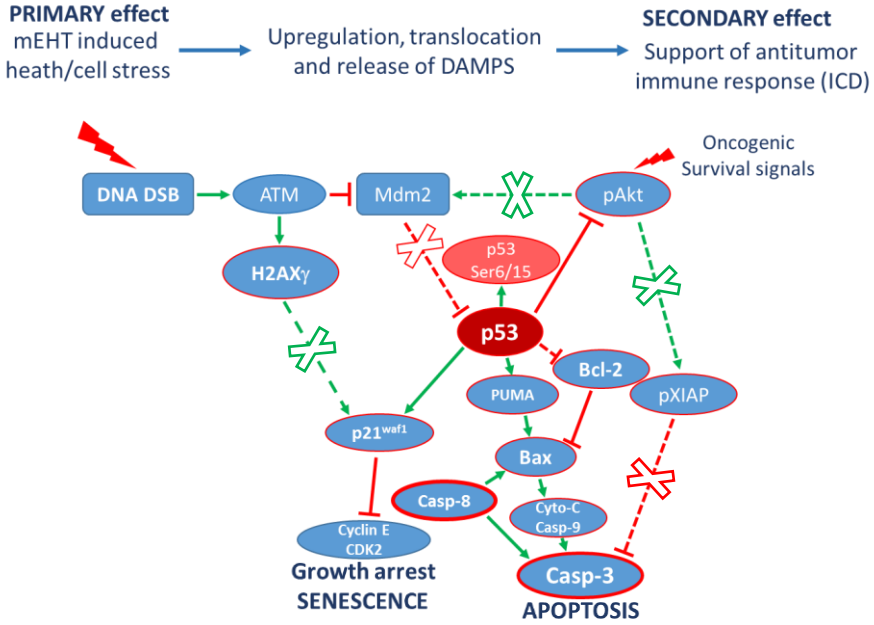

Figure 24. Summary of the main tumor damaging effects of mEHT treatment on C26 colorectal adenocarcinoma. The primary heat and cell stress induces DNA DSBs and the upregulation of phospho-p53, which by escaping under the inhibition of Mdm2 can induce both caspase-dependent apoptosis and $p21^{waf1}$ driven cell cycle arrest (senescence). The release of DAMP signals from damaged cells may induce the accumulation of T-cells and antigen presenting cells contributing to a secondary immune-mediated tumor cell death.

In vitro combination with doxorubicin, mEHT seems to promote the uptake and significantly potentiate tumor destruction and control, merging the efficient apoptosis and necrosis induction by mEHT and Dox, respectively, and the cell cycle arrest contributed by both treatments. *In vivo*, DAMP signals released from mEHT-damaged cells are associated with tumor infiltration by APC and T-cells, which probably contribute to the ongoing secondary immune mediated tumor damage (ICD). Loco-regional mEHT treatment can also facilitate a systemic anti-tumor effect in combination with a T-cell

promoting agent (MTE). The contribution of MTE derived chlorogenic acid in the immune response need to be further elucidated.

Our *in vitro* and *in vivo* mEHT treatment setups and tumor models can serve for pilot testing of mEHT combinations with chemo-, radio- or targeted treatment modalities. Clarifying the mode of action and the molecular pathways activated by mEHT can support more efficient use of this non-invasive treatment to complement traditional and novel options in oncotherapy.

7. Novel observations in the dissertation

Modulated electro-hyperthermia (mEHT) treatment used in C26 colorectal adenocarcinoma cell line models resulted in the significant:

- Early upregulation of cell stress associated Hsp70 and calreticulin proteins and their release into the cytoplasm reaching the cell membranes (*in vitro* and *in vivo).*
- Caspase-dependent apoptotic tumor cell death utilizing both the extrinsic and the mitochondrial pathways (*in vitro* and *in vivo).*
- Upregulation of H2AXγ indicating DNA double strand-breaks, which was likely to contribute to increased nuclear phospho-p53 expression to mediate both apoptosis and $p21^{waf1}$ induced senescence in the tumors (*in vitro*).
- Additive tumor cell destruction when mEHT was combined with doxorubicin *in vitro*.
- Translocation and release of Hsp70, calreticulin and HMGB1 in and from tumor cells were likely to be part of DAMP signaling relevant for an immunogenic cell death response (ICD) *in vivo*.
- Accumulation of cytotoxic T-cells and professional antigen presenting cells (APC) and cell damage caused by a single shot of mEHT confirming the secondary anti-tumor immune response.
- Systemic tumor destruction also on the untreated left-leg tumors when a T-cell promoting agent MTE was additionally used.

DOI:10.14753/SE.2020.2337

8. Summary

Modulated electro-hyperthermia (mEHT), generated at 13.56 MHz radiofrequency, can selectively target tumors due to their elevated glycolysis (Warburg-effect), extracellular ion concentration and conductivity compared to normal tissues. It has been used as a non-invasive complementary to human chemo- and radiotherapy, though its mechanism of actions had been insufficiently clarified. We have used C26 mouse colorectal adenocarcinoma cell cultures and their allografts in immunocompetent (BALB/c) mice to study the molecular background of mEHT induced tumor damage using qPCR, immunocytochemistry, cell viability and clonogenic assays and cell death analysis.

mEHT treatment induced significant tumor damage *in vitro* and *in vivo*. This was preceded by the early downregulation of the anti-apoptotic XIAP, BCL-2 and BCL-XL and elevation of pro-apoptotic BAX and PUMA transcripts *in vitro* and followed by the upregulation of activated caspase-8 and -3 proteins consistent with the activation of both the extrinsic and intrinsic apoptosis. mEHT treatment induced significant DNA double strand-breaks indicated by nuclear deposition of H2AXγ besides the upregulation of phospho-$p53^{Ser15}$ and $p21^{waf1}$. These were in line with the blockade of cell cycle (senescence) and the reduction of tumor stem cell colonies. Also *in vitro,* mEHT induced apoptosis, while doxorubicin (Dox) treatment led to necrosis. Furthermore, mEHT promoted the Dox uptake and the combined treatment additively reduced tumor cell viability and augmented cell death near to synergy. The upregulation and release of damage associated molecular pattern (DAMP) signals including Hsp70, calreticulin and HMGB1 proteins were relevant for inducing immunogenic cell death (ICD) response *in vivo*. Indeed, a single shot of mEHT led to progressive tumor damage and accumulation of CD3+ T-cells (with scant FoxP3+ regulatory T-cells) and S100+ antigen presenting dendritic cells. Immune mediated tumor damage was also observed in the untreated contralateral tumors when mEHT was combined with a chlorogenic acid rich T-cell promoting MTE agent, indicating a systemic anti-tumor effect of mEHT treatment.

In conclusion, mEHT treatment alone can induce irreversible cell stress leading to p53 induced caspase-dependent apoptosis and senescence, which could enhance the effect of Dox. The accompanying release of stress associated DAMP proteins was likely to contribute to the ongoing secondary tumor destruction by an ICD mechanism.

DOI:10.14753/SE.2020.2337

9. Összefoglaló

A 13,56 MHz rádiófrekvenciával generált modulált elektro-hipertermia (mEHT) alkalmas a tumorok szelektív megcélzására, azok a normál szövetekhez képest megemelkedett glikolízise (Warburg-effektus), extracelluláris ion koncentrációja és konduktivitása miatt. A módszert a humán kemo- és radiotrápiák nem-invazív egészítéseként használják, bár hatásmechanizmusa csak kevéssé tisztázott. C26-os egér colorectalis adenocarcinoma sejtkultúrákon és immunkompetens (BALB/c) egerekbe létrehozott allograftokon vizsgáltuk az mEHT-indukálta tumor-károsodás molekuláris hátterét qPCR, immunocitokémia, sejt viabilitás és kolóniaképző próba, valamint sejt-halál analízis segítségével.

Az mEHT kezelés szignifikáns tumor-pusztulást okozott *in vitro* és *in vivo*. Ezt az anti-apoptotikus XIAP, BCL-2, BCL-XL csökkenése és a pro-apoptotikus BAX és PUMA transzkriptumok mennyiségének emelkedése *in vitro*, melyet az aktivált kaszpáz-8 és -3 fehérjék felülregulációja követett, ami a belső és külső apoptotikus útvnal aktivációjára utalt. Az mEHT DNS duplaszál-töréseket okozott, amit a H2AXγ nukleáris felhalmozódása jelzett, ezt pedig a foszfo-p53^{Ser15} és a p21^{waf1} aktivációja kísért. Utóbbiak okozhatják a sejtciklus gátlását (szeneszcencia) és a tumor őssejt kolóniák csökkenését. Ugyancsak *in vitro*, az mEHT apoptózist, míg a doxorubicin (Dox) főleg nekrózist indukált. Az mEHT elősegítette a Dox felvételét, valamint a kombinált kezelés additív módon csökkentette a sejt-viabilitást és közel szinergista módon potencírozta a sejt halált. Az sérülés asszociált molekuláris mintázat (DAMP) fehérjék felszabadulása mint pl.: a Hsp70, calreticulin és HMGB1, fontosak az immunogén sejt halál indukálásában *in vivo*. Az egyszeri mEHT kezelés progresszív tumorkárosodáshoz, CD3+ T-sejt (változatlan menniségű FoxP3+ regulátoros T-sejt) és S100+ antigén prezentáló dendritikus sejt akkumulációhoz vezetett. Immun-mediált tumor-károsodás volt ugyancsak megfigyelhető a kezeletlen ellenoldali tumorokban is, amikor az mEHT kezelés a klorogénsavban gazdag MTE ágenssel volt kombinálva. Ebből az mEHT szisztémás anti-tumorális hatására következtettünk.

Konklúzióként: az mEHT kezelés önmagában irreverzibilis sejt stresszt indukált, amely p53-mediált kaszpáz-függő apoptózishoz és szeneszcenciához vezetett. Mindezek felerősíthetik a Dox hatását. A DAMP felszabadulás pedig leginkább az idővel terjedő, másodlagos tumor-pusztuláshoz járulhat hozzá az ICD mechanizmusán keresztül.

10. References

1. Yang KL, Huang CC, Chi MS, Chiang HC, Wang YS, Hsia CC, Andocs G, Wang HE, Chi KH. (2016) In vitro comparison of conventional hyperthermia and modulated electro-hyperthermia. Oncotarget, 7(51):84082-84092.
2. Andocs G, Rehman MU, Zhao QL, Papp E, Kondo T, Szasz A. (2015) Nanoheating without Artificial Nanoparticles Part II. Experimental Support of the Nanoheating Concept of the Modulated Electro-Hyperthermia Method, Using U937 Cell Suspension Model. Biology and Medicine, 7(4):9.
3. Szasz A, Szasz N, Szasz O. Oncothermia: Principles and Practices: Springer Netherlands; 2011: 174, 202-203.
4. Kim S, You SH, Cha J, Lee JY. (2017) The Synergistic Capacity of Modulated Electro-Hyperthermia in Preoperative Chemoradiation Therapy for Locally Advanced Rectal Cancer: An Interim Report of Phase 2 Trial. International Journal of Radiation Oncology • Biology • Physics, 99(2).
5. Lee SY, Kim JH, Han YH, Cho DH. (2018) The effect of modulated electro-hyperthermia on temperature and blood flow in human cervical carcinoma. Int J Hyperthermia, 34(7):953-960.
6. Roussakow SV. (2017) Clinical and economic evaluation of modulated electrohyperthermia concurrent to dose-dense temozolomide 21/28 days regimen in the treatment of recurrent glioblastoma: a retrospective analysis of a two-centre German cohort trial with systematic comparison and effect-to-treatment analysis. BMJ Open, 7(11):e017387.
7. Andocs G, Szasz O, Szasz A. (2009) Oncothermia treatment of cancer: from the laboratory to clinic. Electromagn Biol Med, 28(2):148-165.
8. Lee SY, Lee NR, Cho DH, Kim JS. (2017) Treatment outcome analysis of chemotherapy combined with modulated electro-hyperthermia compared with chemotherapy alone for recurrent cervical cancer, following irradiation. Oncol Lett, 14(1):73-78.
9. Brenner H, Kloor M, Pox CP. (2014) Colorectal cancer. Lancet, 383(9927):1490-1502.
10. Boland PM, Ma WW. (2017) Immunotherapy for Colorectal Cancer. Cancers (Basel), 9(5).
11. Koido S, Ohkusa T, Homma S, Namiki Y, Takakura K, Saito K, Ito Z, Kobayashi H, Kajihara M, Uchiyama K, Arihiro S, Arakawa H, Okamoto M, Gong J, Tajiri H. (2013) Immunotherapy for colorectal cancer. World journal of gastroenterology, 19(46):8531-8542.
12. Siegel R, DeSantis C, Virgo K, Stein K, Mariotto A, Smith T, Cooper D, Gansler T, Lerro C, Fedewa S, Lin C, Leach C, Cannady RS, Cho H, Scoppa S, Hachey M, Kirch R, Jemal A, Ward E. (2012) Cancer treatment and survivorship statistics, 2012. CA Cancer J Clin, 62(4):220-241.

13. Ramirez LY, Huestis SE, Yap TY, Zyzanski S, Drotar D, Kodish E. (2009) Potential chemotherapy side effects: what do oncologists tell parents? Pediatr Blood Cancer, 52(4):497-502.

14. Pearce A, Haas M, Viney R, Pearson SA, Haywood P, Brown C, Ward R. (2017) Incidence and severity of self-reported chemotherapy side effects in routine care: A prospective cohort study. PLoS One, 12(10):e0184360.

15. Thorn CF, Oshiro C, Marsh S, Hernandez-Boussard T, McLeod H, Klein TE, Altman RB. (2011) Doxorubicin pathways: pharmacodynamics and adverse effects. Pharmacogenet Genomics, 21(7):440-446.

16. Meggyeshazi N, Andocs G, Balogh L, Balla P, Kiszner G, Teleki I, Jeney A, Krenacs T. (2014) DNA fragmentation and caspase-independent programmed cell death by modulated electrohyperthermia. Strahlentherapie und Onkologie : Organ der Deutschen Rontgengesellschaft, 190(9):815-822.

17. Minotti G, Recalcati S, Mordente A, Liberi G, Calafiore AM, Mancuso C, Preziosi P, Cairo G. (1998) The secondary alcohol metabolite of doxorubicin irreversibly inactivates aconitase/iron regulatory protein-1 in cytosolic fractions from human myocardium. FASEB J, 12(7):541-552.

18. Olson RD, Mushlin PS, Brenner DE, Fleischer S, Cusack BJ, Chang BK, Boucek RJ. (1988) Doxorubicin cardiotoxicity may be caused by its metabolite, doxorubicinol. Proc Natl Acad Sci U S A, 85(10):3585-3589.

19. Lynch D, Murphy A. (2016) The emerging role of immunotherapy in colorectal cancer. Ann Transl Med, 4(16):305.

20. Andocs G, Meggyeshazi N, Balogh L, Spisak S, Maros ME, Balla P, Kiszner G, Teleki I, Kovago C, Krenacs T. (2015) Upregulation of heat shock proteins and the promotion of damage-associated molecular pattern signals in a colorectal cancer model by modulated electrohyperthermia. Cell Stress Chaperones, 20(1):37-46.

21. Tsang YW, Huang CC, Yang KL, Chi MS, Chiang HC, Wang YS, Andocs G, Szasz A, Li WT, Chi KH. (2015) Improving immunological tumor microenvironment using electro-hyperthermia followed by dendritic cell immunotherapy. BMC Cancer, 15:708.

22. Chircop M, Speidel D. (2014) Cellular stress responses in cancer and cancer therapy. Front Oncol, 4:304.

23. Csermely P. Stresszfehérjék. Glatz F (editor). Vince Kiadó Kft., Budapest, 2000: 10.

24. Ali YO, Kitay BM, Zhai RG. (2010) Dealing with misfolded proteins: examining the neuroprotective role of molecular chaperones in neurodegeneration. Molecules, 15(10):6859-6887.

25. Kumar P, Ambasta RK, Veereshwarayya V, Rosen KM, Kosik KS, Band H, Mestril R, Patterson C, Querfurth HW. (2007) CHIP and HSPs interact with beta-APP in a proteasome-dependent manner and influence Abeta metabolism. Hum Mol Genet, 16(7):848-864.

26. Kroemer G, Galluzzi L, Vandenabeele P, Abrams J, Alnemri ES, Baehrecke EH, Blagosklonny MV, El-Deiry WS, Golstein P, Green DR, Hengartner M, Knight RA, Kumar S, Lipton SA, Malorni W, Nuñez G, Peter ME, Tschopp J, Yuan J, Piacentini M, Zhivotovsky B, Melino G. (2009) Classification of cell death: recommendations of the Nomenclature Committee on Cell Death 2009. Cell Death Differ. 16(1):3-11.

27. Ziegler U, Groscurth P. (2004) Morphological features of cell death. News Physiol Sci, 19:124-128.

28. Green DR, Ferguson T, Zitvogel L, Kroemer G. (2009) Immunogenic and tolerogenic cell death. Nat Rev Immunol, 9(5):353-363.

29. Galluzzi L, Vitale I, Aaronson SA, Abrams JM, Adam D, Agostinis P, Alnemri ES, Altucci L, Amelio I, Andrews DW et al. (2018) Molecular mechanisms of cell death: recommendations of the Nomenclature Committee on Cell Death 2018. Cell Death Differ, 25(3):486-541.

30. Vila M, Przedborski S. (2003) Targeting programmed cell death in neurodegenerative diseases. Nature reviews Neuroscience, 4(5):365-375.

31. Yu J, Zhang L. (2003) No PUMA, no death: implications for p53-dependent apoptosis. Cancer Cell, 4(4):248-249.

32. Chiang SC, Theorell J, Entesarian M, Meeths M, Mastafa M, Al-Herz W, Frisk P, Gilmour KC, Ifversen M, Langenskiold C, Machaczka M, Naqvi A, Payne J, Perez-Martinez A, Sabel M, Unal E, Unal S, Winiarski J, Nordenskjold M, Ljunggren HG, Henter JI, Bryceson YT. (2013) Comparison of primary human cytotoxic T-cell and natural killer cell responses reveal similar molecular requirements for lytic granule exocytosis but differences in cytokine production. Blood, 121(8):1345-1356.

33. Kalkavan H, Green DR. (2018) MOMP, cell suicide as a BCL-2 family business. Cell Death Differ, 25(1):46-55.

34. Srinivasula SM, Hegde R, Saleh A, Datta P, Shiozaki E, Chai J, LeeRA, Robbins PD, Fernandes-Alnemri T, Shi Y, Alnemri ES. (2001) A conserved XIAP-interaction motif in caspase-9 and Smac/DIABLO regulates caspase activity and apoptosis. Nature, 410(6824):112-116.

35. Niero EL, Rocha-Sales B, Lauand C, Cortez BA, de Souza MM, Rezende-Teixeira P, Urabayashi MS, Martens AA, Neves JH, Machado-Santelli GM. (2014) The multiple facets of drug resistance: one history, different approaches. J Exp Clin Cancer Res, 33:37.

36. Porter AG, Jänicke RU. (1999) Emerging roles of caspase-3 in apoptosis. Cell Death Differ, 6(2):99-104.

37. Segawa K, Suzuki J, Nagata S. (2014) Flippases and scramblases in the plasma membrane. Cell Cycle, 13(19):2990-2991.

38. Segawa K, Nagata S. (2015) An Apoptotic 'Eat Me' Signal: Phosphatidylserine Exposure. Trends Cell Biol, 25(11):639-650.

39. deCathelineau AM, Henson PM. (2003) The final step in programmed cell death: phagocytes carry apoptotic cells to the grave. Essays Biochem, 39:105-117.

40. Kitazumi I, Tsukahara M. (2011) Regulation of DNA fragmentation: the role of caspases and phosphorylation. The FEBS journal, 278(3):427-441.

41. Lomonosova E, Chinnadurai G. (2008) BH3-only proteins in apoptosis and beyond: an overview. Oncogene, 27 Suppl 1:S2-19.

42. Guicciardi ME, Gores GJ. (2009) Life and death by death receptors. FASEB J, 23(6):1625-1637.

43. Ozören N, El-Deiry WS. (2002) Defining characteristics of Types I and II apoptotic cells in response to TRAIL. Neoplasia, 4(6):551-557.

44. Gamrekelashvili J, Greten TF, Korangy F. (2015) Immunogenicity of necrotic cell death. Cell Mol Life Sci, 72(2):273-283.

45. Dhuriya YK, Sharma D. (2018) Necroptosis: a regulated inflammatory mode of cell death. J Neuroinflammation, 15(1):199.

46. Ha HC, Snyder SH. (1999) Poly(ADP-ribose) polymerase is a mediator of necrotic cell death by ATP depletion. Proc Natl Acad Sci U S A, 96(24):13978-13982.

47. Dimri GP. (2005) What has senescence got to do with cancer? Cancer Cell, 7(6):505-512.

48. Cheng Q, Chen L, Li Z, Lane WS, Chen J. (2009) ATM activates p53 by regulating MDM2 oligomerization and E3 processivity. EMBO J, 28(24):3857-3867.

49. Maréchal A, Zou L. (2013) DNA damage sensing by the ATM and ATR kinases. Cold Spring Harb Perspect Biol, 5(9).

50. Georgakilas AG, Martin OA, Bonner WM. (2017) p21: A Two-Faced Genome Guardian. Trends Mol Med, 23(4):310-319.

51. Gottlieb TM, Leal JF, Seger R, Taya Y, Oren M. (2002) Cross-talk between Akt, p53 and Mdm2: possible implications for the regulation of apoptosis. Oncogene, 21(8):1299-1303.

52. Schreiber RD, Old LJ, Smyth MJ. (2011) Cancer immunoediting: integrating immunity's roles in cancer suppression and promotion. Science, 331(6024):1565-1570.

53. Kepp O, Senovilla L, Vitale I, Vacchelli E, Adjemian S, Agostinis P, Apetoh L, Aranda F, Barnaba V, Bloy N et al. (2014) Consensus guidelines for the detection of immunogenic cell death. Oncoimmunology, 3(9):e955691.

54. Kang R, Zhang Q, Zeh HJ, Lotze MT, Tang D. (2013) HMGB1 in cancer: good, bad, or both? Clin Cancer Res, 19(15):4046-4057.

55. Liu W, Wang P, Li Z, Xu W, Dai L, Wang K, Zhang J. (2009) Evaluation of tumour-associated antigen (TAA) miniarray in immunodiagnosis of colon cancer. Scand J Immunol, 69(1):57-63.

56. Restifo NP, Dudley ME, Rosenberg SA. (2012) Adoptive immunotherapy for cancer: harnessing the T cell response. Nat Rev Immunol, 12(4):269-281.

57. Gross G, Margalit A. (2007) Targeting tumor-associated antigens to the MHC class I presentation pathway. Endocr Metab Immune Disord Drug Targets, 7(2):99-109.

58. Farhood B, Najafi M, Mortezaee K. (2018) CD8+ T Cells: Foot Soldiers of the Immune System. J Cell Physiol, 26;35(2):161-8.

59. Neefjes J, Jongsma ML, Paul P, Bakke O. (2011) Towards a systems understanding of MHC class I and MHC class II antigen presentation. Nat Rev Immunol, 11(12):823-836.

60. Fridman WH, Pagès F, Sautès-Fridman C, Galon J. (2012) The immune contexture in human tumours: impact on clinical outcome. Nat Rev Cancer. 12(4):298-306.

61. Barry M, Heibein JA, Pinkoski MJ, Lee SF, Moyer RW, Green DR, Bleackley RC. (2000) Granzyme B short-circuits the need for caspase 8 activity during granule-mediated cytotoxic T-lymphocyte killing by directly cleaving Bid. Mol Cell Biol, 20(11):3781-3794.

62. Zhang S, Zhang H, Zhao J. (2009) The role of CD4 T cell help for CD8 CTL activation. Biochem Biophys Res Commun, 384(4):405-408.

63. Holling TM, Schooten E, van Den Elsen PJ. (2004) Function and regulation of MHC class II molecules in T-lymphocytes: of mice and men. Hum Immunol, 65(4):282-290.

64. Thibodeau J, Bourgeois-Daigneault MC, Lapointe R. (2012) Targeting the MHC Class II antigen presentation pathway in cancer immunotherapy. Oncoimmunology, 1(6):908-916.

65. Melief CJ. (2008) Cancer immunotherapy by dendritic cells. Immunity, 29(3):372-383.

66. O'Sullivan B, Thomas R. (2003) CD40 and dendritic cell function. Crit Rev Immunol, 23(1-2):83-107.

67. Ostroumov D, Fekete-Drimusz N, Saborowski M, Kühnel F, Woller N. (2018) CD4 and CD8 T lymphocyte interplay in controlling tumor growth. Cell Mol Life Sci, 75(4):689-713.

68. Takeuchi A, Saito T. (2017) CD4 CTL, a Cytotoxic Subset of CD4. Front Immunol, 8:194.

69. Ling KL, Pratap SE, Bates GJ, Singh B, Mortensen NJ, George BD, Warren BF, Piris J, Roncador G, Fox SB, Banham AH, Cerundolo V. (2007) Increased frequency of regulatory T cells in peripheral blood and tumour infiltrating lymphocytes in colorectal cancer patients. Cancer Immun, 7:7.

70. Shevach EM. (2009) Mechanisms of foxp3+ T regulatory cell-mediated suppression. Immunity, 30(5):636-645.

71. Raimondi G, Turner MS, Thomson AW, Morel PA. (2007) Naturally occurring regulatory T cells: recent insights in health and disease. Crit Rev Immunol, 27(1):61-95.

72. Maldonado RA, von Andrian UH. (2010) How tolerogenic dendritic cells induce regulatory T cells. Adv Immunol, 108:111-165.

73. Beatty GL, Gladney WL. (2015) Immune escape mechanisms as a guide for cancer immunotherapy. Clin Cancer Res, 21(4):687-692.

74. Rabinovich GA, Gabrilovich D, Sotomayor EM. (2007) Immunosuppressive strategies that are mediated by tumor cells. Annu Rev Immunol, 25:267-296.

75. Evans SS, Wang WC, Bain MD, Burd R, Ostberg JR, Repasky EA. (2001) Fever-range hyperthermia dynamically regulates lymphocyte delivery to high endothelial venules. Blood, 97(9):2727-2733.

76. Ostberg JR, Kabingu E, Repasky EA. (2003) Thermal regulation of dendritic cell activation and migration from skin explants. Int J Hyperthermia, 19(5):520-533.

77. Kobayashi Y, Ito Y, Ostapenko VV, Sakai M, Matsushita N, Imai K, Shimizu K, Aruga A, Tanigawa K. (2014) Fever-range whole-body heat treatment stimulates antigen-specific T-cell responses in humans. Immunol Lett, 162(1 Pt A):256-261.

78. Mace TA, Zhong L, Kilpatrick C, Zynda E, Lee CT, Capitano M, Minderman H, Repasky EA. (2011) Differentiation of CD8+ T cells into effector cells is enhanced by physiological range hyperthermia. J Leukoc Biol, 90(5):951-962.

79. Murshid A, Gong J, Calderwood SK. (2012) The role of heat shock proteins in antigen cross presentation. Front Immunol, 3:63.

80. Breloer M, Dorner B, Moré SH, Roderian T, Fleischer B, von Bonin A. (2001) Heat shock proteins as "danger signals": eukaryotic Hsp60 enhances and accelerates antigen-specific IFN-gamma production in T cells. Eur J Immunol, 31(7):2051-2059.

81. Garrido F, Aptsiauri N, Doorduijn EM, Garcia Lora AM, van Hall T. (2016) The urgent need to recover MHC class I in cancers for effective immunotherapy. Curr Opin Immunol, 39:44-51.

82. Nicholson SE, Keating N, Belz GT. (2017) Natural killer cells and anti-tumor immunity. Mol Immunol, 110:40-47.

83. Ostberg JR, Dayanc BE, Yuan M, Oflazoglu E, Repasky EA. (2007) Enhancement of natural killer (NK) cell cytotoxicity by fever-range thermal stress is dependent on NKG2D function and is associated with plasma membrane NKG2D clustering and increased expression of MICA on target cells. J Leukoc Biol, 82(5):1322-1331.

84. Dayanc BE, Beachy SH, Ostberg JR, Repasky EA. (2008) Dissecting the role of hyperthermia in natural killer cell mediated anti-tumor responses. Int J Hyperthermia, 24(1):41-56.

85. O'Leary JG, Goodarzi M, Drayton DL, von Andrian UH. (2006) T cell- and B cell-independent adaptive immunity mediated by natural killer cells. Nat Immunol, 7(5):507-516.

86. Yagawa Y, Tanigawa K, Kobayashi Y, Yamamoto M. (2017) Cancer immunity and therapy using hyperthermia with immunotherapy, radiotherapy, chemotherapy, and surgery. Journal of Cancer Metastasis and Treatment, 3:218-230.

87. Espinosa E, Zamora P, Feliu J, González Barón M. (2003) Classification of anticancer drugs--a new system based on therapeutic targets. Cancer Treat Rev, 29(6):515-523.

88. Wu XZ. (2006) A new classification system of anticancer drugs - based on cell biological mechanisms. Med Hypotheses, 66(5):883-887.

89. Nussbaumer S, Bonnabry P, Veuthey JL, Fleury-Souverain S. (2011) Analysis of anticancer drugs: a review. Talanta, 85(5):2265-2289.

90. Baskar R, Dai J, Wenlong N, Yeo R, Yeoh KW. (2014) Biological response of cancer cells to radiation treatment. Front Mol Biosci, 1:24.

91. Harrison LB, Chadha M, Hill RJ, Hu K, Shasha D. (2002) Impact of tumor hypoxia and anemia on radiation therapy outcomes. Oncologist, 7(6):492-508.

92. Evans SM, Jenkins WT, Shapiro M, Koch CJ. (1997) Evaluation of the concept of "hypoxic fraction" as a descriptor of tumor oxygenation status. Adv Exp Med Biol, 411:215-225.

93. Teicher BA. (1995) Physiologic mechanisms of therapeutic resistance. Blood flow and hypoxia. Hematology/oncology clinics of North America, 9(2):475-506.

94. Griffin RJ, Dings RP, Jamshidi-Parsian A, Song CW. (2010) Mild temperature hyperthermia and radiation therapy: role of tumour vascular thermotolerance and relevant physiological factors. Int J Hyperthermia, 26(3):256-263.

95. Farkona S, Diamandis EP, Blasutig IM. (2016) Cancer immunotherapy: the beginning of the end of cancer? BMC Med, 14:73.

96. Li Z, Song W, Rubinstein M, Liu D. (2018) Recent updates in cancer immunotherapy: a comprehensive review and perspective of the 2018 China Cancer Immunotherapy Workshop in Beijing. J Hematol Oncol, 11(1):142.

97. Lee S, Margolin K. (2011) Cytokines in cancer immunotherapy. Cancers (Basel). 3(4):3856-3893.

98. Chakrabarty AM, Bernardes N, Fialho AM. (2014) Bacterial proteins and peptides in cancer therapy: today and tomorrow. Bioengineered, 5(4):234-242.

99. Jahrsdörfer B, Weiner GJ. (2008) CpG oligodeoxynucleotides as immunotherapy in cancer. Update Cancer Ther, 3(1):27-32.

100. Bachanova V, Miller JS. (2014) NK cells in therapy of cancer. Crit Rev Oncog, 19(1-2):133-141.

101. Shang N, Figini M, Shangguan J, Wang B, Sun C, Pan L, Ma Q, Zhang Z. (2017) Dendritic cells based immunotherapy. Am J Cancer Res, 7(10):2091-2102.

102. Miliotou AN, Papadopoulou LC. (2018) CAR T-cell Therapy: A New Era in Cancer Immunotherapy. Curr Pharm Biotechnol, 19(1):5-18.

103. Anassi E, Ndefo UA. (2011) Sipuleucel-T (provenge) injection: the first immunotherapy agent (vaccine) for hormone-refractory prostate cancer. P T, 36(4):197-202.

104. Prasad V, Kaestner V. (2017) Nivolumab and pembrolizumab: Monoclonal antibodies against programmed cell death-1 (PD-1) that are interchangeable. Semin Oncol, 44(2):132-135.

105. Seidel JA, Otsuka A, Kabashima K. (2018) Anti-PD-1 and Anti-CTLA-4 Therapies in Cancer: Mechanisms of Action, Efficacy, and Limitations. Front Oncol, 8:86.

106. Gong J, Chehrazi-Raffle A, Reddi S, Salgia R. (2018) Development of PD-1 and PD-L1 inhibitors as a form of cancer immunotherapy: a comprehensive review of registration trials and future considerations. J Immunother Cancer, 6(1):8.

107. Lewith G, Robinson N. (2009) Complementary and alternative medicine: what the public want and how it may be delivered safely and effectively. J R Soc Med. 102(10):411-414.

108. Frass M, Strassl RP, Friehs H, Müllner M, Kundi M, Kaye AD. (2012) Use and acceptance of complementary and alternative medicine among the general population and medical personnel: a systematic review. Ochsner J, 12(1):45-56.

109. Rossi E, Di Stefano M, Firenzuoli F, Monechi MV, Baccetti S. (2017) Add-On Complementary Medicine in Cancer Care: Evidence in Literature and Experiences of Integration. Medicines (Basel), 4(1).

110. Cassileth BR, Deng G. (2004) Complementary and alternative therapies for cancer. Oncologist, 9(1):80-89.

111. Roussakow S. (2013) The History of Hyperthermia Rise and Decline. Conference Papers in Medicine, 2013:40.

112. Chicheł A, Skowronek J, Kubaszewska M, Kanikowski M. (2007) Hyperthermia – description of a method and a review of clinical applications. Reports of Practical Oncology & Radiotherapy, 12(5):267-275.

113. Kaur P, Hurwitz MD, Krishnan S, Asea A. (2011) Combined hyperthermia and radiotherapy for the treatment of cancer. Cancers (Basel), 3(4):3799-3823.

114. Kong G, Dewhirst MW. (1999) Hyperthermia and liposomes. Int J Hyperthermia, 15(5):345-370.

115. Ponce AM, Vujaskovic Z, Yuan F, Needham D, Dewhirst MW. (2006) Hyperthermia mediated liposomal drug delivery. Int J Hyperthermia. 22(3):205-213.

116. Ohno S, Siddik ZH, Kido Y, Zwelling LA, Bull JM. (1994) Thermal enhancement of drug uptake and DNA adducts as a possible mechanism for the effect of sequencing hyperthermia on cisplatin-induced cytotoxicity in L1210 cells. Cancer Chemother Pharmacol, 34(4):302-306.

117. Nagaoka S, Kawasaki S, Sasaki K, Nakanishi T. (1986) Intracellular uptake, retention and cytotoxic effect of adriamycin combined with hyperthermia in vitro. Jpn J Cancer Res, 77(2):205-211.

118. Park BJ, Alexander HR, Libutti SK, Wu P, Royalty D, Kranda KC, Bartlett DL. (1999) Treatment of primary peritoneal mesothelioma by continuous hyperthermic peritoneal perfusion (CHPP). Ann Surg Oncol, 6(6):582-590.

119. Newton AD, Bartlett EK, Karakousis GC. (2016) Cytoreductive surgery and hyperthermic intraperitoneal chemotherapy: a review of factors contributing to morbidity and mortality. J Gastrointest Oncol, 7(1):99-111.

120. Behrouzkia Z, Joveini Z, Keshavarzi B, Eyvazzadeh N, Aghdam RZ. (2016) Hyperthermia: How Can It Be Used? Oman Med J, 31(2):89-97.

121. Brace C. (2011) Thermal tumor ablation in clinical use. IEEE Pulse, 2(5):28-38.

122. Chatterjee DK, Diagaradjane P, Krishnan S. (2011) Nanoparticle-mediated hyperthermia in cancer therapy. Ther Deliv, 2(8):1001-1014.

123. Sapareto SA, Dewey WC. (1984) Thermal dose determination in cancer therapy. Int J Radiat Oncol Biol Phys, 10(6):787-800.

124. Robins HI, Cohen JD, Schmitt CL, Tutsch KD, Feierabend C, Arzoomanian RZ, Alberti D, d'Oleire F, Longo W, Heiss C. (1993) Phase I clinical trial of carboplatin and 41.8 degrees C whole-body hyperthermia in cancer patients. J Clin Oncol, 11(9):1787-1794.

125. Amichetti M, Graiff C, Fellin G, Pani G, Bolner A, Maluta S, Valdagni R. (1993) Cisplatin, hyperthermia, and radiation (trimodal therapy) in patients with locally advanced head and neck tumors: a phase I-II study. Int J Radiat Oncol Biol Phys, 26(5):801-807.

126. Abdel-Wahab OI, Grubbs E, Viglianti BL, Cheng TY, Ueno T, Ko S, Rabbani Z, Curtis S, Pruitt SK, Dewhirst MW, Tyler DS. (2004) The role of hyperthermia in regional alkylating agent chemotherapy. Clin Cancer Res, 10(17):5919-5929.

127. Issels RD, Lindner LH, Verweij J, Wessalowski R, Reichardt P, Wust P, Ghadjar P, Hohenberger P, Angele M, Salat C, Vujaskovic Z, Daugaard S, Mella O, Mansmann U, Dürr HR, Knösel T, Abdel-Rahman S, Schmidt M, Hiddemann W, Jauch KW, Belka C, Gronchi A. (2018) Effect of Neoadjuvant Chemotherapy Plus Regional Hyperthermia on Long-term Outcomes Among Patients With Localized High-Risk Soft Tissue Sarcoma: The EORTC 62961-ESHO 95 Randomized Clinical Trial. JAMA Oncol, 4(4):483-492.

128. Issels RD, Lindner LH, Verweij J, Wust P, Reichardt P, Schem BC, Abdel-Rahman S, Daugaard S, Salat C, Wendtner CM, Vujaskovic Z, Wessalowski R, Jauch KW, Dürr HR, Ploner F, Baur-Melnyk A, Mansmann U, Hiddemann W, Blay JY,

Hohenberger P. (2010) Neo-adjuvant chemotherapy alone or with regional hyperthermia for localised high-risk soft-tissue sarcoma: a randomised phase 3 multicentre study. Lancet Oncol, 11(6):561-570.

129. Lee S, Son B, Park G, Kim H, Kang H, Jeon J, Youn H, Youn B. (2018) Immunogenic Effect of Hyperthermia on Enhancing Radiotherapeutic Efficacy. Int J Mol Sci, 19(9).

130. Atanackovic D, Nierhaus A, Neumeier M, Hossfeld DK, Hegewisch-Becker S. (2002) 41.8 degrees C whole body hyperthermia as an adjunct to chemotherapy induces prolonged T cell activation in patients with various malignant diseases. Cancer Immunol Immunother, 51(11-12):603-613.

131. Vujaskovic Z, Kim DW, Jones E, Lan L, McCall L, Dewhirst MW, Craciunescu O, Stauffer P, Liotcheva V, Betof A, Blackwell K. (2010) A phase I/II study of neoadjuvant liposomal doxorubicin, paclitaxel, and hyperthermia in locally advanced breast cancer. Int J Hyperthermia, 26(5):514-521.

132. Kouloulias VE, Dardoufas CE, Kouvaris JR, Gennatas CS, Polyzos AK, Gogas HJ, Sandilos PH, Uzunoglu NK, Malas EG, Vlahos LJ. (2002) Liposomal doxorubicin in conjunction with reirradiation and local hyperthermia treatment in recurrent breast cancer: a phase I/II trial. Clin Cancer Res, 8(2):374-382.

133. Gianni L, Eiermann W, Semiglazov V, Manikhas A, Lluch A, Tjulandin S, Zambetti M, Vazquez F, Byakhow M, Lichinitser M, Climent MA, Ciruelos E, Ojeda B, Mansutti M, Bozhok A, Baronio R, Feyereislova A, Barton C, Valagussa P, Baselga J. (2010) Neoadjuvant chemotherapy with trastuzumab followed by adjuvant trastuzumab versus neoadjuvant chemotherapy alone, in patients with HER2-positive locally advanced breast cancer (the NOAH trial): a randomised controlled superiority trial with a parallel HER2-negative cohort. Lancet, 375(9712):377-384.

134. Neef DW, Jaeger AM, Thiele DJ. (2011) Heat shock transcription factor 1 as a therapeutic target in neurodegenerative diseases. Nat Rev Drug Discov, 10(12):930-44.

135. Kampinga HH. (2006) Cell biological effects of hyperthermia alone or combined with radiation or drugs: a short introduction to newcomers in the field. Int J Hyperthermia, 22(3):191-196.

136. van der Zee J, González GD. (2002) The Dutch Deep Hyperthermia Trial: results in cervical cancer. Int J Hyperthermia, 18(1):1-12.

137. Franckena M, Stalpers LJ, Koper PC, Wiggenraad RG, Hoogenraad WJ, van Dijk JD, Wárlám-Rodenhuis CC, Jobsen JJ, van Rhoon GC, van der Zee J. (2008) Long-term improvement in treatment outcome after radiotherapy and hyperthermia in locoregionally advanced cervix cancer: an update of the Dutch Deep Hyperthermia Trial. Int J Radiat Oncol Biol Phys, 70(4):1176-1182.

138. Franckena M, Lutgens LC, Koper PC, Kleynen CE, van der Steen-Banasik EM, Jobsen JJ, Leer JW, Creutzberg CL, Dielwart MF, van Norden Y, Canters RA, van Rhoon GC, van der Zee J. (2009) Radiotherapy and hyperthermia for treatment of

primary locally advanced cervix cancer: results in 378 patients. Int J Radiat Oncol Biol Phys, 73(1):242-250.

139. Takeda T, Kobayashi S, Takeda H. (2012) Immunotherapy with hyperthermia for advanced or recurrent breast cancer patients in whom standard therapy showed no effect or was refused. Gan To Kagaku Ryoho, 39(12):1766-1769.

140. Takeda T, Takeda H, Tanaka C, Maruhashi S. (2014) The effect of immunotherapy and hyperthermia for advanced or recurrent head and neck cancer - 74 clinical cases. Gan To Kagaku Ryoho, 41(10):1283-1285.

141. Hegyi G, Szigeti GP, Szász A. (2013) Hyperthermia versus Oncothermia: Cellular Effects in Complementary Cancer Therapy. Evid Based Complement Alternat Med, 2013:672873.

142. Hegyi G, Szasz O, Szasz A. (2013) Oncothermia: a new paradigm and promising method in cancer therapies. Acupuncture & electro-therapeutics research, 38(3-4):161-197.

143. Szasz A. (2014) Current status of oncothermia therapy for lung cancer. The Korean journal of thoracic and cardiovascular surgery, 47(2):77-93.

144. Foster KR. Dielectric Properties of Tissues. In: Bronzo JD (editor). The Biomedical Engineering Handbook, Second Edition. 2. CRC Press LLC, USA, Boca Raton, 1999: 1606.

145. Raoof M, Cisneros BT, Corr SJ, Palalon F, Curley SA, Koshkina NV. (2013) Tumor selective hyperthermia induced by short-wave capacitively-coupled RF electric-fields. PLoS One, 8(7):e68506.

146. Zou Y, Guo Z. (2003) A review of electrical impedance techniques for breast cancer detection. Medical engineering & physics, 25(2):79-90.

147. Pethig R, Gascoyne PR, McLaughlin JA, Szent-Gyorgyi A. (1984) Interaction of the 2,6-dimethoxysemiquinone and ascorbyl free radicals with Ehrlich ascites cells: a probe of cell-surface charge. Proc Natl Acad Sci U S A, 81(7):2088-2091.

148. Blad B, Baldetorp B. (1996) Impedance spectra of tumour tissue in comparison with normal tissue; a possible clinical application for electrical impedance tomography. Physiol Meas, 17 Suppl 4A:A105-115.

149. O'Rourke AP, Lazebnik M, Bertram JM, Converse MC, Hagness SC, Webster JG, Mahvi DM. (2007) Dielectric properties of human normal, malignant and cirrhotic liver tissue: in vivo and ex vivo measurements from 0.5 to 20 GHz using a precision open-ended coaxial probe. Physics in medicine and biology, 52(15):4707-4719.

150. Khramtsov VV, Gillies RJ. (2014) Janus-faced tumor microenvironment and redox. Antioxid Redox Signal, 21(5):723-729.

151. Romero-Garcia S, Moreno-Altamirano MM, Prado-Garcia H, Sanchez-Garcia FJ. (2016) Lactate Contribution to the Tumor Microenvironment: Mechanisms, Effects on Immune Cells and Therapeutic Relevance. Front Immunol, 7:52.

152. Morimoto T, Kimura S, Konishi Y, Komaki K, Uyama T, Monden Y, Kinouchi Y, Iritani T. (1993) A study of the electrical bio-impedance of tumors. Journal of investigative surgery : the official journal of the Academy of Surgical Research, 6(1):25-32.

153. Scholoz B, Anderson R. (2000) On electrical impedance scanning-principles and simulations. Electromedica, 68:35-44.

154. Alon L, Sodickson DK, Deniz CM. (2016) Heat equation inversion framework for average SAR calculation from magnetic resonance thermal imaging. Bioelectromagnetics. 37(7):493-503.

155. Mátay G, Zombory L. A rádiófrekvenciás sugárzás élettani hatásai és orvosbiológiai alkalmazásai. Műegyetemi Kiadó, Budapest, 2000: 7-193.

156. Office IL. SAFETY IN THE USE OF RADIOFREQUENCY DIELECTRIC HEATERS AND SEALERS: International Labour Office; 1998: 7.

157. Andocs G, Renner H, Balogh L, Fonyad L, Jakab C, Szasz A. (2009) Strong synergy of heat and modulated electromagnetic field in tumor cell killing. Strahlentherapie und Onkologie : Organ der Deutschen Rontgengesellschaft, 185(2):120-126.

158. Yang W, Han GH, Shin HY, Lee EJ, Cho H, Chay DB, Kim JH. (2019) Combined treatment with modulated electro-hyperthermia and an autophagy inhibitor effectively inhibit ovarian and cervical cancer growth. Int J Hyperthermia, 36(1):9-20.

159. Cha J, Jeon TW, Lee CG, Oh ST, Yang HB, Choi KJ, Seo D, Yun I, Baik IH, Park KR, Park YN, Lee YH. (2015) Electro-hyperthermia inhibits glioma tumorigenicity through the induction of E2F1-mediated apoptosis. Int J Hyperthermia, 31(7):784-792.

160. Qin W, Akutsu Y, Andocs G, Suganami A, Hu X, Yusup G, Komatsu-Akimoto A, Hoshino I, Hanari N, Mori M, Isozaki Y, Akanuma N, Tamura Y, Matsubara H. (2014) Modulated electro-hyperthermia enhances dendritic cell therapy through an abscopal effect in mice. Oncol Rep, 32(6):2373-2379.

161. Pang CLK, Zhang X, Wang Z, Ou J, Lu Y, Chen P, Zhao C, Wang X, Zhang H, Roussakow SV. (2017) Local modulated electro-hyperthermia in combination with traditional Chinese medicine vs. intraperitoneal chemoinfusion for the treatment of peritoneal carcinomatosis with malignant ascites: A phase II randomized trial. Molecular and clinical oncology, 6(5):723-732.

162. Zhao L, Xiang B, Tan X. (2010) Fingerprinting of Marsdenia tenacissima by capillary electrophoresis compared to HPLC. J Chromatogr Sci, 48(5):417-420.

163. Fan W, Sun L, Zhou JQ, Zhang C, Qin S, Tang Y, Liu Y, Lin SS, Yuan ST. (2015) Marsdenia tenacissima extract induces G0/G1 cell cycle arrest in human esophageal carcinoma cells by inhibiting mitogen-activated protein kinase (MAPK) signaling pathway. Chinese journal of natural medicines, 13(6):428-437.

164. Han SY, Zhao MB, Zhuang GB, Li PP. (2012) Marsdenia tenacissima extract restored gefitinib sensitivity in resistant non-small cell lung cancer cells. Lung Cancer, 75(1):30-37.

165. Li W, Yang Y, Ouyang Z, Zhang Q, Wang L, Tao F, Shu Y, Gu Y, Xu Q, Sun Y. (2013) Xiao-Ai-Ping, a TCM Injection, Enhances the Antigrowth Effects of Cisplatin on Lewis Lung Cancer Cells through Promoting the Infiltration and Function of CD8(+) T Lymphocytes. Evid Based Complement Alternat Med, 2013:879512.

166. Yan Y, Li J, Han J, Hou N, Song Y, Dong L. (2015) Chlorogenic acid enhances the effects of 5-fluorouracil in human hepatocellular carcinoma cells through the inhibition of extracellular signal-regulated kinases. Anticancer Drugs, 26(5):540-546.

167. Kang TY, Yang HR, Zhang J, Li D, Lin J, Wang L, Xu X. (2013) The studies of chlorogenic Acid antitumor mechanism by gene chip detection: the immune pathway gene expression. J Anal Methods Chem, 2013:617243.

168. Vancsik T, Kovago C, Kiss E, Papp E, Forika G, Benyo Z, Meggyeshazi N, Krenacs T. (2018) Modulated electro-hyperthermia induced loco-regional and systemic tumor destruction in colorectal cancer allografts. Journal of Cancer, 9(1):41-53.

169. Andocs G, Rehman MU, Zhao QL, Tabuchi Y, Kanamori M, Kondo T. (2016) Comparison of biological effects of modulated electro-hyperthermia and conventional heat treatment in human lymphoma U937 cells. Cell Death Discov, 2:16039.

170. Vancsik T, Forika G, Balogh A, Kiss E, Krenacs T. (2019) Modulated electro-hyperthermia induced p53 driven apoptosis and cell cycle arrest additively support doxorubicin chemotherapy of colorectal cancer in vitro. Cancer Med, 00:1–12.

171. Kurywchak P, Tavormina J, Kalluri R. (2018) The emerging roles of exosomes in the modulation of immune responses in cancer. Genome Med, 10(1):23.

172. Collett GP, Redman CW, Sargent IL, Vatish M. (2018) Endoplasmic reticulum stress stimulates the release of extracellular vesicles carrying danger-associated molecular pattern (DAMP) molecules. Oncotarget, 9(6):6707-6717.

173. Garg AD, Martin S, Golab J, Agostinis P. (2014) Danger signalling during cancer cell death: origins, plasticity and regulation. Cell Death Differ, 21(1):26-38.

174. Piccinini AM, Midwood KS. (2010) DAMPening inflammation by modulating TLR signalling. Mediators Inflamm, 2010:672395.

175. Schaefer L. (2014) Complexity of danger: the diverse nature of damage-associated molecular patterns. J Biol Chem, 289(51):35237-35245.

176. Elmore S. (2007) Apoptosis: a review of programmed cell death. Toxicol Pathol, 35(4):495-516.

177. Yuan S, Akey CW. (2013) Apoptosome structure, assembly, and procaspase activation. Structure, 21(4):501-515.

178. Korchak HM, Rich AM, Wilkenfeld C, Rutherford LE, Weissmann G. (1982) A carbocyanine dye, DiOC6(3), acts as a mitochondrial probe in human neutrophils. Biochem Biophys Res Commun, 108(4):1495-1501.

179. Ozgen U, Savaşan S, Buck S, Ravindranath Y. (2000) Comparison of DiOC(6)(3) uptake and annexin V labeling for quantification of apoptosis in leukemia cells and non-malignant T lymphocytes from children. Cytometry, 42(1):74-78.

180. Plesca D, Mazumder S, Almasan A. (DNA) damage response and apoptosis. Methods Enzymol, 446:107-122.

181. Joerger AC, Fersht AR. (2016) The p53 Pathway: Origins, Inactivation in Cancer, and Emerging Therapeutic Approaches. Annu Rev Biochem, 85:375-404.

182. Kastenhuber ER, Lowe SW. Putting p53 in Context. Cell. 2017;170(6):1062-1078.

183. Fragkos M, Jurvansuu J, Beard P. (2009) H2AX is required for cell cycle arrest via the p53/p21 pathway. Mol Cell Biol, 29(10):2828-2840.

184. Coloff JL, Mason EF, Altman BJ, Gerriets VA, Liu T, Nichols AN, Zhao Y, Wofford JA, Jacobs SR, Ilkayeva O, Garrison SP, Zambetti GP, Rathmell JC. (2011) Akt requires glucose metabolism to suppress puma expression and prevent apoptosis of leukemic T cells. J Biol Chem, 286(7):5921-5933.

185. Plas DR, Thompson CB. (2002) Cell metabolism in the regulation of programmed cell death. Trends Endocrinol Metab, 13(2):75-78.

186. Gu L, Zhu N, Zhang H, Durden DL, Feng Y, Zhou M. (2009) Regulation of XIAP translation and induction by MDM2 following irradiation. Cancer Cell, 15(5):363-375.

187. Huang X, Wu Z, Mei Y, Wu M. (2013) XIAP inhibits autophagy via XIAP-Mdm2-p53 signalling. EMBO J, 32(16):2204-2216.

188. Mayo LD, Donner DB. (2001) A phosphatidylinositol 3-kinase/Akt pathway promotes translocation of Mdm2 from the cytoplasm to the nucleus. Proc Natl Acad Sci U S A, 98(20):11598-11603.

189. Greene RF, Collins JM, Jenkins JF, Speyer JL, Myers CE. (1983) Plasma pharmacokinetics of adriamycin and adriamycinol: implications for the design of in vitro experiments and treatment protocols. Cancer Res, 43(7):3417-3421.

190. Gunvén P, Theve NO, Peterson C. (1986) Serum and tissue concentrations of doxorubicin after IV administration of doxorubicin or doxorubicin-DNA complex to patients with gastrointestinal cancer. Cancer Chemother Pharmacol, 17(2):153-156.

191. Janigro D, Perju C, Fazio V, Hallene K, Dini G, Agarwal MK, Cucullo L. (2006) Alternating current electrical stimulation enhanced chemotherapy: a novel strategy to bypass multidrug resistance in tumor cells. BMC Cancer, 6:72.

192. Brown DC, Gatter KC. (2002) Ki67 protein: the immaculate deception? Histopathology, 40(1):2-11.

193. Mukhopadhaya A, Mendecki J, Dong X, Liu L, Kalnicki S, Garg M, Alfieri A, Guha C. (2007) Localized hyperthermia combined with intratumoral dendritic cells induces systemic antitumor immunity. Cancer Res, 67(16):7798-7806.

194. Skitzki JJ, Repasky EA, Evans SS. (2009) Hyperthermia as an immunotherapy strategy for cancer. Curr Opin Investig Drugs, 10(6):550-558.

195. Repasky EA, Evans SS, Dewhirst MW. (2013) Temperature matters! And why it should matter to tumor immunologists. Cancer Immunol Res, 1(4):210-216.

196. Han SY, Zhao W, Sun H, Zhou N, Zhou F, An G, Li PP. (2015) Marsdenia tenacissima extract enhances gefitinib efficacy in non-small cell lung cancer xenografts. Phytomedicine, 22(5):560-567.

197. Lee CH, Yoon SJ, Lee SM. (2013) Chlorogenic acid attenuates high mobility group box 1 (HMGB1) and enhances host defense mechanisms in murine sepsis. Mol Med, 18:1437-1448.

198. Derer A, Deloch L, Rubner Y, Fietkau R, Frey B, Gaipl US. (2015) Radio-immunotherapy-induced immunogenic cancer cells as basis for induction of systemic anti-tumor immune responses - pre-clinical evidence and ongoing clinical applications. Frontiers in Immunology, 6:505.

11. Publications

Publications relevant to the dissertation

Vancsik T, Kovago C, Kiss E, Papp E, Forika G, Benyo Z, Meggyeshazi N, Krenacs T. Modulated electro-hyperthermia induced loco-regional and systemic tumor destruction in colorectal cancer allografts. Journal of Cancer. 2018;9(1):41-53.

Vancsik T, Forika G, Balogh A, Kiss E, Krenacs T. Modulated electro-hyperthermia induced p53 driven apoptosis and cell cycle arrest additively support doxorubicin chemotherapy of colorectal cancer in vitro. Cancer Medicine. 2019;00:1–12.

Publications not directly related to the dissertation

Rajnai H, Teleki I, Kiszner G, Meggyeshazi N, Balla P, Vancsik T, Muzes Gy, Csomor J, Matolcsy A, Krenacs T. Connexin 43 communication channels in follicular dendritic cell development and in follicular lymphomas. Journal of immunology research. 2015;2015:528098.

12. Acknowledgements

I am grateful for Dr. Tibor Krenács for providing the opportunity to work in his laboratory and for supervising my work all the time.

I am thankful to Prof. András Matolcsy to let me work in his institution and to Prof. Ilona Kovalszky that I could study in the Pathology Doctoral School.

I am grateful for all the members of the laboratory, especially for Edit Parsch† and Éva Mátrainé Balogh for their excellent technical support in the laboratory work, to András Sztodola for his help in the animal experiments, and to Marica Csorba Gézáné † and Titanilla Dankó for their support in cell culturing.

I am also thankful for all of my former and recent colleagues: Éva Kiss, Gertrúd Fórika, Nóra Meggyesházi, Péter Balla, Lilla Füleki for their help and friendly atmosphere; and to Dr. Csaba Kővágó, who guided me at the first steps in the animal experiments and to Edina Papp for helping in data analysis.

I am thankful to Dr. Gábor Barna and Orsi Szabó for their patient teaching and help in flow cytometry.

Many thanks to Prof. Zoltán Benyó for his motivating attitude and for letting me work with his colleagues in the Institute of Clinical Experimental Research, in particular to Andrea Balogh for her advices and guidance in the *in vitro* studies.

I am also grateful to all members of the 1st Department of Pathology and Experimental Cancers Research who helped me in any aspect of my studies.

Furthermore, I am thankful to Prof. András Szász for supporting me with professional advice.

Finally, but not least, I am truly grateful to my beloved family and friends who give me the stable background and motivation throughout my work.